

FACILITY FORM 802

N65-27297 (ACCESSION NUMBER)	(THRU)
122 (PAGES)	1 (CODE)
(NASA CR OR TMX OR AD NUMBER)	25 (CATEGORY)



GPO PRICE \$ _____
 OTS PRICE(S) \$ _____
 Hard copy (HC) 4.00
 Microfiche (MF) 1.00

NASA CR-54353
 GA-6117

SUMMARY REPORT

**THE EFFECT OF HIGH PRESSURES ON
 THE CONDUCTIVITY OF VAPORS**

by

S. W. Kurnick and J. F. Colwell

prepared for

**NATIONAL AERONAUTICS AND SPACE ADMINISTRATION
 CONTRACT NAS 3-4119**

May 28, 1965

GENERAL ATOMIC
 DIVISION OF
GENERAL DYNAMICS

JOHN JAY HOPKINS LABORATORY FOR PURE AND APPLIED SCIENCE
 P.O. BOX 608, SAN DIEGO 12, CALIFORNIA

NOTICE

This report was prepared as an account of Government sponsored work. Neither the United States, nor the National Aeronautics and Space Administration (NASA), nor any person acting on behalf of NASA:

- A.) Makes any warranty or representation, expressed or implied, with respect to the accuracy, completeness, or usefulness of the information contained in this report, or that the use of any information, apparatus, method, or process disclosed in this report may not infringe privately owned rights; or
- B.) Assumes any liabilities with respect to the use of, or for damages resulting from the use of any information, apparatus, method or process disclosed in this report.

As used above, "person acting on behalf of NASA" includes any employee or contractor of NASA, or employee of such contractor, to the extent that such employee or contractor of NASA, or employee of such contractor prepares, disseminates, or provides access to, any information pursuant to his employment or contract with NASA, or his employment with such contractor.

Requests for copies of this report should be referred to
National Aeronautics and Space Administration
Office of Scientific and Technical Information
Attention: AFSS-A
Washington, D.C. 20546

WASHINGTON

NASA CR-54353
GA-6117

SUMMARY REPORT

THE EFFECT OF HIGH PRESSURES ON
THE CONDUCTIVITY OF VAPORS

by

S. W. Kurnick and J. F. Colwell

prepared for

NATIONAL AERONAUTICS AND SPACE ADMINISTRATION

May 28, 1965

CONTRACT NAS 3-4119

Technical Management
NASA Lewis Research Center
Cleveland, Ohio
Space Electric Power Office
N. J. Stevens

General Atomic Division of General Dynamics
Corporation, Box 608, San Diego, California

FOREWORD

This summary report was prepared by the General Atomic Division of General Dynamics Corporation, San Diego, California, on NASA Contract NAS3-4119, "The Effect of High Pressure on the Conductivity of Vapors". Work was performed during the period of January 22, 1964 through January 21, 1965 under the technical direction of Dr. S. W. Kurnick, the General Atomic Principal Investigator for this program.

The NASA Technical Monitor for this contract was Mr. N. J. Stevens. The contractors report number is GA-6117 and its project number is 401. This report completes the requirements of this contract.

THE EFFECT OF HIGH PRESSURES ON
THE CONDUCTIVITY OF VAPORS

by

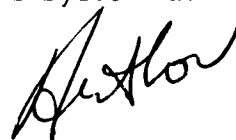
S. W. Kurnick and J. F. Colwell

ABSTRACT

27297

Studies were conducted to determine whether increasing the density of metallic vapors would cause them to exhibit electrical conductivity. Theories based on a one-electron model indicate that metals having low ionization potentials (i. e. , the alkali metals) should have the highest conductivity. Calculations indicated that the conductivity of Hg:Cs alloys should be high enough to be of interest. Theories based on a many-body model also indicated that Hg:Cs alloys should be a good candidate.

Experiments in a high pressure autoclave were conducted on pure Hg vapor at pressures up to 735 atm. No conductivity attributable to the vapor was observed, indicating a conductivity $\sigma \leq 10^{-2} \Omega/\text{m}$. Measurements on 95% Hg:5% Cs were made at temperatures up to 1460°C and at pressures up to 965 atm. A decrease in electrical losses was observed and may have been caused by conductivity within the vapor, however, the evidence is not conclusive. Thus, the question of the effect of pressure on the conductivity of the system remains unresolved. However, it does not appear that useful conductivities can be attained in the Hg:Cs system at reasonable pressures (up to 300 atm).



SUMMARY

An experimental and theoretical research program was conducted to investigate the possibility of increasing the electrical conductivity of vapors by increasing the pressure (up to 1000 atm). Qualitative theoretical estimates, using a one-electron conduction band model, showed that the best conductivities would be expected from materials with low ionization energies and high polarizability. The role of electron-electron correlation in causing a sharp transition between insulation and conduction was also studied. If the transition is sharp, it is expected that the transition must be accompanied by a density change. No conclusive evidence for or against this theory was found.

Materials having high vapor pressures were selected for experimentation so that the pressure and temperature range of interest would be applicable. Delays in designing and manufacturing the required high pressure experimental apparatus and in solving certain experimental problems (e. g., heat losses), restricted the number of experimental runs that could be performed in the available time. Experimentation was therefore limited to measurements of Hg, P and 0.95 Hg:0.05 Cs. Results are summarized as follows:

- a. Measurements on P vapor were limited to 700°C and 1250 psi (85 atm). No conductivity ascribable to the sample was detected.
- b. Up to 10,800 psi (735 atm), Hg vapor exhibited no detectible conductivity. Attempts to make measurements at higher pressures were discontinued to permit concentration on the Hg:Cs system during the limited time remaining in the program.
- c. Measurements were made on 0.95 Hg:0.05 Cs up to 1460°C and 965 atm. While an anomalous behavior was observed between 1100°C and 1460°C, no conclusive evidence for appreciable conductivity was established. This anomalous behavior requires further study.

As a result of this program, it is concluded that the Hg:Cs system is most likely to conduct at high pressures. However, confirmation of the theory must await further experimentation.

CONTENTS

	<u>Page</u>
I. INTRODUCTION	1
II. THEORETICAL PROGRAM	3
2.1 Pressure and Density Calculations	5
2.2 Conductivity Calculations	7
2.3 More Elaborate Calculations	30
III. EXPERIMENTAL PROGRAM	35
3.1 Experimental Method	35
3.2 Experimental Apparatus	37
3.3 Experiments with Interim Apparatus	47
3.4 Experiments with the Autoclave	59
IV. CONCLUSIONS	75
V. RECOMMENDATIONS	77
VI. PERSONNEL	79
REFERENCES AND FOOTNOTES	81
APPENDIXES	
I. The Electronic and Thermodynamic Nature of Dense Vapors	83
II. Mathematical Details	113
III. Conversion of Q Measurements to Resistance	117

FIGURES

		<u>Page</u>
1.	Liquid and solid density on the saturated vapor pressure curve of Hg as a function of temperature. The streamers are superheated vapor densities at constant pressure.	8
2.	Vapor pressure of Hg as a function of temperature	9
3.	Vapor pressure for Cs as a function of temperature	10
4.	Effective mass, \bar{m} , of Cs and Hg versus interatomic distance (r). Atomic energy level (E_0) in atomic units, as a parameter	18
5.	Interatomic distance r , as a function of pressure for Hg and Cs	19
6.	Theoretical estimate of the conductivity of pure Cs vapor versus temperature. Also shown is the conductivity due to the Saha mechanism	21
7.	Energy levels of Hg versus atomic distance, r	24
8.	Estimate of the conductivity of pure Hg vapor versus temperature	26
9.	Liquidus curve for Hg-Cs (see Reference 19)	28
10.	Conductivity of 95% Hg:5% Cs as a function of the vapor pressure of Hg	29
11.	The absolute value of the product $P V/r$ versus r , where P/r is the wave function and V/r the potential for a 6s Cs electron	32
12.	Effective mass \bar{m} versus interatomic distance r (in A.U.) showing differences between the two methods of calculation	33
13.	Relative change in dissipative factor ($\Delta R/\omega L_0$) versus $(\omega \sigma \mu_V)^{\frac{1}{2}} a$	36
14.	Arrangement for eliminating end effects in a "capacitance-coupled" resistivity measurement. Thermocouples are located close by for temperature measurements.	38
15.	Resistance of an electrolytic solution in an Alundum tube plotted versus length	39

FIGURES (Cont'd.)

	<u>Page</u>
16. Rupture strength of Lucalox as a function of temperature (see Ref. 26)	40
17. Detailed drawing of high pressure autoclave	42
18. Schematic of pressure control and monitoring system	44
19. High pressure control panel. Items numbered are identified in Figure 18	45
20. Thermocouple and conductivity band locations in the autoclave. Each band is a platinum strip ~ 1.5 cm wide; the distance between their inner edges is 2.0 cm	46
21. Schematic of interim apparatus. Each conductivity band is a Pt strip ~ 1 cm wide and the distance between their inner edges is 2.5 cm	48
22. Measured Q of sample tube with and without Hg vapor as a function of temperature. The pressure at 1100°C was about 290 atm. $\omega = 20$ Mc, $C_o \approx 240$ pF	50
23. Q as function of temperature for 0.13 g of P in a quartz sample tube	52
24. Q as function of temperature for 0.3 g of P in a quartz sample tube	53
25. Q of empty quartz tube from which P has been removed. Interior of tube was open to air.	55
26. Measured $Q(Q_s)$ and computed apparent resistance (R_z) of AgBr as functions of temperature. $\omega = 20$ Mc, $C_o \approx 237$ pF. The equivalent capacitance in series was 10.7 pF.	56
27. Conductivity σ_s of AgBr as a function of temperature compared with that of Teltow. Based on R_z of Figure 26 with a C_3 of 10.7 pF. $\sigma_s = 14/R_s \text{ ohm}^{-1} \text{ cm}^{-1}$	57
28. Modified sample filling system for use with Hg:C s	58
29. Temperature versus time for experiment with Hg vapor	62
30. Sample tube pressure and Q versus time for experiment with Hg	63
31. Q as a function of temperature for pure Hg	64
32. Resistance of powdered alumina	66

FIGURES (Cont'd.)

	<u>Page</u>
33. Q as a function of temperature for 95% Hg:5% Cs	68
34. ΔQ and \bar{Q} as functions of pressure for 95% Hg:5% Cs	70
35. Vapor pressures of pure Hg and 95% Hg:5% Cs as function of temperature	72
36. $(Q_d - Q)/Q_d Q$ versus R/R_3 for various values of $\omega C_3 R_3$	122

INTRODUCTION

This summary report describes the progress achieved during a twelve-month theoretical and experimental research program on the effect of pressures up to about 1000 atm on the electrical conductivity of vapors. This limit was set arbitrarily as the maximum pressure of interest. If proven valid, the concept had possible application for MHD generators.

The electrical nature of matter at densities between one and ten per cent of that of normal solid or liquid metals is a problem of great importance. On the basic side, it is of the essence of a "many-body" system where electron correlations play an important role in determining both the equilibrium and transport properties. An increasing amount of theoretical attention is currently being devoted to this subject.⁽¹⁻³⁾ However, because of the extreme temperatures and moderately high pressures, little experimental work has been conducted in this field.^(4, 5)

Technologically, the possibility of achieving essentially metallic conductivity at fractional densities of solids or liquids is of great potential importance, both in MHD and thermoelectric systems.

Theoretically, the possible increase of conductivity at high pressure is explainable in terms of overlapping discrete energy levels. An increase in pressure decreases the interatomic distance until the wave functions of the valence electrons overlap, with a resultant broadening of the atomic levels into a conduction band. The theories of solid-state physics have long postulated that a sharp increase in electrical conductivity occurs when this conduction band occurs. It is conceivable that under high pressure, an atom with the proper electron configuration might be brought close enough to its neighbor for this to happen. Before the start of the program, it was estimated that the required pressure would be of the order of several hundred atmospheres.

The theoretical aspect of this program had as its ultimate purpose the establishment of the relation between electrical conductivity and density. The experimental part was to provide measurements of the electrical conductivity of vapors of choice at moderate temperatures ($\leq 1600^{\circ}\text{C}$) and at pressures up to 1000 atm. The measurement of other properties, such as the optical properties, were to be postponed until such an augmented conductivity was experimentally established.

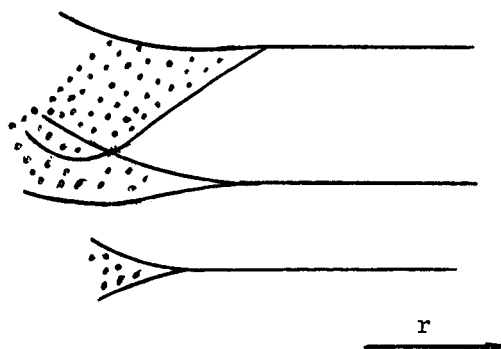
The theoretical background for this program is discussed in Section II. The experimental program is described in Section III. Section IV and V contain conclusions and recommendations for future work while the personnel who contribute to this program are listed in Section VI.

II

THEORETICAL PROGRAM

From the theoretical point of view, the problem can be reduced to its essence by imagining that the atoms are fixed on lattice points with nearest neighbor distances r . The question is, what happens to the electrical conductivity as r is varied from very large to very small values? One knows the answer for two regions of the curve; if r is very large, there can be no interaction between the atoms (in particular, no transfer of charge through the lattice) and the system is a non-conducting vapor. If r has the value normally encountered in liquids or solids, then (if one starts with atoms that are known to be metallic) the conductivity will be quite high. Thus the question becomes, at what r does conductivity become apparent and how rapidly does the conductivity rise as r is made even smaller?

Although there is much question as to the specific details, the general behavior is believed to be well known. As shown in the sketch, the sharp atomic energy levels broaden into energy bands. The width of these bands is related to the effective mass of the electrons, which determine the acceleration in response to an external field. In other words, the effective mass will determine the conductivity. It might be mentioned that the formation of energy bands is an effect that is analogous to the lowering of the ionization energy in a plasma as found by Ecker and Kröll.⁽⁶⁾ The mechanism is somewhat different, however. In a plasma, the interaction between an atom and the microfields of the charged particles lowers the ionization energy. In a dense vapor (or a liquid or solid) it is the interactions between the neutral atoms themselves that change the energy levels.



At this point, we digress to discuss the applicability of the calculations to the experiment. Obviously, the atoms in a vapor are not fixed on regular lattice points. Nonetheless, the fiction of a regular lattice is such a computational convenience that one is loath to relinquish it. Rather, one imagines that the gross features of the conductivity do not depend on the detailed atomic positions but on the mean density. Thus, it is convenient to do the calculation for a given lattice position and then, at some point in the computation, to take an ensemble average over the atomic positions. This average would hopefully not change the value of the conductivity by a large amount. In fact, the average was not carried out in this work, and only a rough estimate of the conductivity was obtained.

One further point should be raised. In principle, the conduction bands, as envisioned here, would be formed even at zero degrees Kelvin and would require no thermal activation. The experiments were carried out at high temperature, however, so that Saha ionization and the consequent transport of free electrons may also occur. This effect has been estimated and found to be small for the pressures and temperatures of interest here, at least for the cases of mercury and the alloy of mercury-cesium investigated.

The theoretical work is described in two separate parts. The first, and shorter, is concerned with calculating the vapor pressure and density of pure Hg and Cs using van der Waals' law. The second part is concerned with calculating the conductivity as a function of the density. Both parts may be regarded as providing a guide for the design of the experiment, and, in addition, information from the density calculation is needed to make the conductivity estimates.

In addition to these two parts, Appendix I contains a discussion of the role played by electron-electron correlations in the problem of the onset of conductivity. This Appendix also contains a thermodynamical analysis of the nature of the insulating-conducting transition. This analysis shows that the insulating-conducting transition will be accompanied by a density transition; i. e., the transition will be similar to an ordinary phase transition and a conducting gas does not exist. If these conclusions are correct, they bode ill for this program. It is possible, however, that the analysis is based on an oversimplified model which in no case would predict the existence of a critical point. Further, Birch's⁽⁵⁾ data appear to show that conducting gases do exist. For these reasons, it became even more interesting to carry out the experiments to see what behavior is actually observed.

In general, for the vapor of a material to be a good conductor, it must have a low ionization energy and high polarizability. Furthermore, there is the experimentally desirable condition that the vapor pressure be

in a range such that the pressure-temperature region of interest remains accessible. These requirements limit the metals to be considered to Hg and the alkalis (preferably Cs). The explicit calculations made in the theoretical program were limited to these two metals. No actual calculations were attempted for the non-metals, but certain qualitative considerations described in the experimental section indicated that phosphorous should be promising.

2.1 Pressure and Density Calculations

Data on the vapor pressure as a function of temperature was required to permit the design conditions of the autoclave to be calculated. The interatomic distance as a function of temperature, required for theoretical calculations of conductivity, may be derived from the vapor density provided by these pressure and density calculations.

The required data on pressure, density and temperature of mercury and other vapors in the elevated pressure and temperature region could be taken from the literature^(7, 8); unfortunately, an ideal gas is assumed as the basis of these tabulations. It seemed desirable to use a somewhat more realistic equation of state, so some computations were programmed for the IBM-7044 for van der Waals' equation,

$$\left(p + \frac{a}{v^2}\right) (v - b) = RT \quad (1)$$

which is fairly successful in describing gas behavior near and above the critical temperature. It was further felt that data derived from this equation would be useful in calculating the dynamics of a gas in an experimental apparatus when applied pressure or temperature is changed.

For Hg, the constants

$$a = 8.093 \frac{\text{liter}^2 \text{ atm}}{\text{mole}^2}, \text{ and}$$

$$b = 0.01696 \frac{\text{liter}}{\text{mole}},$$

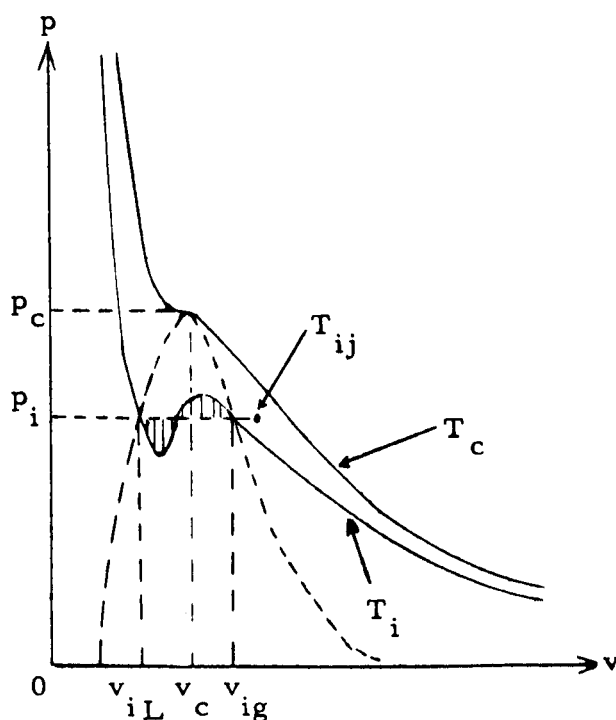
were taken from the Handbook of Chemistry and Physics, with the universal gas constant, $R = 0.08206 \text{ liter atm/mole-}^\circ\text{K}$ in these units. Since the critical values are related⁽⁹⁾ to a and b by

$$P_c = \frac{a}{27b^2}, \quad v_c = 3b, \quad T_c = \frac{8a}{27Rb}, \quad (2)$$

this choice of a and b leads to $p_c \approx 1040$ atm, $T_c \approx 1450^\circ\text{C}$, and, calling A the atomic mass, the density ρ is

$$\rho = \frac{A \times 10^{-3}}{v_c} \approx \frac{4g}{\text{cm}^3}$$

As is well known, below T_c , the isotherms of van der Waals' equation (plotted in the $p - v$ plane) have an oscillation which does not correspond to thermodynamic equilibrium. The latter is obtained by drawing a horizontal isobar at a pressure which intersects the isotherm, T_i , at three points in such a way that the two areas defined between the isobar and the isotherm, (with one area below the isobar, the other above), are equal (see sketch). The two extreme intersection points correspond to the liquid and gaseous specific volumes, respectively. The pressure p_i defining the isobar is the saturation pressure, and the line between the extreme points of intersection gives the $p-v$ curve at T_i in the liquid-gas mixed phase. The region under the dashed curve represents this mixed phase, the region to its left and to the left of the T_c isotherm indicates the liquid phase, and the region to its right and below the T_c isotherm represents the gas phase. To the right of the T_c isotherm only one phase is defined.



In the computer program, T_i ranged over values from 450°C to T_c , and for each isotherm, the saturation pressure, p_i , and the liquid and gas densities, ρ_{iL} and ρ_{iG} , were computed from van der Waals' equation. For each saturation pressure p_i , gas density values were also computed for the superheated vapor at temperature T_{ij} up to 200° above T_i . Finally, the derivatives $(\partial\rho_g/\partial T_p)_p$ and $(\partial\rho_g/\partial p)_T$, which are useful for computations of the dynamics of the experiment, were evaluated over the pertinent range.

Similar computations were also made for the alkali metals, where no reliable critical data are available. Here $T_c = 2500^\circ\text{K}$ and $p_c = 300 \text{ atm}$ were assumed,* leading to van der Waals' constants

$$a = 59.18 \frac{\text{liter}^2 \text{ atm}}{\text{mole}^2}, \text{ and}$$

$$b = 0.08548 \frac{\text{liter}}{\text{mole}}.$$

It would be fortuitous if these values gave more than a qualitative picture of the vapor behavior of one of the alkalis, let alone of all of them from Li to Cs.

Figure 1 shows the density-temperature relationship at saturation for mercury. The streamers are isobars for vapor heated above the saturation temperature. Figures 2 and 3 gives pressure versus temperature for Hg and Cs.

2.2 Conductivity Calculation

2.2.1 Outline of method

The problem of calculating the conductivity of a collection of atoms is not inordinately complicated provided the energy levels for the electrons are adequately given by a band structure that can be calculated from a one-electron theory.⁽¹⁰⁾ The procedure is first, to find the energy levels (or rather the effective mass of the electrons which is known once the energy levels are found), and then to derive the coupling between the electrons and the ion density fluctuations that scatter the electrons from one state to another (in a solid, these are phonons) and, finally, to find the conductivity by averaging over all filled energy levels. We have, in fact, adopted this procedure here, using suitable approximations at various steps to permit rapid estimates to be made on a variety of materials.

* See page 143 of Ref. 8.

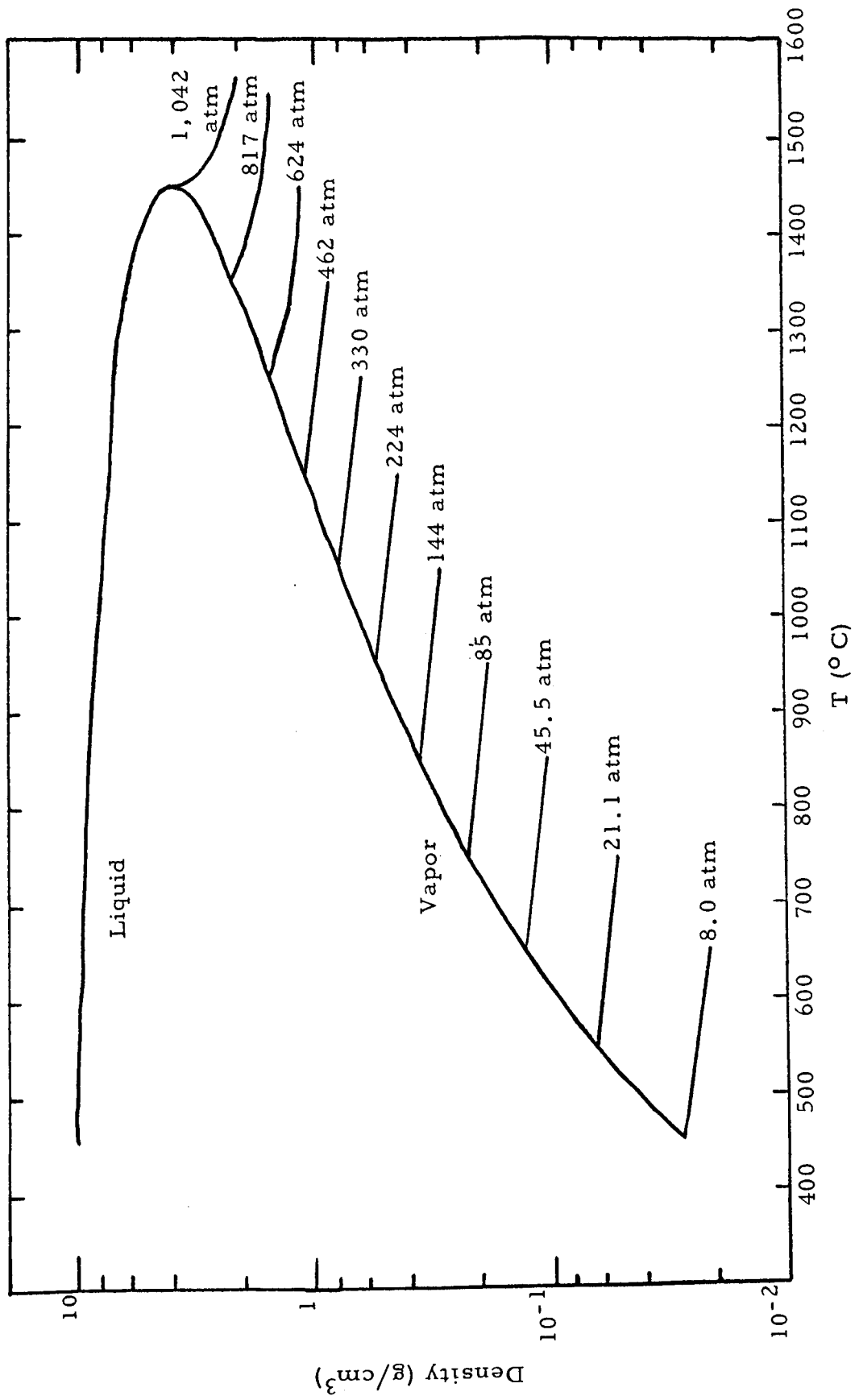


Fig. 1--Liquid and solid density on the saturated vapor pressure curve of Hg as a function of temperature. The streamers are superheated vapor densities at constant pressure.

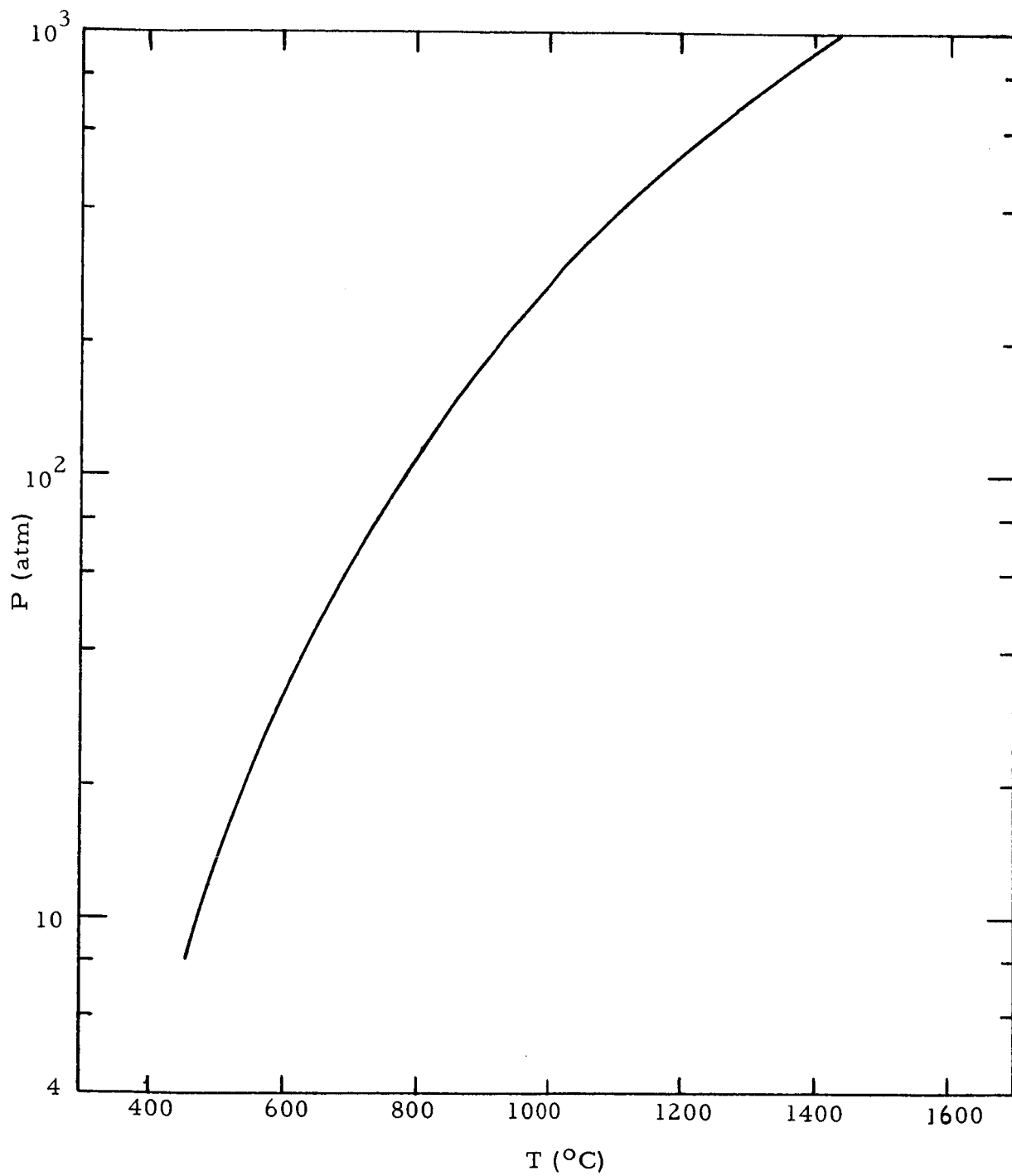


Fig. 2--Vapor pressure of Hg as a function of temperature

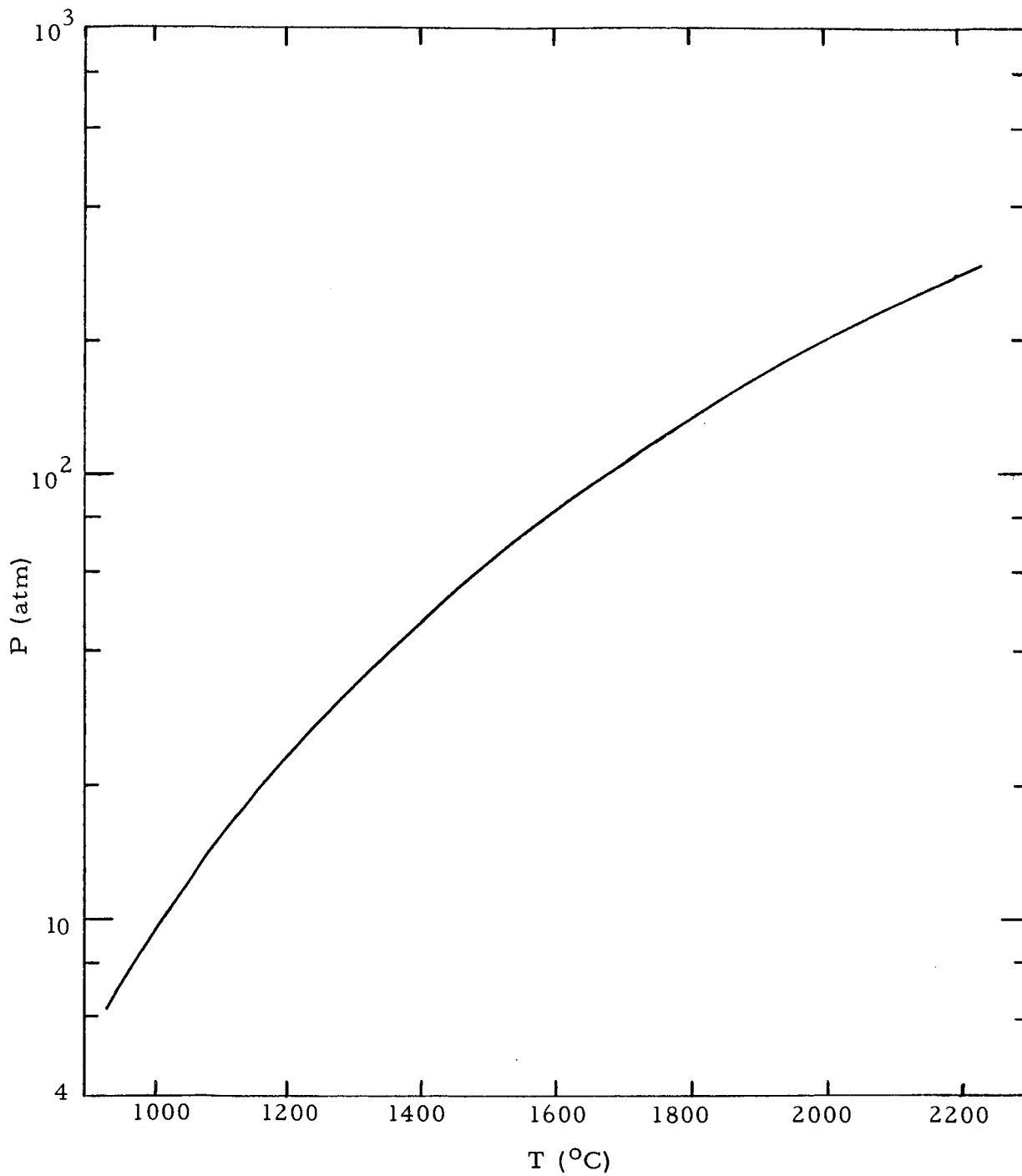


Fig. 3--Vapor pressure for Cs as a function of temperature

According to many physicists^(11, 12) the role of electron correlations is such as to prevent the continuous formation of bands as the density is continuously increased. Instead, there will be no formation of bands until the density is greater than some critical value. Thus the procedure outlined above is incorrect in principle. Whether such a critical density does exist at the elevated temperatures of concern here is by no means an established fact experimentally. In fact, from the point of view of the final effect, there may be little difference between the one-electron theory and a more complete many-body theory that takes into account the electron correlations. The reason is that the one-electron calculation, while in principle continuous, actually predicts a very rapid change in conductivity with pressure so that it may be difficult experimentally to determine whether the actual onset is discontinuous or merely a very strong function of pressure.

The above discussion about the conductivity does not take into account the possible implications regarding density changes that may accompany the conduction changes. This is discussed in Appendix I, where it is assumed that there are two distinct states, the conducting or metallic state and the insulating state, and that one knows, qualitatively, how the free energy of these two states varies with density. It is then shown that a transition to a metallic state of intermediate densities is thermodynamically unstable: the material is either a metal with a large density or an insulator with a small density.

In spite of the above objections, it remains an experimental fact that none of the points have been verified in any detail; on the other hand, the one-electron picture has worked fairly well for solid and liquid metals. For this reason, it was felt to be useful to use the simple picture to obtain estimates of the conductivity. Even though these estimates are not based on a solid formal foundation, it was hoped that they would be accurate enough to provide some guide in planning experiments and would be of some use in interpreting any data that were found. Unfortunately, in view of the somewhat ambiguous nature of the data collected, the second function was utilized in only a cursory fashion and it is not really known how well the first function was performed.

The calculations outlined in this section will now be done. First, the formal expression for the effective mass will be derived and a very simple expression for this mass will be found and is expected to be qualitatively correct. This simple expression is not expected to be very accurate for large densities but it is designed to be useful for surveying qualitatively the behavior of different metals in the small density limit. This simple expression is then used to estimate the conductivity for Hg, Cs, and Hg:Cs alloys. Finally, a more detailed calculation that might be carried out for a metal with one valence electron is indicated for Cs at small densities.

We have not been bold enough to try to make any predictions for substances (such as P) which in the normal liquid state are either insulators or semiconductors. This is not because we do not think these substances may become conductors; it is merely because the simple theory developed here ignores any formation of chemical bonds which, in fact, must actually form in insulators or semiconductors.

2.2.2 Formal calculation of effective mass

We shall use a model due to Knight and Peterson⁽¹³⁾ which gives the energy of an interacting system of atoms in terms of a sum over the reciprocal lattice space (this model was developed for the case where the atoms are located on a given lattice). It will be more convenient for our work to transform this into a sum in coordinate space because the reciprocal lattice vector has a magnitude $1/r$ (where r is the separation distance) and a sum in this space may be expected to converge very slowly if r is large. A sum over r itself should be rapidly convergent. We also prefer to work in coordinate space since the dense vapor is not, of course, a perfect solid, so that we must take an ensemble average over the position of the particles. This is most easily done in coordinate space rather than in the reciprocal lattice space.

The dispersion relation giving the energy, written in atomic units (1 A.U. of length $\approx 0.53 \text{ \AA}$, and 1 A.U. of energy $\approx 13.5 \text{ eV}$), as derived by Knight and Peterson⁽¹³⁾ (their Eq. 18), is

$$1 = \left(\frac{1}{\Omega}\right) \sum_{\vec{b}} \frac{|\tilde{v}(\vec{k} + \vec{b})|^2}{(\vec{k} + \vec{b})^2 + E_k}, \quad (3)$$

where Ω is the volume of a unit cell, \vec{b} is a reciprocal lattice vector, and \tilde{v} is the Fourier transform of a "pseudo-potential" to be discussed later. We have used $+E_k$ for the electron energy rather than their more conventional $-E_k$; the conventional E_k is a negative number since we are dealing with bound states. To carry out the transformation to coordinate space we define the summand of Eq. (3) as $\tilde{f}(\vec{k} + \vec{b})$. It has a Fourier transform which we call $f(r)$;

$$f(r) = \frac{1}{(2\pi)^3} \int d^3q \frac{|\tilde{v}(q)|^2}{q^2 + E_k} e^{-iq \cdot r}, \quad (4)$$

so that we can write

$$\tilde{f}(\vec{b} + \vec{k}) = \int d^3r f(r) e^{i\vec{b} \cdot r} e^{i\vec{k} \cdot r}. \quad (5)$$

The actual rather complicated mechanics of finding $f(\mathbf{r})$ will be discussed in later sections.

To carry out the sum over \mathbf{b} , we expand $\vec{\mathbf{b}}$ in terms of the reciprocal lattice basis vector $\vec{\mathbf{b}}_i$ and $\vec{\mathbf{r}}$ in terms of the lattice vectors $\vec{\mathbf{a}}_i$:

$$\vec{\mathbf{b}} = 2\pi \sum_i n_i \vec{\mathbf{b}}_i, \quad \mathbf{r} = \sum_i x_i \vec{\mathbf{a}}_i / |\mathbf{a}_i| \quad (6)$$

with

$$\mathbf{b}_i \cdot \mathbf{a}_j = \delta_{ij}, \quad \Omega = \prod_i a_i. \quad (7)$$

The use of Eqs. (5) and (6) in Eq. (3) yields

$$1 + (1/\Omega) \sum_{\vec{\mathbf{b}}} \tilde{f}(\vec{\mathbf{b}} + \vec{\mathbf{k}}) = (1/\Omega) \int d^3 r f(\mathbf{r}) e^{i\mathbf{k} \cdot \mathbf{r}} \prod_i \sum_{|n_i| < N} \exp(2\pi i x_i n_i / a_i) \quad (8)$$

$$1 = (1/\Omega) \int d^3 r f(\mathbf{r}) e^{i\mathbf{k} \cdot \mathbf{r}} \prod_i \frac{\sin(2\pi x_i N/a_i)}{\sin(\pi x_i/a_i)}. \quad (9)$$

The last member of Eq. (9) is familiar from diffraction grating theory; it is of the order N (the number of atoms contained along one edge of the sample, and thus a very large number) whenever the denominator is zero, and is of the order 1 elsewhere. In other words it is well approximated by a delta-function:

$$\frac{\sin(2\pi x_i N/a_i)}{\sin(\pi x_i/a_i)} \approx \sum_n \frac{\sin(2\pi x_i N/a_i)}{\pi (x_i/a_i - n)} \rightarrow a_i \sum_n \delta(x_i - na_i) \quad \text{as } N \rightarrow \infty. \quad (10)$$

The lattice positions are given by

$$\vec{\mathbf{r}} = \sum_i n_i \vec{\mathbf{a}}_i, \quad (11)$$

where the set of n_i 's are all integers. Equations (10) and (11) imply that the factor which occurs in Eq. (9) may be written

$$\prod_i \frac{\sin(2\pi x_i N/a_i)}{\sin(\pi x_i/a_i)} = \Omega \sum_{\vec{\mathbf{l}}} \delta(\vec{\mathbf{r}} - \vec{\mathbf{l}}). \quad (12)$$

Now insert Eq. (12) in Eq. (9) to find

$$1 = \sum_{\vec{\ell}} f(\vec{\ell}) e^{i\vec{k} \cdot \vec{\ell}} \quad (13)$$

Equation (13) is the desired dispersion relation for the energy $E_{\vec{k}}$. The expression, $f(\vec{\ell})$, as defined by Eq. (4), must be varied by varying $E_{\vec{k}}$, until Eq. (13) is satisfied. This value of $E_{\vec{k}}$ is the correct eigenvalue.

The effective mass tensor, which we actually need, is defined by

$$\frac{\vec{1}}{m^*} = - \vec{\nabla}_{\vec{k}} \vec{\nabla}_{\vec{k}} E_{\vec{k}} \quad (14)$$

If the gradient in \vec{k} is applied twice to Eq. (13), one obtains

$$0 = \sum_{\vec{\ell}} \left(\frac{\partial^2 f}{\partial E_{\vec{k}}^2} \vec{\nabla}_{\vec{k}} E_{\vec{k}} \vec{\nabla}_{\vec{k}} E_{\vec{k}} + \frac{\partial f}{\partial E_{\vec{k}}} \vec{\nabla}_{\vec{k}} \vec{\nabla}_{\vec{k}} E_{\vec{k}} + 2i \vec{\ell} \vec{\nabla}_{\vec{k}} E_{\vec{k}} f - \vec{\ell} \vec{\ell} \right) e^{i\vec{k} \cdot \vec{\ell}} \quad (15)$$

One usually wants the effective mass at an extremum in the energy band, at which point the derivative of E is 0; for these cases, Eq. (15) reduces to

$$\frac{\vec{1}}{m^*} = \frac{- \sum_{\vec{\ell}} e^{i\vec{k} \cdot \vec{\ell}} \vec{\ell} \vec{\ell} f(\vec{\ell})}{\sum_{\vec{\ell}} \frac{\partial f}{\partial E_{\vec{k}}} e^{i\vec{k} \cdot \vec{\ell}}} \quad (16)$$

Finally, we shall be content with an average effective mass, which we define as \bar{m} . It is the average over the diagonal elements of Eq. (16),

$$\frac{1}{\bar{m}} = 1/3 \frac{- \sum_{\vec{\ell}} \ell^2 f(\vec{\ell}) e^{i\vec{k} \cdot \vec{\ell}}}{\sum_{\vec{\ell}} \frac{\partial f}{\partial E_{\vec{k}}} e^{i\vec{k} \cdot \vec{\ell}}} \quad (17)$$

2.2.3 Approximate effective mass

Before proceeding with a general calculation, we shall develop an approximation which is probably not too far wrong and which is very useful for obtaining quick estimates. Recall that $\tilde{v}(q)$ is the Fourier transform of a pseudo-potential occurring in the Knight-Peterson model. Since the atom has a certain size, $\tilde{v}(q)$ must approach zero as q approaches infinity because of the general principle that the product of the uncertainty in the position times the uncertainty in the momentum is fixed. The approximation consists of assuming that $\tilde{v}(q)$ is very small for q greater than some q_0 , and that this q_0 is much less than the square-root of the energies involved. If this is the case, then Eq. (4) reduces to

$$f(\vec{\ell}) = \frac{1}{E_k (2\pi)^3} \int d^3 q |\tilde{v}(q)|^2 e^{i\vec{q} \cdot \vec{\ell}} . \quad (18)$$

But, according to Fourier transform theory, this is merely the convolution of the Fourier transform of $\tilde{v}(q)$; which is $v(\vec{\ell})$, the pseudo-potential itself:

$$f(\vec{\ell}) = \frac{1}{E_k} \int d^3 r v(\vec{r}) v(\vec{r} - \vec{\ell}) . \quad (19)$$

Equation (19) is a very physical result since it says that the broadening in energy levels and the effective masses calculated above are due to a function which depends on the overlap between various atoms. That is, if the atoms are very localized in space and very far apart, then there will be no interactions and all energy levels must reduce to the free atomic states. This may be expressed more formally by letting R go to infinity in Eq. (13) so that only the term with $l = 0$ in the sum remains,

$$1 = \frac{1}{E_k} \int d^3 r v^2(\vec{r}) . \quad (20)$$

Since Equation (20) is independent of k , the solution is

$$E_k = E_0 = \int d^3 r v^2(\vec{r}) . \quad (20')$$

The fact that the atoms are now isolated and do not interact implies that E_0 is the free atom energy level.

Equation (19) can, in principle, be found for any potential. We shall work it out now for a particular potential which, on one hand, can be done quite simply, and on the other hand represents fairly well the normal state of atoms. Namely, we take

$$v(r) = \frac{\Lambda e^{-\lambda r}}{r}. \quad (21)$$

Equation (20') shows that the strength, A , and the size, λ , must be related to E_0 via

$$E_0 = \frac{2\pi A^2}{\lambda}. \quad (22)$$

The task of actually performing the integration in Eq. (19) is relegated to Appendix II. The result is

$$f(\vec{\ell}) = \frac{E_0}{E_k} e^{-\lambda \ell}. \quad (23)$$

We now insert Eq. (23) into Eq. (13) to obtain the energy

$$E_k = E_0 \left[1 + \sum_{\ell} e^{-\lambda \ell} e^{i\vec{k} \cdot \vec{\ell}} \right]. \quad (24)$$

The effective mass is most easily found by differentiating Eq. (24) directly, rather than by using the more complicated Eq. (17); the result is

$$\frac{1}{\bar{m}} = \frac{E_0}{3} \sum_{\ell} \ell^2 e^{-\lambda \ell} e^{i\vec{k} \cdot \vec{\ell}}. \quad (25)$$

For the initial estimate, we shall take λ from the asymptotic value of the wave functions to be

$$\lambda = \sqrt{E_0}. \quad (26)$$

With this, all parameters in Eq. (25) for the effective mass are known and we can make numerical estimates. For convenience, we do this for $k=0$ (the bottom of the band) and for a simple cubic lattice. This latter state-

ment implies that there are 6 atoms with $l = r$ (r is the interatomic separation), 12 atoms with $l = r\sqrt{2}$, and 8 with $l = r\sqrt{3}$, etc. The results for the Cs s-band and Hg p-band are reproduced in Figure 4 which plots the effective mass versus r . Since the experimental variable is the pressure, we must convert r to density and then, using Figure 1, to pressure. This is done in Figure 5.

2.2.4 Estimation of conductivities

We shall now compute conductivities to be expected on the basis of the preceding estimates. It must be emphasized that the numbers we obtain are very unreliable for several reasons; first, the work in the preceding section was very approximate and designed to give a quick estimate. The second proviso is that the scattering time has not been calculated. We merely estimate it on what is known for other electron systems. The estimates were undertaken in spite of their lack of finality because it was hoped that they would provide some guidance as regards the range of pressures and temperatures which must be reached as well as some guidance as to the most promising materials.

For the conductivity, we take the usual expression

$$\sigma = ne\mu \quad (27)$$

where n is the number of carriers per unit volume, e the electric charge, and μ the mobility. Either simple kinetic theory arguments, or more elaborate calculations, ⁽¹⁴⁾ show that the mobility is of the form

$$\mu = \mu_o (T_o) (T_o/T)(1/\bar{m})^2 \quad (28)$$

for metals, and of the form

$$\mu = \mu_o (T_o)(T_o/T)^{3/2} (1/\bar{m})^{5/2} \quad (29)$$

for semiconductors. The difference between these two expressions is immaterial for our present crude estimate; we take Eq. (28) for definiteness and also because it is somewhat simpler.

By using Eq. (28), Eq. (27) can be rewritten in the form

$$\sigma = \sigma_o (n/n_o)(T_o/T)(1/\bar{m})^2 \quad (30)$$

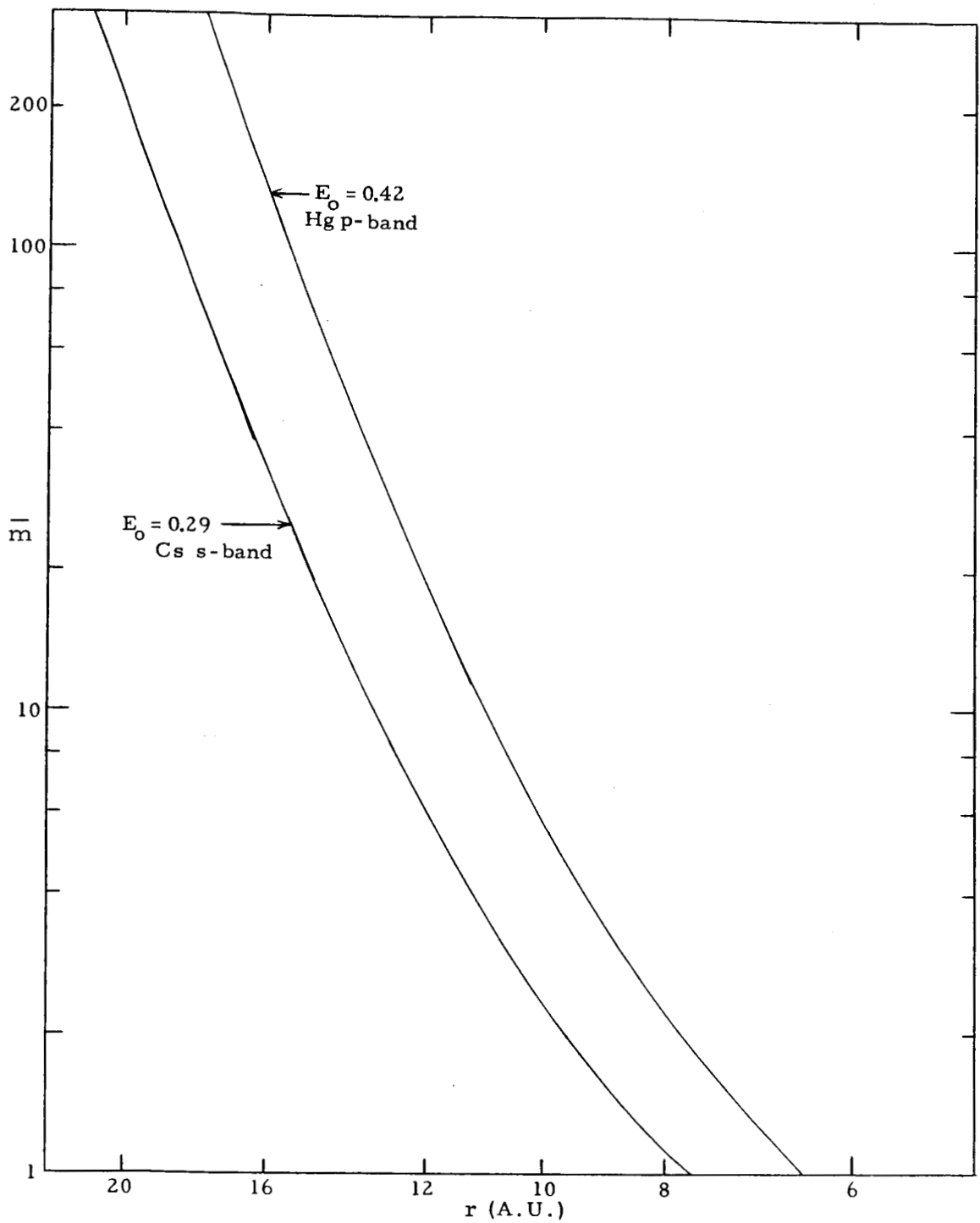


Fig. 4--Effective mass, \bar{m} , of Cs and Hg versus interatomic distance (r). Atomic energy level (E_0) in atomic units, as a parameter

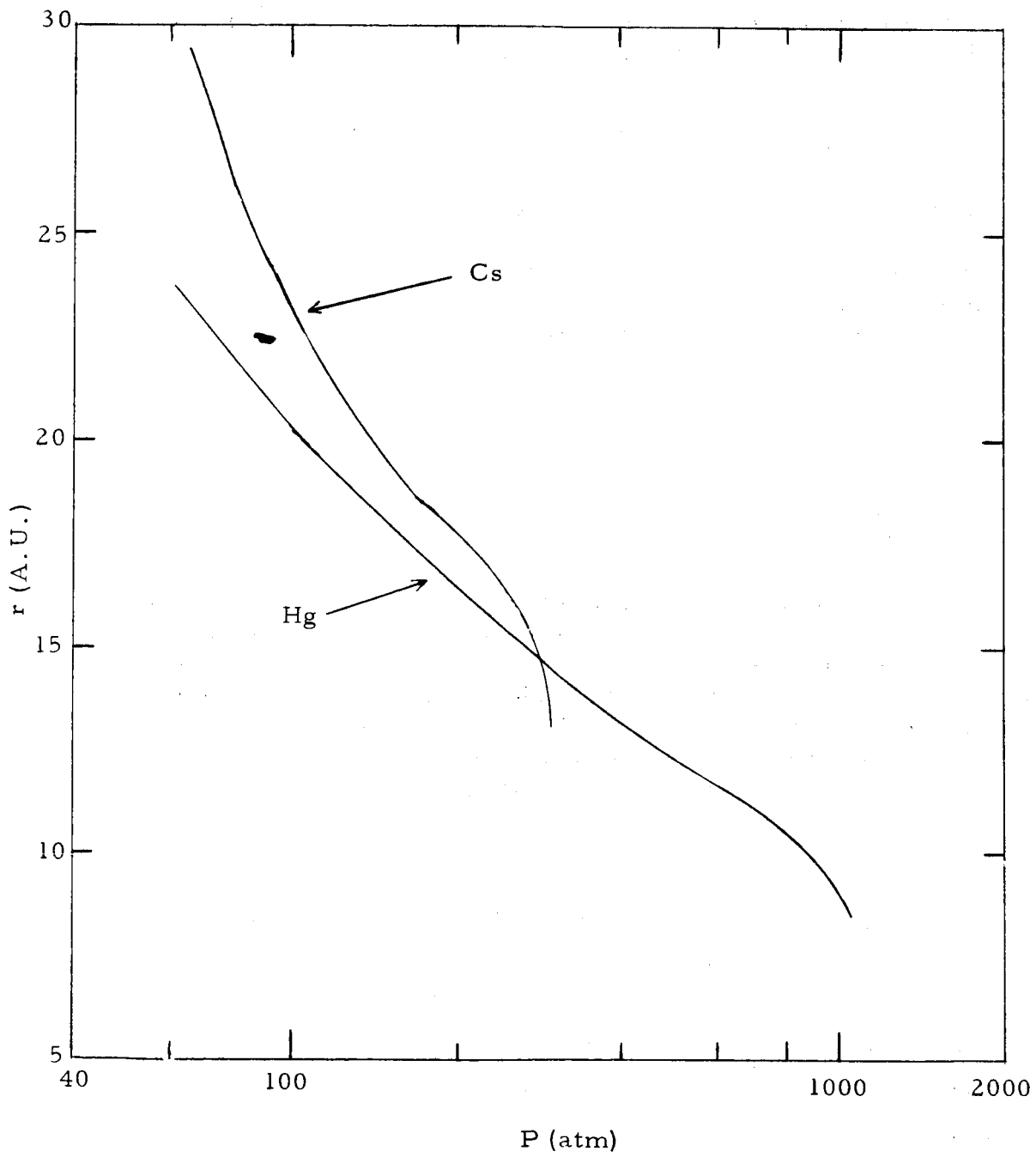


Fig. 5--Interatomic distance r , as a function of pressure for Hg and Cs

where σ_0 is the conductivity at some convenient temperature, T_0 and density, n_0 , and where the effective mass is about 1. We take this state to be the normal liquid.

We shall now discuss some specific materials, starting with Cs. The liquid resistivity, depending on which data is used, ⁽¹⁵⁾ is about 0.36 μ ohm-meter. The density is about 2 g/cm³, so

$$n_0 = 6 \times 10^{23} \times \frac{2}{133} = 0.9 \times 10^{22}/\text{cm}^3.$$

We round this off to 10^{22} for future work.

The conductivity is now estimated as a function of pressure for Cs vapor in equilibrium with the liquid, by first using Figure 5 to find r for a given pressure and then using Figure 4 to find \bar{m} for that r . Finally the density is given by

$$n = r^{-3} \tag{31}$$

where r in Eq. (31) must be in cm. All of the quantities so found are substituted into Eq. (30) to find the conductivity.

The chain of numbers is given in Table I; the result is graphed in Figure 6. This Figure shows that rather large conductivities can be obtained at modest pressures. This is still not an easy experimental regime, as can be seen from Table I, since these pressures correspond to very large liquid temperatures. The temperatures are, in fact, considerably over the rating of the furnace which was used in this research so pure Cs was not explored experimentally.

Table I

EFFECTIVE MASS AND CONDUCTIVITY OF Cs

T (°K)	P (atm)	r (A.U.)	r (cm) ($\times 10^{-7}$)	n/cm ³ ($\times 10^{20}$)	\bar{m}	σ (ohm ⁻¹ /m)
2000	115	22.9	1.21	5.64	$\approx 10^3$	0.025
2100	144	21.2	1.12	7.10	300	0.30
2200	176	19.7	1.04	8.90	160	1.47
2300	213	18.2	.96	11.24	90	5.4
2400	250	16.7	.88	14.54	34	55
2500	300	14.2	.75	23.5	11	690

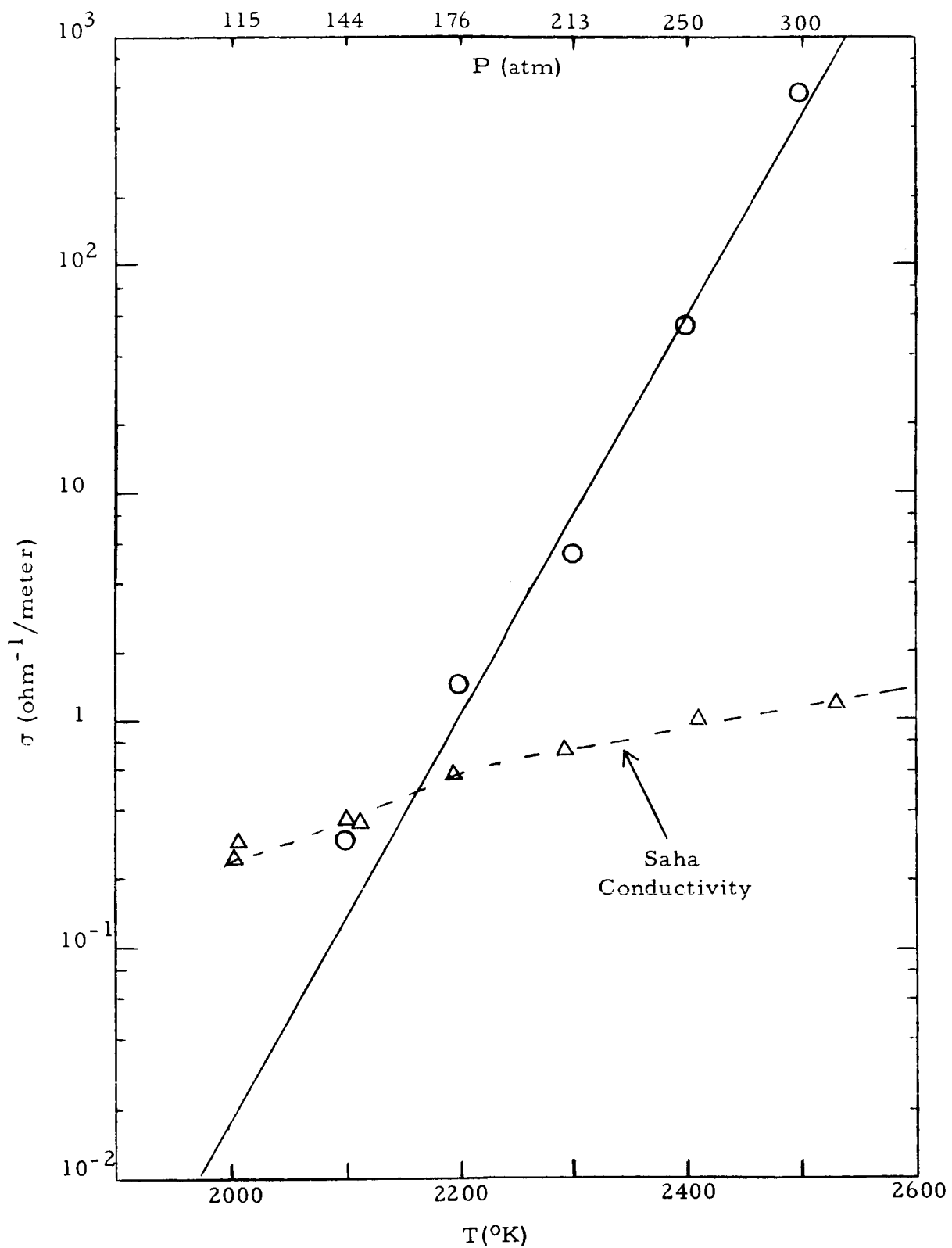


Fig. 6--Theoretical estimate of the conductivity of pure Cs vapor versus temperature. Also shown is the conductivity due to the Saha mechanism

In addition to the formation of bands as envisioned above, ordinary Saha (thermal) ionization of the Cs vapor may occur and a conductivity due to the resulting free electrons will be observed. The number of these free electrons n_i is given by the Saha equation, written here in the approximation of small percentage ionization:

$$n_i^2 = n \left(\frac{2\pi mkT}{h^2} \right)^{3/2} e^{-E/kT} , \quad (32)$$

where

n is the number density of Cs atoms,
 m is the free electron mass,
 h is Planck's constant, and
 E is the Cs ionization energy (3.88 eV).

The ionization energy would actually be expected to be lowered somewhat by the same sort of interactions that form the energy bands and by the fluctuating plasma potentials, as found by Ecker and Kröll.⁶ The effects have been ignored, however, so the Saha conductivity may actually be higher than found here.

The conductivity of a free plasma is

$$\sigma = \frac{n_i e^2}{m n \bar{\nu}} , \quad (33)$$

where e is the electronic charge, and $\bar{\nu}$ is the mean scattering frequency. Following Robinson,⁽¹⁶⁾ we judge that neutral-electron scattering is the most important for the values of n of interest here and thus adopt his value of

$$\bar{\nu} \approx 10^{-6} \text{ (cm}^3/\text{sec)} . \quad (34)$$

The value of σ due to Saha ionization is shown as the dashed line in Figure 6. For the lower temperatures, it is actually greater than that due to band formation. This is perhaps another reason why pure Cs is not a good material in which to search for band formation. The effect will be partially masked by the more common plasma conductivity.

We now turn to Hg, which has a liquid conductivity of about 10^6 ohm⁻¹/m; and a density of about $n = 4 \times 10^{22}$ /cm³. Since the ionization energy of Hg is 10.38 eV, there is negligible Saha ionization and any conductivity must be due to band formation. The processes that occur in Hg may be quite different from those that occur in Cs because the s level in

Hg is filled, indicating that the resulting energy band can be filled. By analogy with solids, conduction can occur in one of three ways:

- a. Metallic conduction in which the next band (originating from the atomic p state) overlaps the s band--(this presumably happens in the liquid),
- b. Intrinsic semiconduction (thermal excitation from the s to the p band), and
- c. Extrinsic semiconduction (in which impurities are deliberately added to contribute their electrons to the p level).

For all conduction processes, one must know the position of the top of the s band and the bottom of the p band. To find the top of the s band, we assume it occurs when

$$\begin{aligned} e^{\vec{k} \cdot \vec{\ell}} &= -1 \text{ for nearest neighbors, and} \\ e^{\vec{k} \cdot \vec{\ell}} &= 1 \text{ for next nearest neighbors.} \end{aligned} \quad (35)$$

Thus, for the p band

$$E_{\text{bottom}} = E_p \left[1 + 6 \exp(-r/\bar{E}_p) + 12 \exp(-r/\sqrt{2}\bar{E}_p) + \dots \right]. \quad (36)$$

For the s band,

$$E_{\text{top}} = E_s \left[1 - 6 \exp(-r/\bar{E}_s) + 12 \exp(-r/\sqrt{2}\bar{E}_s) - \dots \right]. \quad (37)$$

The results are shown in Figure 7. It can be seen at once that metallic conduction (case a) will not be reached until the density approaches that for a normal liquid. In fact, the figure shows the energies crossing at a separation smaller than for the liquid. Equation (22) for the potential is only valid for large r , however, so the model is not expected to give quantitative results for small r .

We now estimate the conductivity for the other two cases listed above. First, we estimate case b, for which there is an equal number of holes and electrons. If they have equal mobilities, the conductivity is

$$\sigma = 2\sigma_0 (n/n_0) (T_0/T) (1/\bar{m})^2. \quad (38)$$

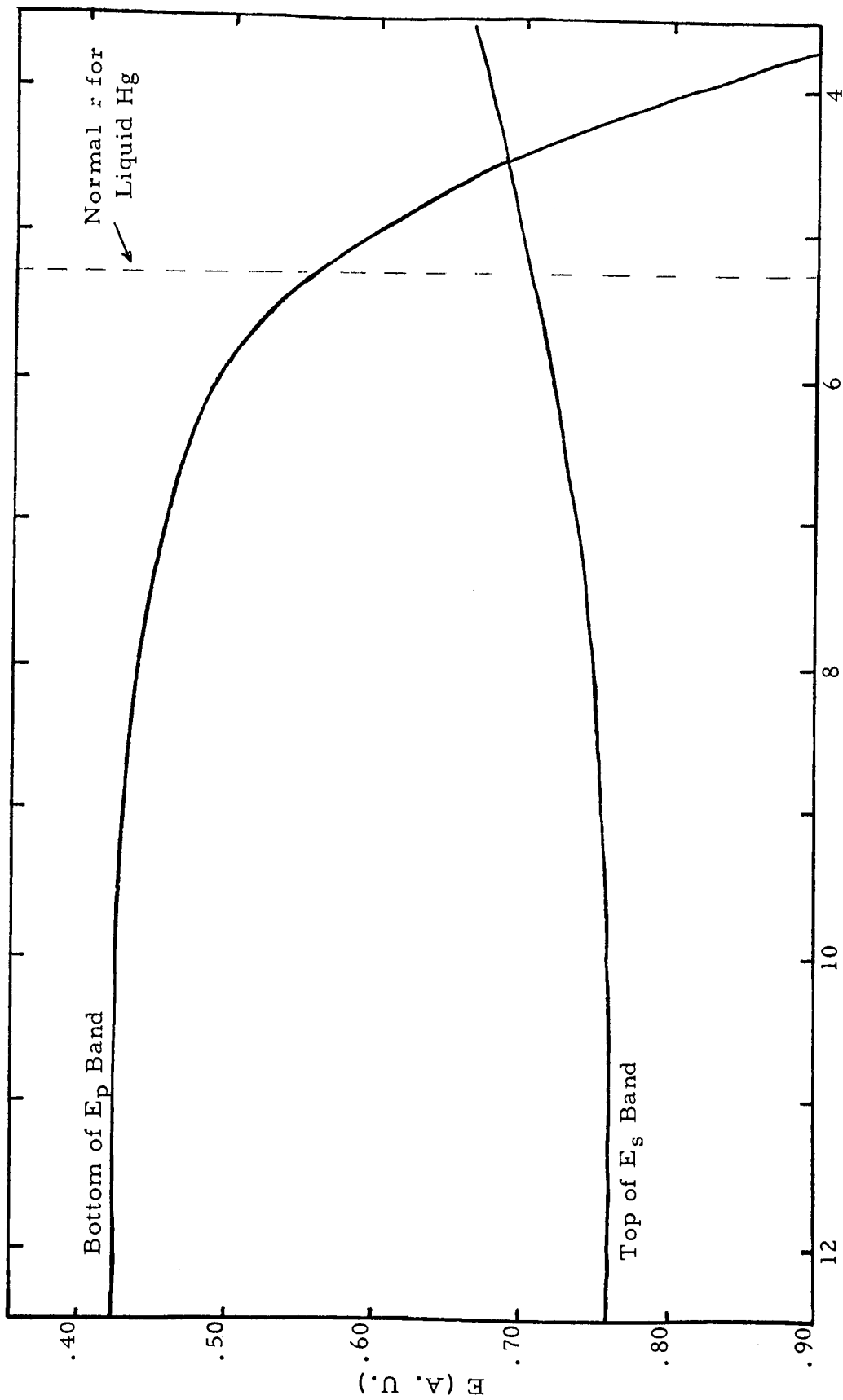


Fig. 7 -- Energy levels of Hg versus atomic distance, r

Now, for an intrinsic semiconductor, ⁽¹⁷⁾

$$n \approx 2 \times 10^{19} (T/T_0)^{3/2} \bar{m}^{-3/2} \exp \left[- \frac{E_s - E_p}{2kT} \right] \quad (39)$$

so

$$\sigma \approx \sigma_0 10^{-2} (T/\bar{m}T_0)^{1/2} \exp \left[- \frac{E_s - E_p}{2kT} \right] \quad (40)$$

We now calculate this, as shown in Table II and plotted in Figure 8, by taking $E_s - E_p$ from Figure 7 and \bar{m} from Figure 4, using the electron (the p state) mass.

Figure 8 shows that for Hg, reasonable conductivities may be reached by 1000 atm (at which point the temperature is 1700°K) which makes it the more reasonable first choice for proof testing. One may even engage in a bit of optimism on this point since Figure 8 may underestimate the conductivity because σ is proportional to $\exp[-(E_s - E_p)/2kT]$ and we know that $E_s - E_p$ is too large in magnitude at $r \approx 5$. We may also hope it is too large for larger r as well.

Table II

EFFECTIVE MASS AND CONDUCTIVITY OF Hg

T (°K)	P (atm)	r (A.U.)	n/cm ³ (× 10 ²⁰)	$\frac{E_s - E_p}{2kT}$	\bar{m}	σ (ohm ⁻¹ /m)
1200	200	16.5	14.8	22.3	130	3.7×10^{-5}
1300	300	14.4	22.0	20.5	70	3.1×10^{-4}
1400	430	13.0	30.6	19.1	25	2.9×10^{-3}
1500	550	11.7	43.0	17.4	14	1.7×10^{-2}
1600	770	10.6	60	16.1	8	8.3×10^{-2}
1700	990	9.4	90	14.8	4	0.44

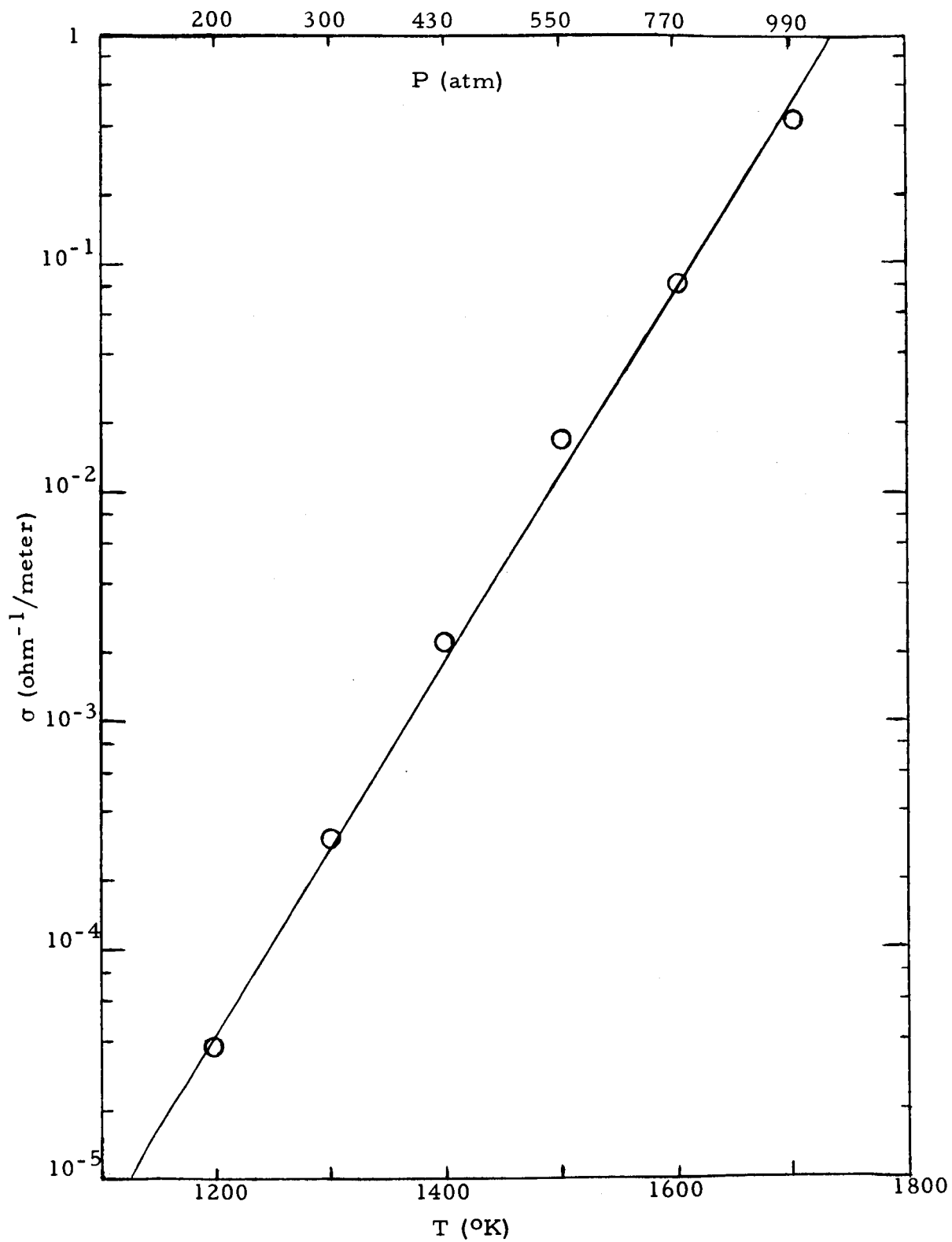


Fig. 8 -- Estimate of the conductivity of pure Hg vapor versus temperature

We now turn to case c mentioned above: using mercury as a doped semiconductor. We shall suppose that the experiment consists of mixing mercury with some other metal and observing the conductivity of the vapor of this alloy. We assume that all the "impurity" atoms in the vapor donate an electron to the p band that is formed by the mercury so the conductivity takes place within the mercury but via electrons from the other species. We shall take cesium as the donor since it has a high vapor pressure and can be expected to contribute the most electrons to the conduction process.

According to Raoult's law, ⁽¹⁸⁾ the number of atoms of species, n_A , in the vapor is related to the percentage, X_A , in the liquid by

$$n_A = X_A n_A^0 \quad (41)$$

where n_A^0 is the number of atoms in the vapor above the pure liquid A. The vapor pressure P_A is similarly given by

$$P_A = X_A P_A^0 \quad (42)$$

where P_A^0 is the vapor pressure of the pure liquid A. It should be mentioned that Raoult's law is known to be inaccurate for many substances. ⁽¹⁸⁾ It is not expected to be invalid by large amounts, however, so it is not unreasonable to use it here.

The procedure used to calculate the conductivity uses Eq. (30), in which n is the number of Cs atoms given by Eq. (41) and \bar{m} is the effective mass of Hg at the pressure given by Eq. (42). Table III shows how the conductivity varies with X_{Cs} if the temperature is held constant. The maximum that is evident in Table III is not hard to understand; the number of electrons increases as X_{Cs} increases, but \bar{m} decreases because the mercury pressure decreases. At some point the decrease in \bar{m} starts to dominate.

The phase diagram for Hg-Cs alloys (see Fig. 9 and Ref. 19) shows that the alloy is a liquid at room temperature only when X_{Cs} is less than about 5 percent. Since the experiment is much easier to perform if the sample is a liquid at room temperature and since Table III does not show large improvements if the Cs concentration is increased above this value, it was decided to perform the experiments with 5 percent Cs. The conductivities estimated for this case are given in Table IV and shown in Figure 10. These conductivities are sufficiently higher than those for pure Hg to warrant an experimental study of this system.

Table III

CONDUCTIVITY OF Hg-Cs ALLOY FOR
VARIOUS Cs CONCENTRATION, T = 1600°K

X_{Cs}	n_{Cs} ($\times 10^{20} \text{ cm}^{-3}$)	P_{Hg} (atm)	σ ohm^{-1}/m
.05	.097	760	.65
.10	.19	720	1.20
.15	.29	680	1.40
.20	.38	640	1.45
.25	.49	600	1.41
.40	.76	480	.91

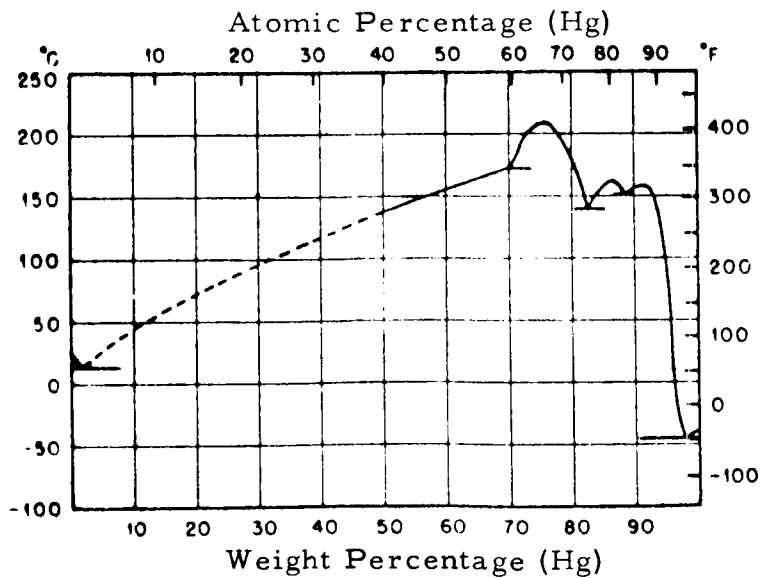


Figure 9---Liquidus curve for Hg-Cs
(see Reference 19)

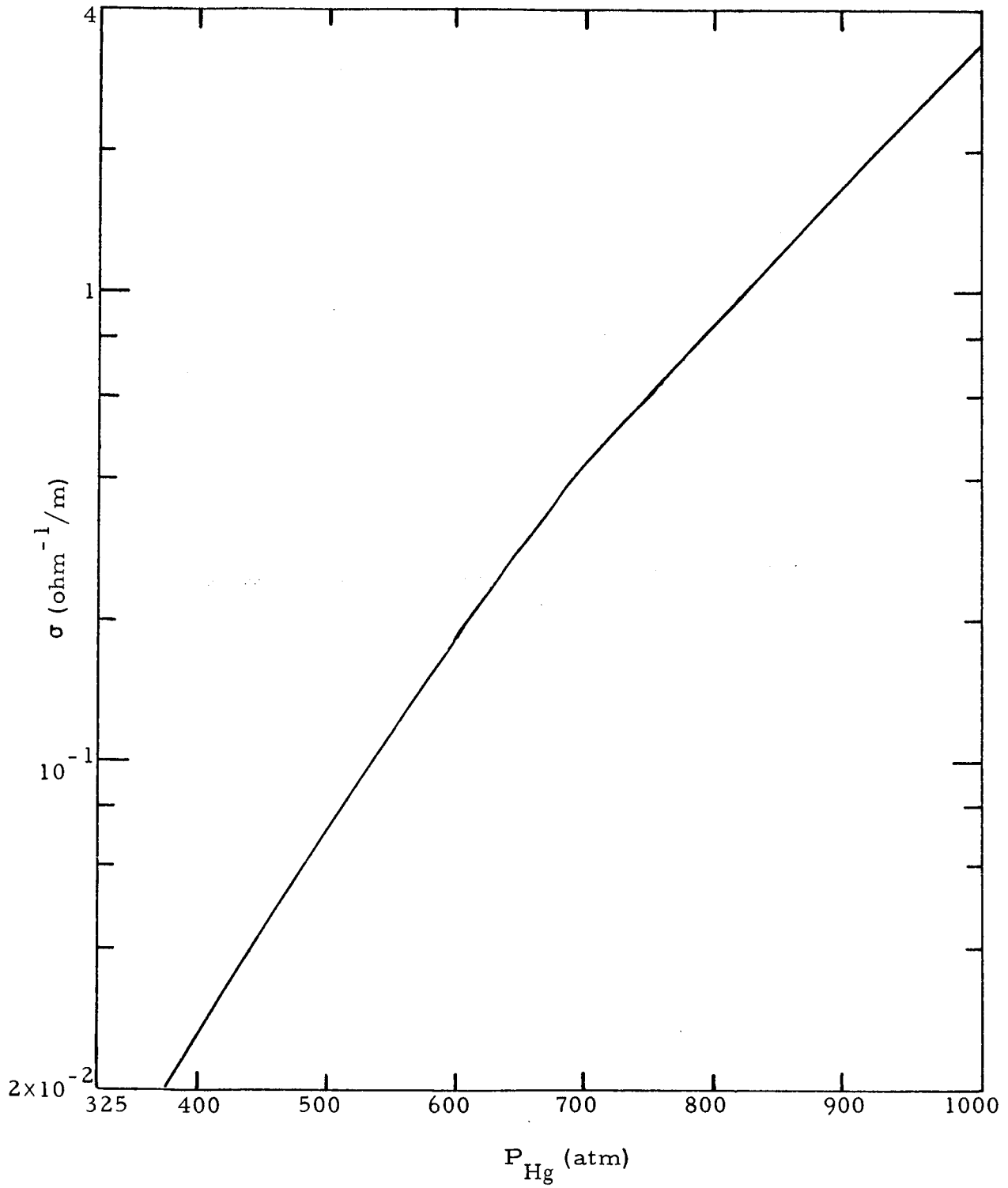


Fig. 10--Conductivity of 95% Hg:5% Cs as a function of the vapor pressure of Hg

Table IV

CONDUCTIVITY OF 0.95 Hg:0.05 Cs AS A
FUNCTION OF PRESSURE

T (°K)	n_{Cs} ($\times 10^{20} \text{ cm}^{-3}$)	P_{Hg} (atm)	σ (band formation) (ohm^{-1}/m)	σ (plasma) (ohm^{-1}/m)
1300	.032	300	.003	7.7×10^{-5}
1400	.046	420	.032	2.3×10^{-4}
1500	.075	570	.187	6.5×10^{-4}
1600	.097	760	.650	1.4×10^{-3}
1700	.110	950	2.40	2.4×10^{-3}

The percent ionization of the Cs atoms at the temperature given in Table IV is rather small. An explicit calculation of the conductivity based on such ionization is also given in Table IV and is seen to be negligible compared to σ brought about by band formation. To compute the conductivity of the Saha contribution, σ (plasma), it was assumed that the main scattering was between an electron and neutral mercury atoms. Since the scattering cross section is expected to scale somewhat as the polarizability, ⁽¹⁶⁾ $\bar{\nu}$ was arbitrarily taken to be one tenth as large as it is for neutral cesium atom scattering.

2.3 More Elaborate Calculations

We shall now outline a method for improving on the potential given by Eq. (21). The pseudo-potential $v(r)$ was introduced into the model we are using⁽¹³⁾ in the following way: the term in Schrödinger's equation, which is of the form of the actual potential times the wave function, was replaced by $v(r)$ times an integral of $v(r)$ times the wave function. For our present purpose, the integral is a disposable normalization that will be used to reproduce the correct atomic level, therefore we omit it in the following. We call the actual potential $V(r)/r$ and the wave function $\Psi(r)$, thus the preceding implies the formula

$$v(r) = V(r)\Psi(r)/r \quad . \quad (43)$$

We use a statistical model⁽²⁰⁾ for $V(r)$, which should be valid for the large atoms we are considering. The wave function is found by integrating Schrödinger's equation numerically, using this same potential.

These numerical wave functions are used to fit $v(r)$ with functions of the form

$$v(r) = A \sum_n B_n (1/r) \exp(-\lambda_n r) \quad . \quad (44)$$

This is done for analytic convenience because it is only relatively tedious to find $f(\ell)$ with no approximations if Eq. (44) is used. If Slater functions⁽²¹⁾ are used, then the analytic work is very tedious. The actual derivation of $f(\ell)$, using Eq. (44), is done in Appendix II.

The form of the pseudo-potential found numerically is shown in Figure 11. Note that it exhibits the exponential decay with large distance as expected but that near the origin it grows to very large values. The value of the pseudo-potential near the origin is not expected to affect the values of the effective mass to any extent so the fit indicated by Eq. (44) has been broken off with the first few terms and no attempt has been made to fit the oscillations at small r . (Parenthetically, it may be remarked that this method could probably be made more accurate, as well as less arbitrary, if a pseudo-potential in the more common sense of the term, as used by Phillips and Kleinman,⁽²²⁾ were used for the potential $V(r)$. If this were done, both $V(r)$ and $v(r)$ would be replaced by functions which, near the origin, are small and vary slowly. This was not done however.)

Because the pseudo-potential has this peak at the origin, the fit was not completely satisfactory. The values of the calculated effective mass depend to some extent on the number of terms used in Eq. (44). By the time this was realized, it had become apparent that Cs would not be measured experimentally, so this phase of the theoretical work was not pursued.

The numbers that were found for the mass, using this second method, are shown in Figure 12, where they are compared with the earlier approximation. It can be seen that the new calculations are far smaller and would predict a conductivity far larger than the one given in Table I. The reason why the new calculation is smaller can be attributed to two factors: the wave function falls off more slowly than had previously been assumed and the more accurate calculation of the overlap integrals, taking into account a correct treatment of the denominator in Eq. (4), brings in factors which tend to lower the value of \bar{m} . The relative amount by which these two effects change \bar{m} can be judged by the third curve in Figure 12 which shows \bar{m} calculated by the first method but using the decay (λ) which is used in the second method.

Which of the three curves in Figure 4 is more nearly the truth is a moot question. Probably the truth lies close to the middle one.

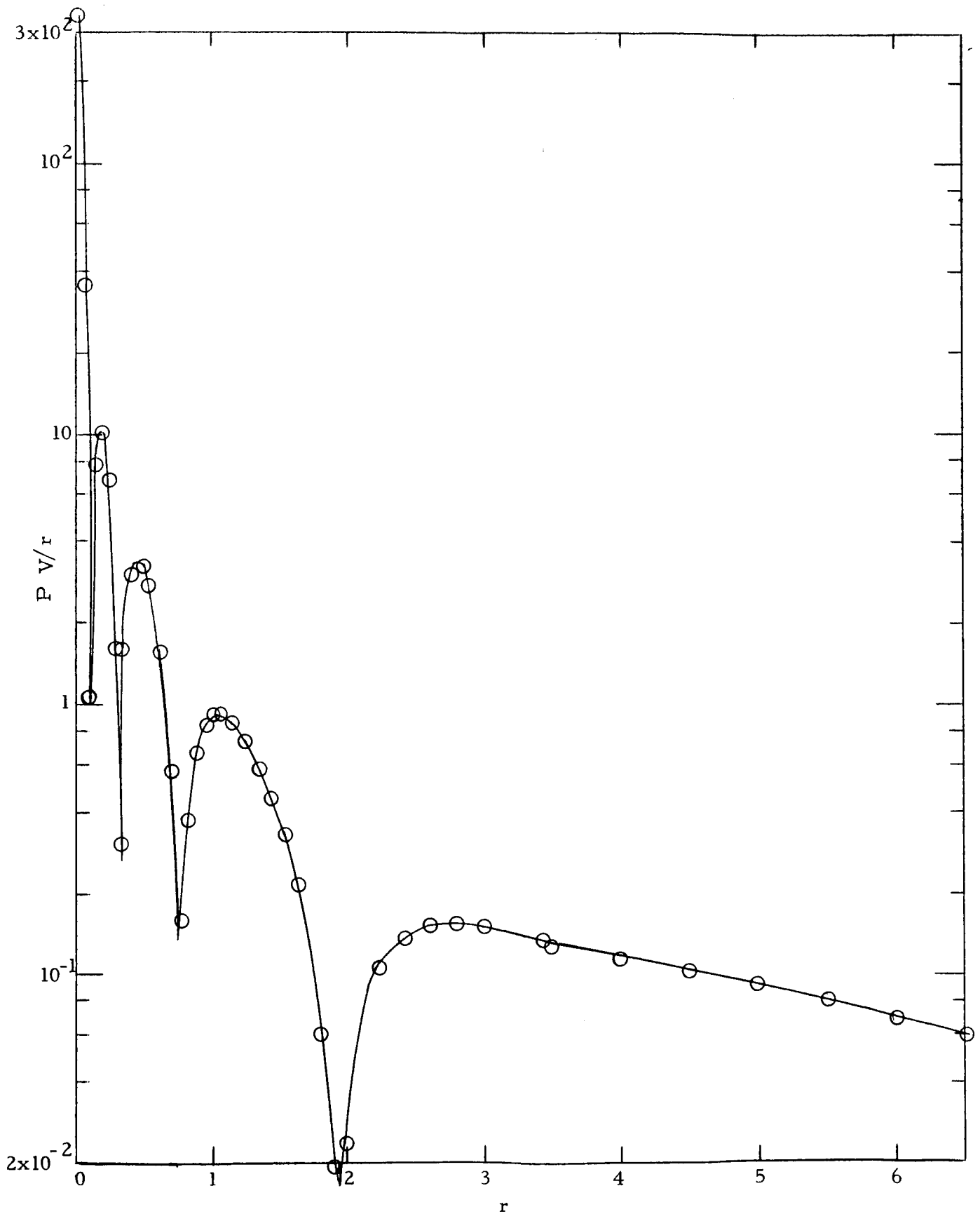


Fig. 11--The absolute value of the product $P V/r$ versus r , where P/r is the wave function and V/r the potential for a 6s Cs electron

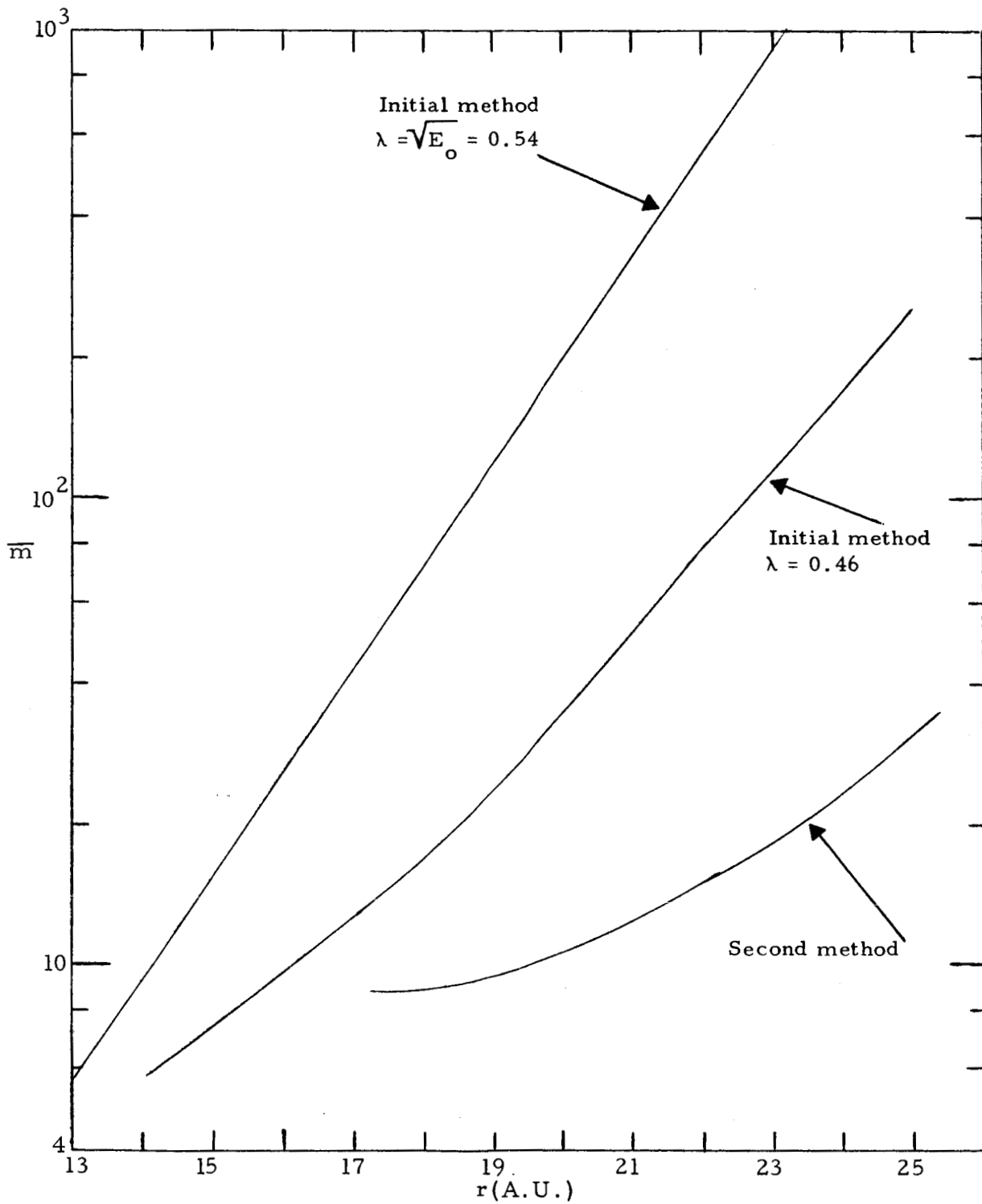


Fig. 12--Effective mass \bar{m} versus interatomic distance r (in A.U.) showing differences between the two methods of calculation

III

EXPERIMENTAL PROGRAM

3.1 Experimental Method

During the first few weeks of this program, various methods of measuring the electrical conductivity of a vapor at temperatures up to 1500°C and pressures up to 1000 atm were considered. Initially, it was intended to use the transformer-bridge technique long employed in physical chemistry for measuring the conductivity of electrolytes.⁽²³⁾ This method avoided direct-contact difficulties caused by the immersion of electrodes in the fluids. On further evaluation, this method was dropped for the following reasons:

- a. The difficulty of using a toroid in any high pressure apparatus because of its sprawling geometry,
- b. The difficulty of subjecting the toroid to a uniform temperature as high as 1500°C, and
- c. The unavailability of a suitable transformer material with a sufficiently high curie temperature for operation in the range of temperatures selected.

The problem then was how to maintain the one advantage of the toroidal bridge, i. e., electrodeless measurements taken through the toroidal walls, and at the same time, to avoid the disadvantages listed above.

To solve the problem, the first approach considered was to adapt the technique of measuring the change in inductance, ascribable to the eddy current loss in a closely-coupled conductor, used by Zimmerman⁽²⁴⁾ in the determination of the low electrical resistivity of metals. In this technique, an electrical conductor is introduced into the field of an inductor and the modified resistance and inductance is indicated by a "Q" meter or rf bridge. Figure 13 shows the change in the dissipative factor $\Delta R/\omega L_0$ as a function of $(\omega\sigma\mu_v)^{1/2}a$, which is a measure of the ratio of the coil radius, a , relative to the "skin depth" $(\omega\sigma\mu_v/2)^{-1/2}$ of the conductor. Notice the sharp peak in the dissipation factor ($\sim 1/Q$) when $(\omega\sigma\mu_v)^{1/2}a \approx 2.5$ which enables one to isolate the maximum response. At this point, and from the known values of ω , a , and $\mu_v (= 4\pi \times 10^{-7}$ for free space), one can readily evaluate σ . If we apply this technique for $\sigma = 100 \text{ ohm}^{-1}/\text{m}$ (larger than

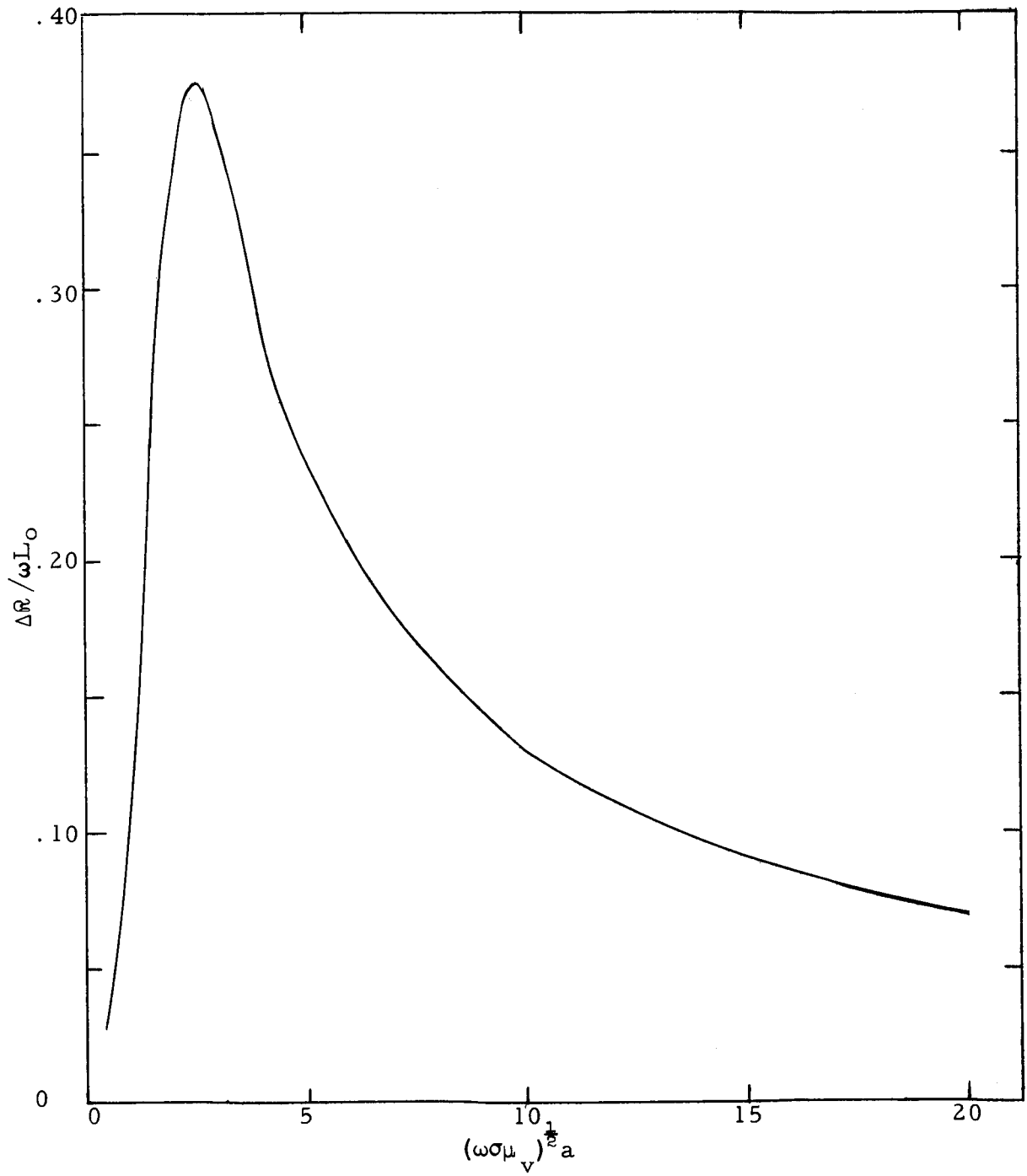


Fig. 13--Relative change in dissipative factor ($\Delta R / \omega L_0$) versus $(\omega \sigma \mu_v)^{1/2} a$

any conductivity expected) and $a = 1/200$ meter and solve for ω , we determine that $\omega = 10^{11}$, a frequency corresponding to wavelengths of the order of centimeters.

Because of the high frequencies involved and because it would be rather difficult to pipe our signal out of the pressure vessel, this technique was set aside for the conductivities expected ($< 100 \text{ ohm}^{-1}/\text{m}$). If the conductivities had turned out to be higher than expected, this technique would have been reconsidered.

Another method investigated, based on capacitive coupling, which we adopted for our initial experiments, is capable of measuring higher resistivities than that ascribed for the inductor technique at a given frequency. Again, measurements are taken by means of a "Q" meter or a high frequency bridge. In this method (see Fig. 14a), the resistance is measured between two tabs. This technique was tested on an electrolytic solution in an Alundum tube and the resistance values plotted versus the length between tabs. As shown in Figure 15, the linear plot does not go through the origin because of the finite contribution of the end effects; however, the slope of the curve may be determined to within 5 percent. Actually, to avoid end effects, the resistance should be measured between tabs 1 and 3 (see Fig. 14b), which are ~ 8 cm apart. By repeating the measurement between tabs 2 and 3 and using the difference between these two measured values, one obtains a resistance value for the distance between tabs 1 and 2 (3 cm) which is free of end effects. This technique was suggested by that employed by Weingarten and Rothberg in evaluating the resistivity of silicon bars.⁽²⁵⁾ The conversion of "Q" meter readings to resistance measurements is described in Appendix III.

3.2 Experimental Apparatus

In measuring the conductivity of a vapor by the method described in Section 3.1, the sample tube must either be capable of withstanding the high internal pressures or a compensating pressure must be applied to the tube exterior to keep the pressure differential across the tube walls at a safe level, say 200 psi. Obviously, a combination of the two features would be highly desirable.

Of the various ceramics considered for use as a sample tube, Lucalox* (very high density, multicrystalline Al_2O_3) was selected because of its reported high tensile strength⁽²⁶⁾ (see Fig. 16) and because it will

* A General Electric product

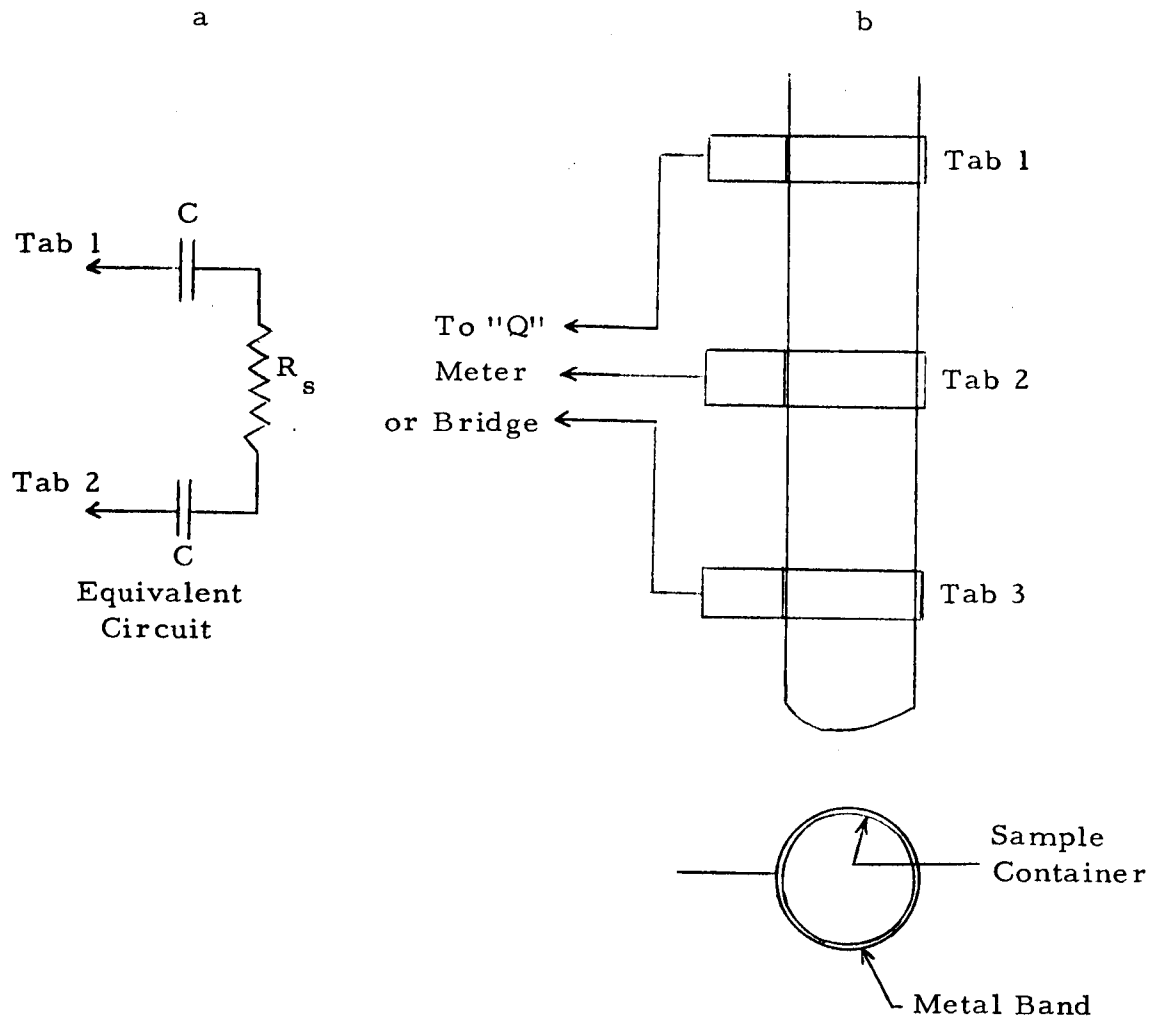


Fig. 14--Arrangement for eliminating end effects in a "capacitance-coupled" resistivity measurement. Thermocouples are located close by for temperature measurements.

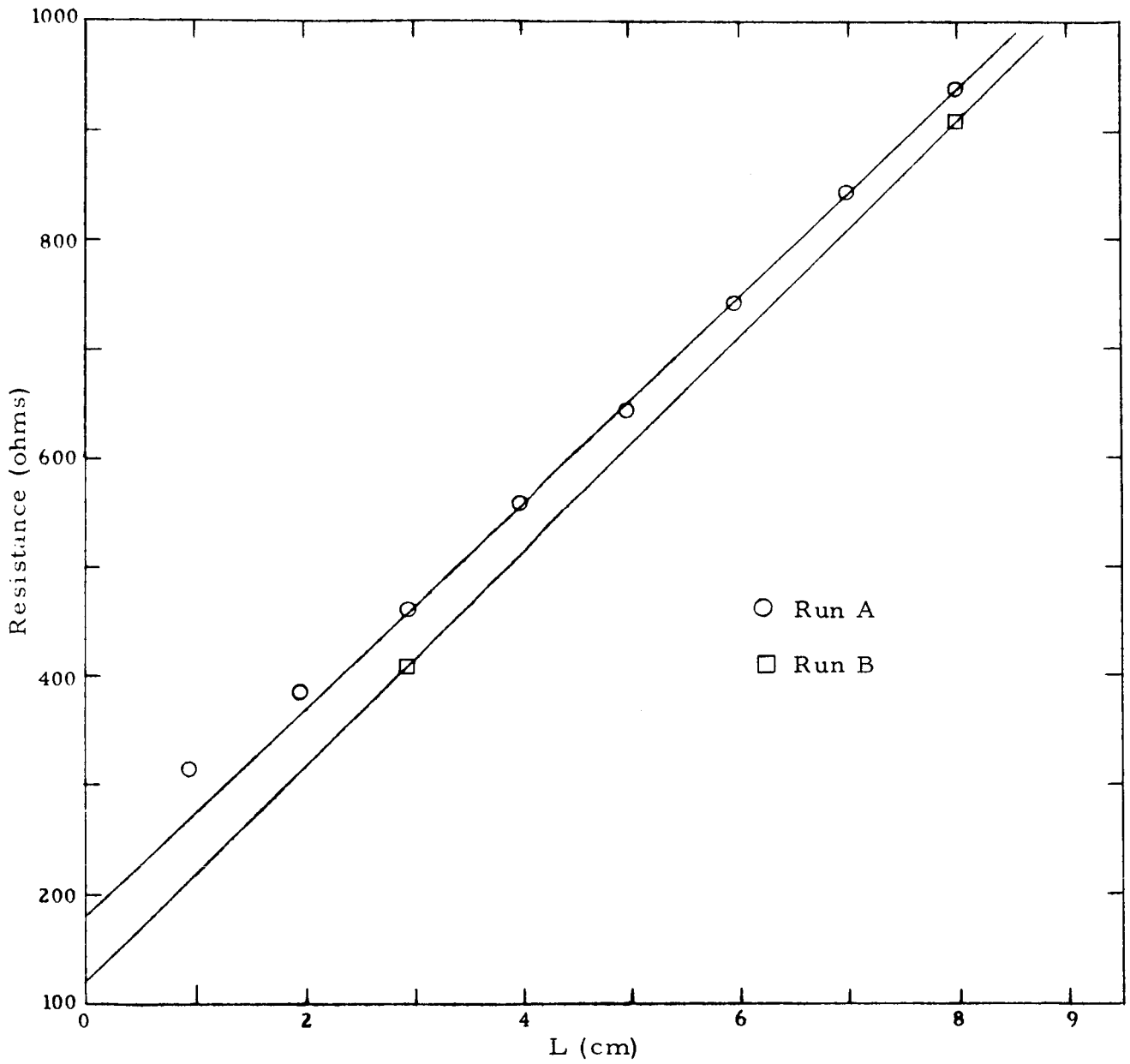


Fig. 15--Resistance of an electrolytic solution in an Alundum tube plotted versus length

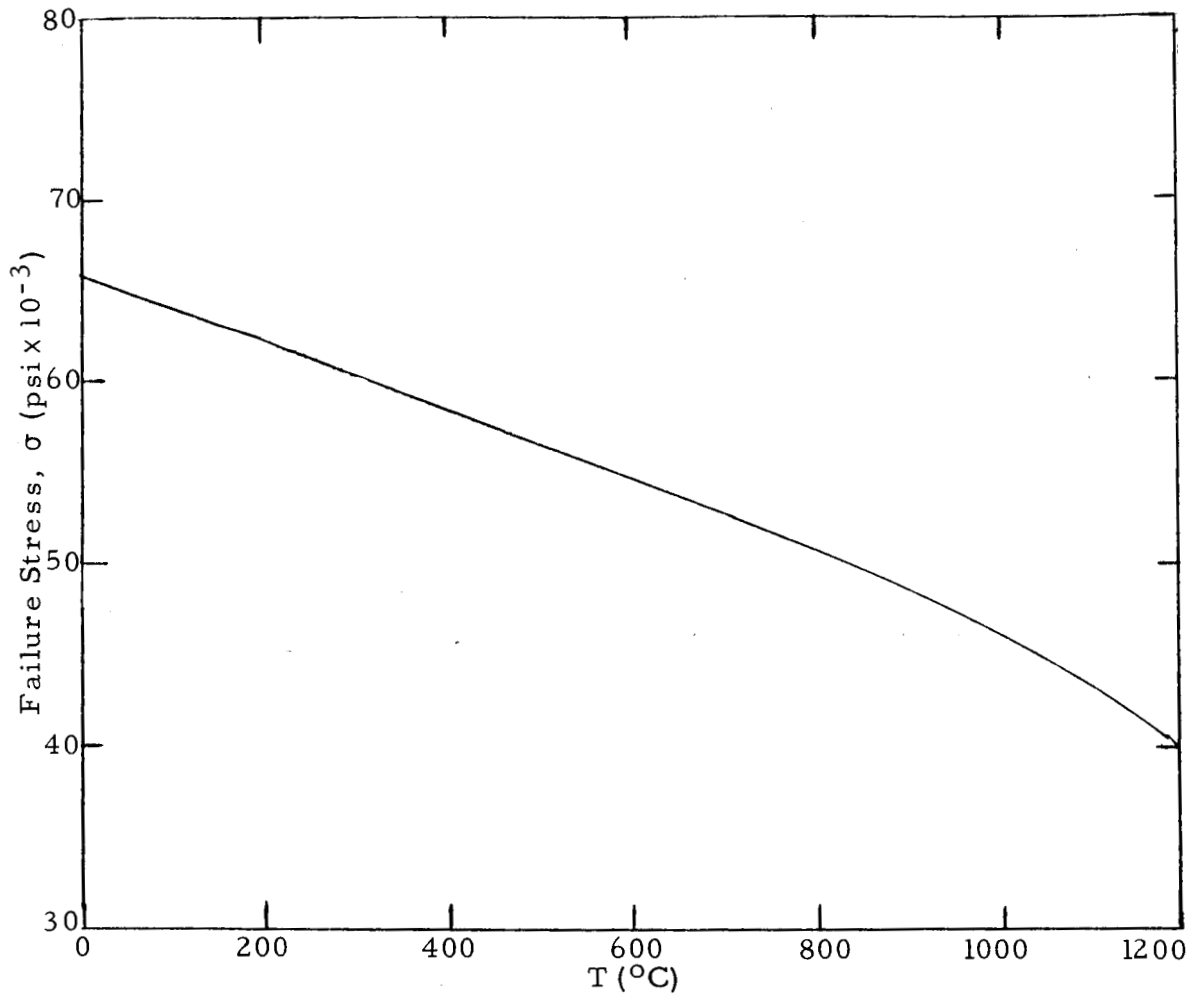


Fig. 16--Rupture strength of Lucalox as a function of temperature (see Ref. 26)

not react with cesium vapor as will ceramics containing Si. If the reported high tensile strength of Lucalox could be realized in a configuration such as we require, one could safely conduct experiments at temperatures up to $1,600^{\circ}\text{C}$ and at pressures of a few hundred atmospheres. However, in fact, under the conditions of our experiment, the various sample tubes ruptured with pressure differentials ranging from 3000 to 4250 psi (204 to 290 atm). These conditions included a large thermal gradient.

3.2.1 High pressure autoclave

In view of the uncertain strength of the best available material (Lucalox) for sample containment, prudence dictated the design and construction of a suitable autoclave to contain the sample tube and to maintain a high pressure (of helium) on the tube exterior. Such a unit (see Fig. 17) was designed and constructed of high strength steel. It contains an internal heater purchased from Marshall Furnace Products. The autoclave itself was constructed by the Autoclave Engineering Co. of Erie, Pennsylvania, and was delivered early in September, 1964.

The autoclave drawing in Figure 17 does not show the furnace which is described separately below. The autoclave itself consists of a gun steel body, $41\text{-}1/2$ in. long with an i. d. of $7\text{-}3/4$ in. and an o. d. of $12\text{-}1/4$ in. It is lined internally with a grooved stainless steel liner used for cooling and to minimize corrosion in case of sample tube failure. The liner reduces the internal working diameter to $6\text{-}1/2$ in. Pressure is maintained by the Viton O-rings and both body covers are maintained in position by the help of separate nuts. The body covers are non-rotatable thus enabling one to maintain electrical leads without twisting off the leads in sealing. Electrical leads for the furnace come through the water-cooled electrodes of the body cover and electrical leads for the measuring system come through Conax glands. These leads are actually thermocouple wires of Pt and Pt:Rh and Cu and Cu:Ni. The Cu and Cu:Ni wires were used for passage through the Conax glands because Pt and Pt:Rh are too ductile for gland packing.

The furnace, which was specially built by Marshall Furnace Products, contains two heater zones, each separately controlled and powered by two powerstats working into the primary coils of step-down power transformers. Attached to its furnace coils, made of an alloy of Mo and Re, are leads which are coiled for ease in making connections to the water-cooled terminals in the top cover. One costly error (in terms of time) in its construction was that it was improperly packed with bubble alumina. At low pressure, the insulation ability of this material was adequate. However, it provided inadequate insulation at the higher pressures, where furnace power loss became an important factor in limiting the highest temperatures obtainable. This was eventually corrected by

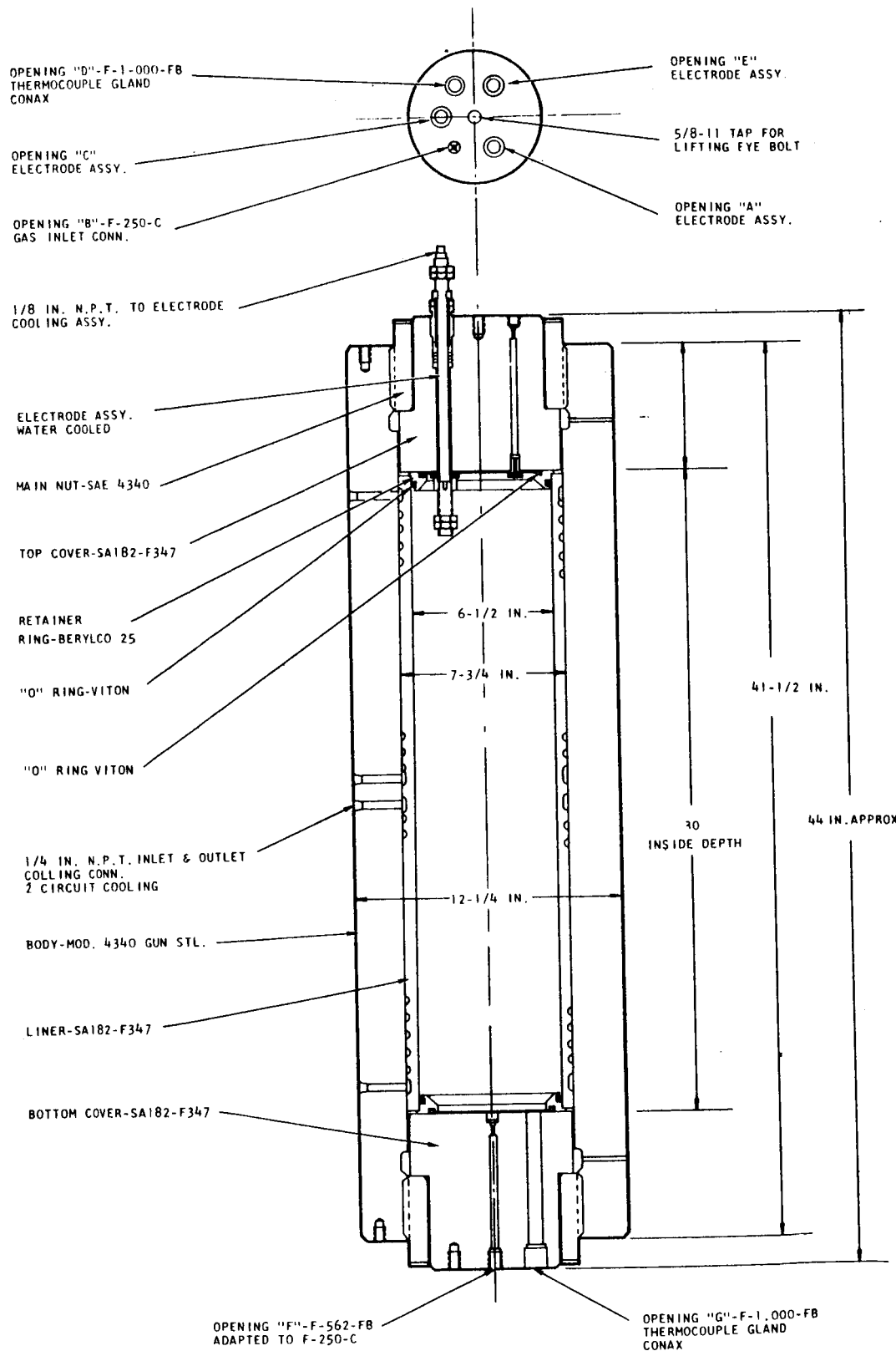


Fig. 17--Detailed drawing of high pressure autoclave

repacking the furnace with a higher-density alumina powder, of about 80 grit size. This alumina was obtainable as ordinary reagent-grade aluminum oxide.

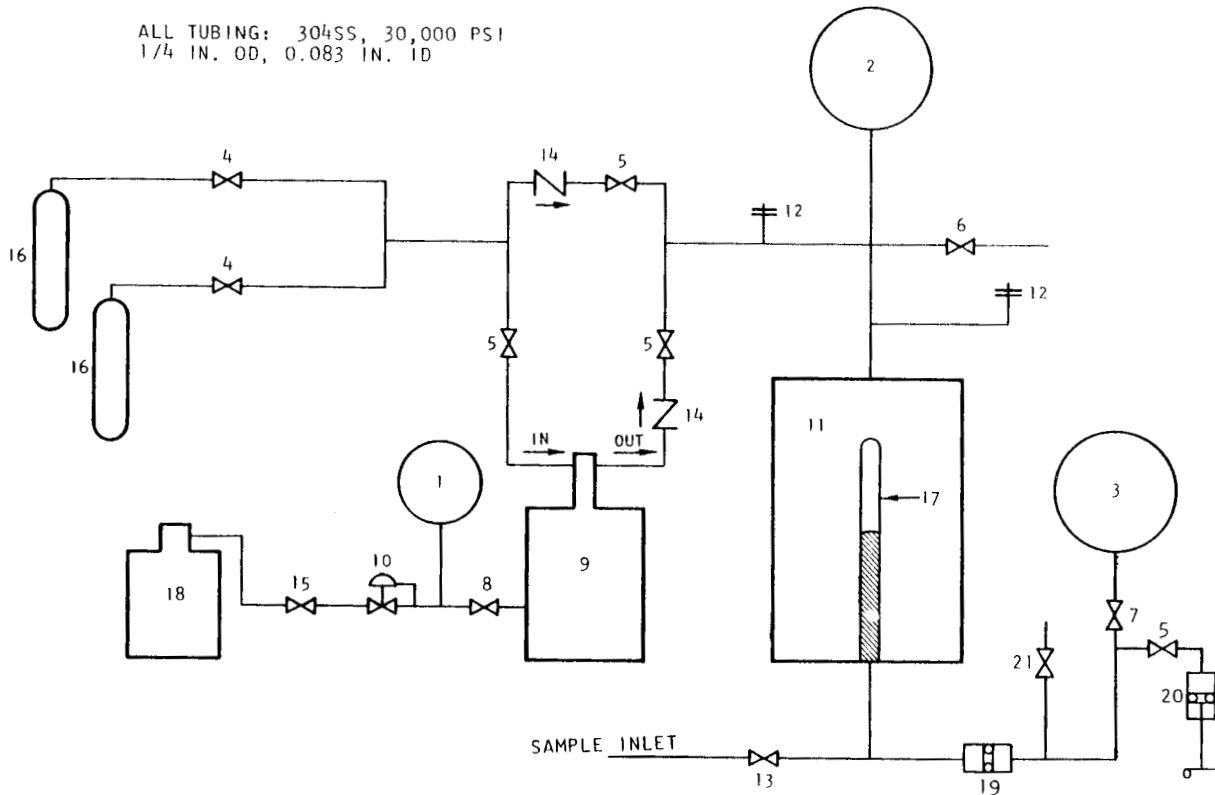
For simplicity, and since the initial runs were required to show evidence of conductivity, only two measuring bands were placed around the sample tube. In addition, a metal strip was mounted on the sample tube to permit accurate positioning of the sample liquid-vapor interface. When the tube contains the liquid sample, the strip constitutes one plate of a capacitor and the liquid is the other. By using a "Q" meter, the capacitance is measured as the liquid level rises and falls and, by proper calibration, the level can thus be positioned accurately.

For safety considerations, the autoclave was positioned in a wood, sand, and chain-mail safety enclosure. Controls and monitoring equipment were contained in an adjoining building.

A schematic diagram of the pressure control and monitoring system is shown in Figure 18. All pressure gauges and the principal controls are installed on a convenient control panel (see Fig. 19). As shown in Figure 18, the system incorporates rupture discs (see 12), which have a burst pressure of 18,000 psi (\sim 1200 atm). All valves and tubing are made of stainless steel. Helium for pressurizing the autoclave is supplied from 2 standard pressure cylinders at an initial pressure of \sim 2500 psi (16). After the autoclave pressure stabilizes at 2000 psi, a Haskel air-driven gas compressor (9) raises the pressure to the desired level (\sim 1000 atm). The Haskel compressor, which is rated at 1.2 scfm, 20,000 psi maximum output, is controlled by a needle-type speed-adjust valve and an air pressure regulator (8 and 10) on the control panel. Air pressure to the gas compressor is maintained by a Joy compressor and is indicated by an Ashcroft gauge (1), while the autoclave pressure and the pressure in the sample tube are indicated by 2 Heise bourdon gauges (2 and 3). The sample tube shutoff valves (7 and 13) and the sample pressure gauge (3) are all modified for use with mercury. Late in the program an adjustable, manually-operated piston was connected to the sample-pressure measuring system (20) to permit the height of the liquid-vapor interface to be adjusted in a temperature gradient, thus allowing the vapor pressure to be varied without changing the vapor temperature.

Temperatures at various points in the high pressure apparatus are monitored by means of thermocouples (T.C.) positioned as shown in Figure 20. The temperature of the vapor is measured by means of T.C. 2 and that of the liquid-vapor interface by T.C. 5.

ALL TUBING: 304SS, 30,000 PSI
 1/4 IN. OD, 0.083 IN. ID



- | | |
|--|---|
| <ol style="list-style-type: none"> 1. Air pressure gauge, Ashcroft, 0 to 160 psi, $\frac{1}{2}$% accuracy 2. Autoclave pressure gauge, Heise, 0 to 20,000 psi, 1/10% accuracy 3. Sample pressure gauge, Heise, 0 to 20,000 psi, 1/10% accuracy 4. Helium selector valves, Autoclave PV-4071, 6,000 psi 5. Helium shutoff valves, Autoclave 30VM-4072, 30,000 psi 6. Autoclave vent valve, Autoclave 30 VM-4071, 30,000 psi 7. Shutoff valve for sample pressure gauge, Autoclave 30VM-4071, 30,000 psi 8. Gas compressor speed-adjust valve, needle type, 300 psi 9. Gas compressor, air operated, Haskel AG-152, 1.2 scfm, 20,000 psi max. output 10. Air pressure regulator, 300 psi max. in, 0-125 psi out | <ol style="list-style-type: none"> 11. Autoclave, 1000 atm, 1700°C 12. Safety head assy, disc type, 18,000 psi burst 13. Sample tube shutoff valves, Autoclave 30VM-4071, 30,000 psi 14. Check valve, O-ring type, 30,000 psi 15. Compressed air shutoff valve, gate type, 300 psi 16. Standard helium supply bottles, initial pressure ~2500 psi 17. Lucalox sample tube 18. Air compressor, 100-125 lbs/in², > 100 scfm 19. Gauge protector, 30,000 psi 20. Adjustable piston for controlling level of sample in sample tube 21. High pressure shut-off valve for hydraulic fluid fill line <p>Note: Valves 7 and 13 and gauge 3 are modified for use with mercury</p> |
|--|---|

Fig. 18--Schematic of pressure control and monitoring system

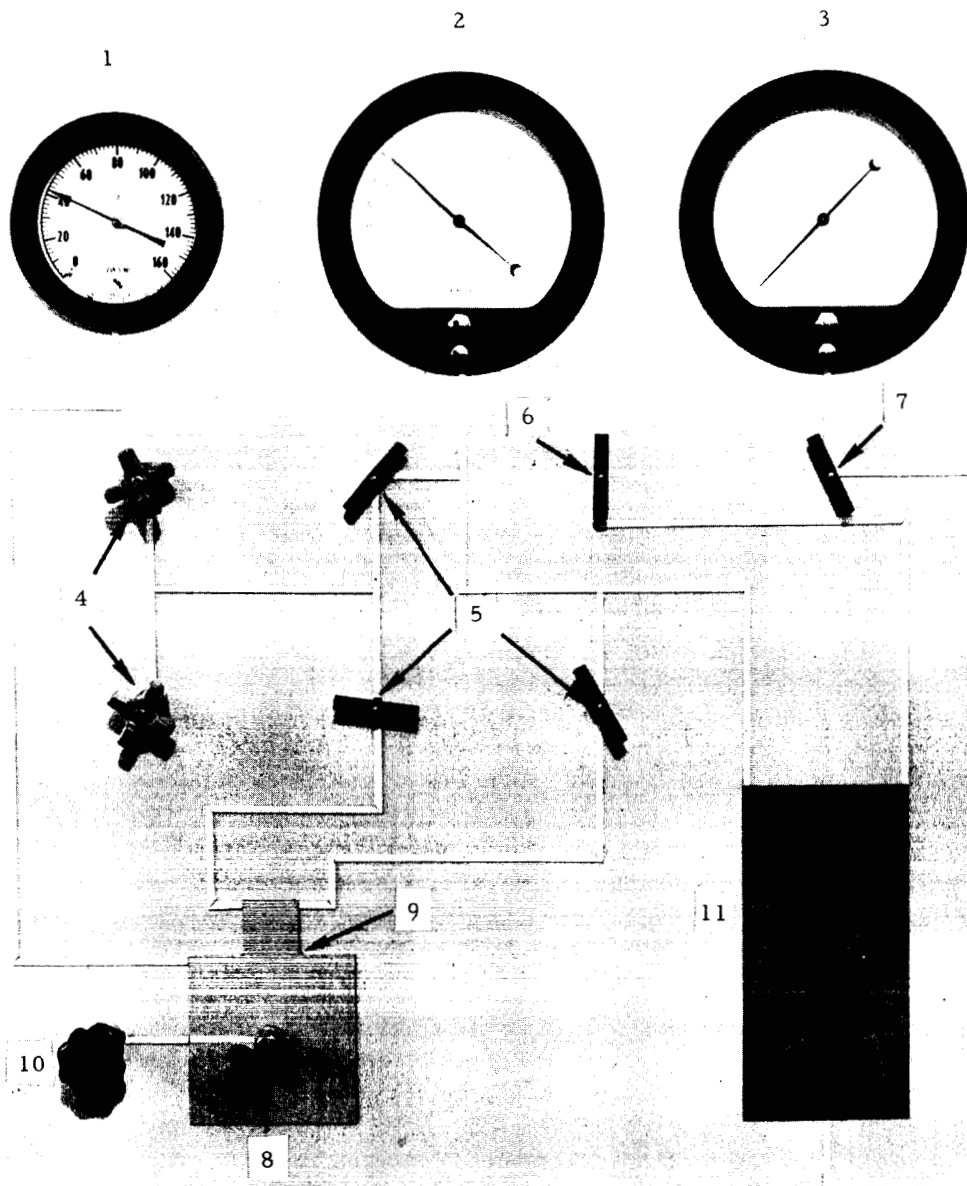


Fig. 19--High pressure control panel. Items numbered are identified in Figure 18

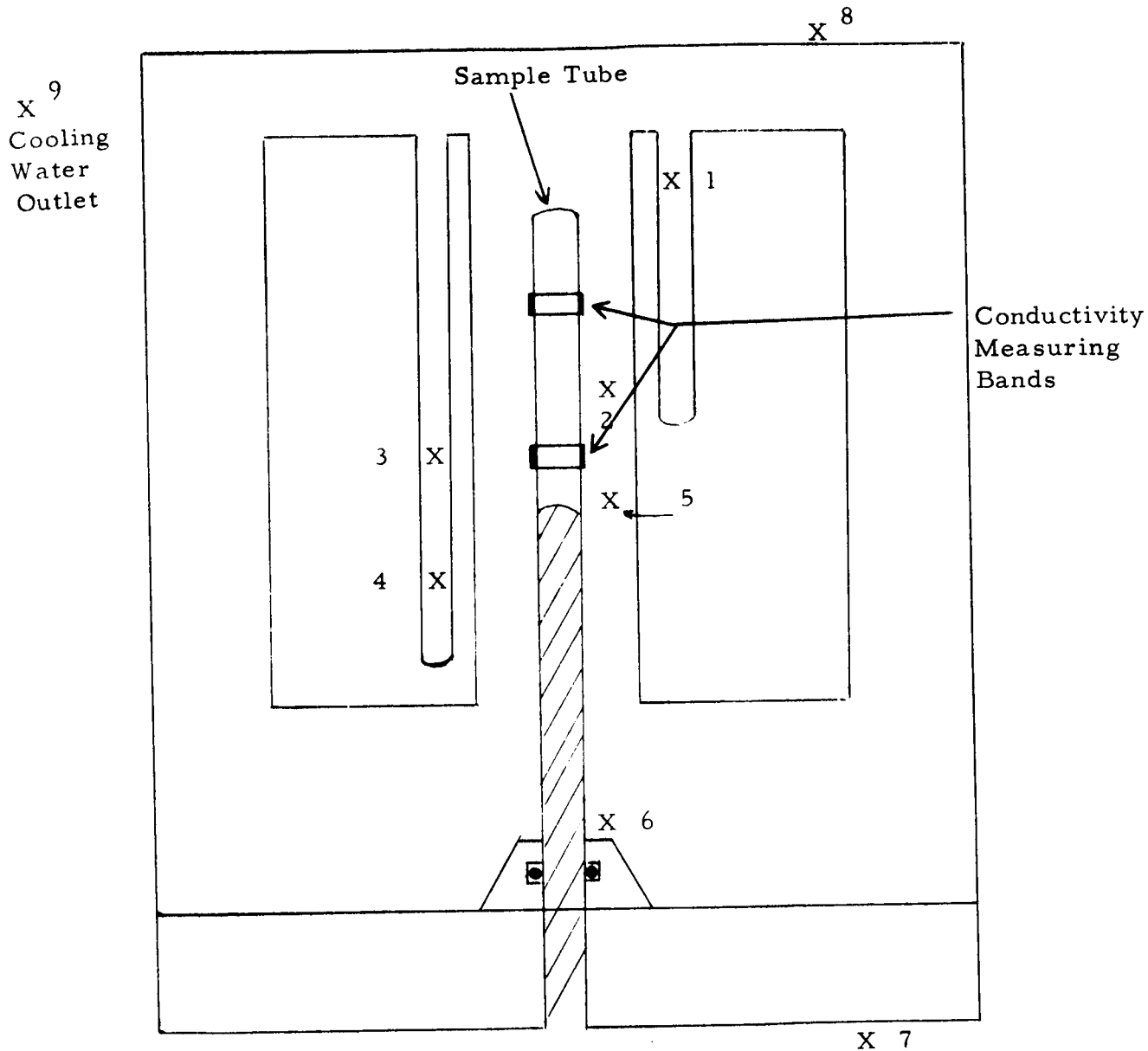


Fig. 20- - Thermocouple and conductivity band locations in the autoclave. Each band is a platinum strip ~ 1.5 cm wide; the distance between their inner edges is 2.0 cm

3.2.2 Interim apparatus

Because of the delay in placing the high-pressure autoclave system in operation, an interim experimental arrangement was constructed to permit the experimental method to be proofed and to obtain preliminary data on the conductivity of vapors of Hg, P, and an alloy of Hg and Cs. As shown in Figure 21, this apparatus consisted of a Lucalox sample tube installed in an unpressurized metal container which served as a safety barricade to contain the sample material in case of a sample tube failure. The container had an O-ring pressure seal between the sample tube and high-pressure tubing which connects the sample tube to the necessary valves and the Heise pressure gauge (3, Figs. 18 and 19) on the control panel. This gauge and its shutoff valve (7) are the only items on the control panel that were used with the interim equipment. The adjustable piston (20) was not used with the interim equipment.

As shown in Figure 21, the apparatus incorporated 2 independently-controlled heaters, H_1 and H_2 . H_1 controls the surface temperature of the liquid/vapor interface and thus the vapor pressure. H_2 controls the temperature of the vapor without changing the pressure.

As already described for the high pressure autoclave, only two measuring bands were used with the sample tube in the interim apparatus. The sample liquid-vapor interface was also positioned as described for the autoclave.

For reasons of safety, the interim apparatus was operated in the wood, sand and chain-mail safety enclosure mentioned previously. The containment vessel was not pressurized but was evacuated to reduce heat losses.

3.3 Experiments with Interim Apparatus

Before the autoclave was placed in operation in October 1964, experiments with vapors of Hg, P, and Hg doped with 5 percent Cs were performed. These experiments were limited in temperature to a maximum of $\sim 1100^\circ\text{C}$ (the maximum capacity of the furnace). Since the sample pressure was uncompensated by any external pressure, the maximum pressure attainable in these experiments depended on the strength of the Lucalox tubes. For individual tests, the Lucalox bursting points ranged from ~ 3000 psi (204 atm) to ~ 4250 psi (290 atm). In spite of these limitations, experiments with the interim apparatus verified the validity of the experimental method and provided some worthwhile preliminary data. In addition to the above tests, the reliability of our measuring technique was further verified by using the interim apparatus to measure the Q of solid AgBr.

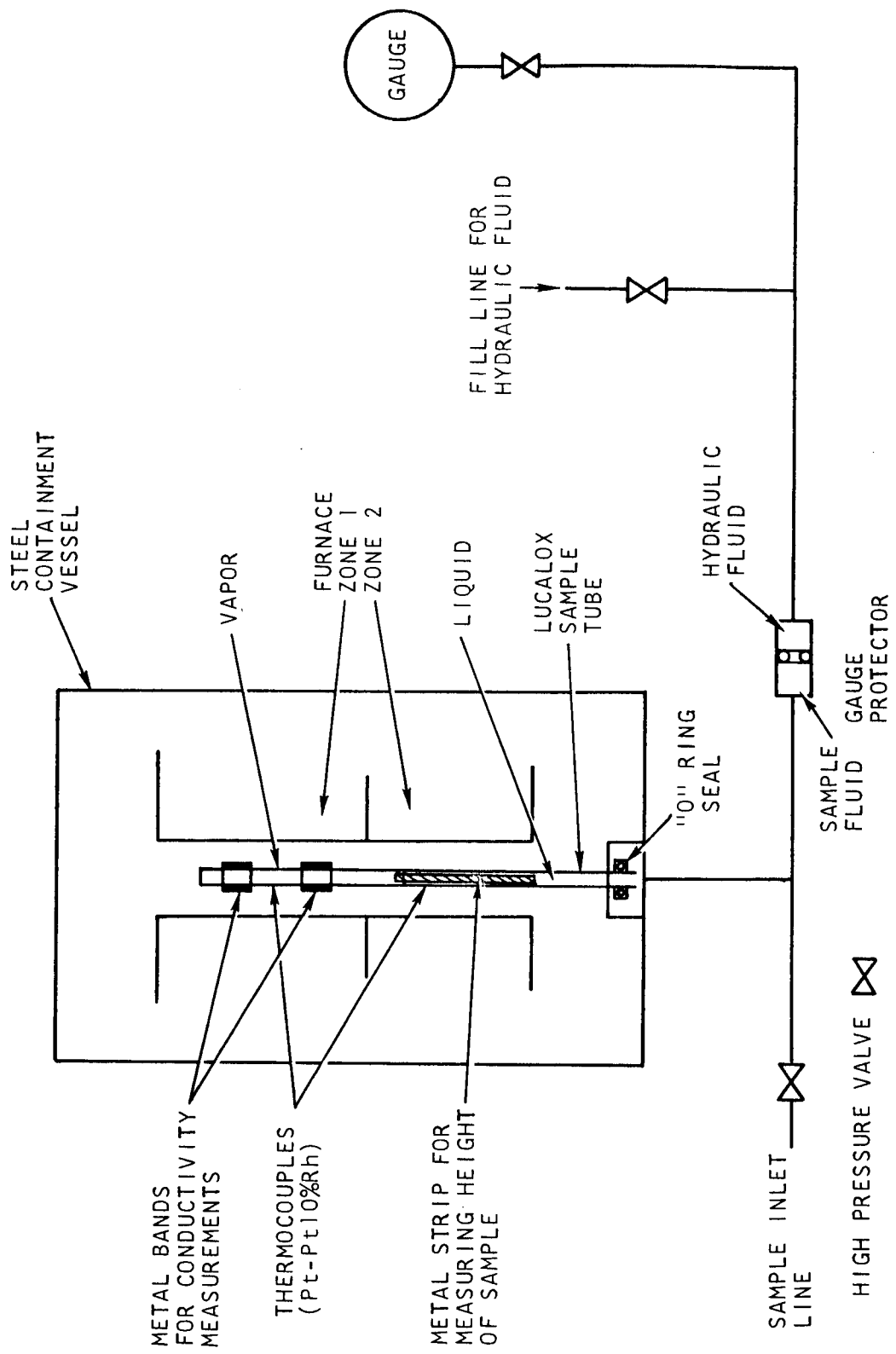


Fig. 21--Schematic of interim apparatus. Each conductivity band is a Pt strip ~ 1 cm wide and the distance between their inner edges is 2.5 cm

3.3.1 Measurements with pure Hg vapor

Two experiments with Hg vapor were conducted with the interim experimental apparatus at significant temperatures and pressures. These experiments closely simulated those which were conducted in the high-pressure autoclave, except that the Lucalox sample tube containing the pressurized vapor had no compensating pressure on its exterior walls.

The results of the experiments may be summarized as follows:

- a. The Lucalox sample tube ruptured at a pressure of 4250 psi (≈ 290 atm) and a temperature of $\approx 1140^\circ\text{C}$.
- b. The conductivity measuring technique showed no erratic behavior and performed as expected.
- c. The O-ring seal remained within its temperature limitation without water cooling and withstood the pressure of 4250 psi without leakage.
- d. Electrical conductivity of mercury vapor could not be detected at temperatures up to 1140°C and at pressures up to 290 atm.

The first experiment with Hg vapor was terminated, at a vapor temperature of $\approx 1000^\circ\text{C}$ and a pressure of 1765 psi (120 atm), to evaluate the data before pushing the temperature and pressure to the point of sample tube failure.

In the second experiment with Hg, Q_s , the Q of the sample tube with the vapor present, was recorded as the temperature was increased to about 1140°C , at which point the tube ruptured. The vapor pressure was 4250 psi (≈ 290 atm). Data from this experiment are plotted in Figure 22 in which Q_s is compared with Q_o (the Q of the empty tube) as a function of temperature. The apparent resistance of the vapor is derived from

$$R_z = \frac{Q_o Q_s}{\omega C_o (Q_o - Q_s)} \quad (45)$$

as described in Appendix III. Here, ω is the angular frequency and C_o is the added capacitance required to tune the "Q" meter. As seen in the figure, no significant difference between Q_o and Q_s is observed. From sensitivity estimates of the measuring system, the slight difference at $\approx 1140^\circ\text{C}$ indicates a resistance for the vapor of $> 2.4 \times 10^4$ ohm, i. e., a conductivity of $\approx 6 \times 10^{-2}$ ohm $^{-1}$ /m. More than likely the difference in Q_o and Q_s was due to the gradual drift of either the sensitivity control or the zero control of the "Q" meter. Later data from autoclave measurements verified this.

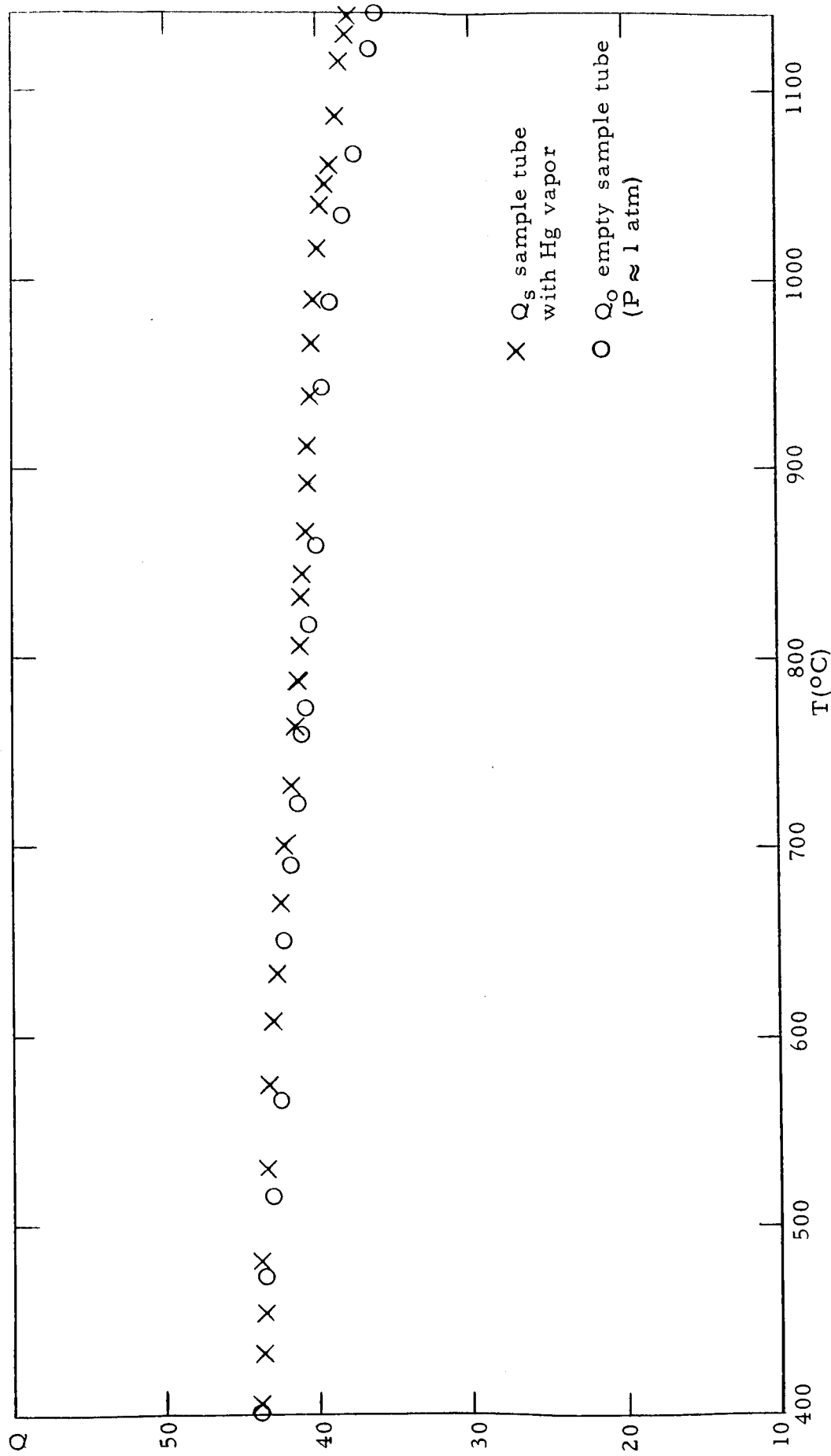


Fig. 22--Measured Q of sample tube with and without Hg vapor as a function of temperature. The pressure at 1100°C was about 290 atm. $\omega = 20$ Mc, $C_o \approx 240$ pF

3.3.2 Measurements with phosphorus

Three experiments were conducted on phosphorus vapor using the interim equipment. Phosphorus was chosen because it has a solid phase which is conducting, indicating that for some configurations of P atoms, electron transfer will take place. The critical point for phosphorus is about 690°C and 83 atm, so that the fluid can be forced above the critical point with relative ease.

Because of the corrosive and poisonous nature of phosphorus, the pressure measuring apparatus was not used. Instead, a measured amount of P was distilled into a thick-walled quartz tube which was then sealed off. The pressure and density were found from the published equation of state.²⁷

In the first experiment, white phosphorus was placed in a quartz tube (~ 15 cm long) having a 2 mm i.d. and an 8 mm o.d. (3 mm wall thickness). About $1/3$ of the tube volume was filled with the sample. The tube was then evacuated before it was sealed off. Unfortunately, the tube failed at $\sim 600^{\circ}\text{C}$ (43 atmospheres) and no useful data were taken.

The second and third experiments were conducted in heavier-walled quartz tubing (4 mm wall thickness) having the same internal volume as the first tube (2 mm i.d.). Red phosphorus was used for these experiments (instead of white P) because it is much easier and safer to handle. As the literature on phosphorus indicates, the liquid existing above the melting point of red P (590°C at 43 atm) is identical regardless of which form one starts with. In particular, when white P is heated in its own vapor, it converts to red P at temperature above 200°C .

Each of the experiments started with a fresh sample tube and differed only in the amount of sample in the tube. In the first experiment, the tube contained 0.13 g of red P which resulted in a vapor density of 0.2 g cm^{-3} at the critical point (690°C at 83 atm). The second tube contained 0.3 g of red P to give a density of 0.5 g cm^{-3} at the critical point. In each case, the Q of the empty tube was measured first and then measurements were made with the sample in the tube. In Figures 23 and 24, these measured values of Q are plotted as a function of temperature. In each figure, the divergence between the empty tube plot and that of the tube-with-sample plot is large enough to be significant.

We did not believe that these losses were really due to the P vapor, however, because the conductivity persisted as the temperature was lowered. It was therefore suspected that the quartz (SiO_2) had been

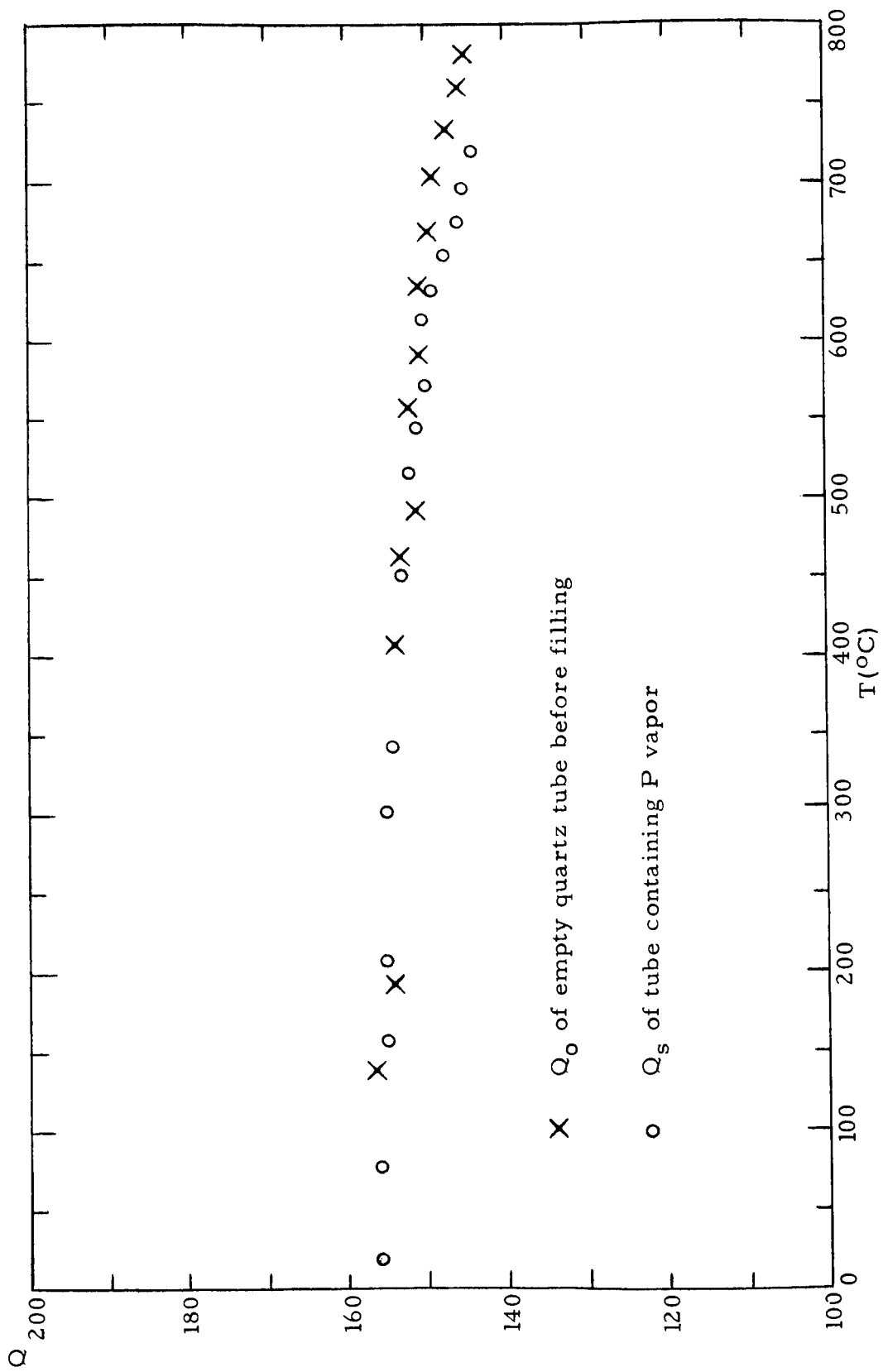


Fig. 23--Q as function of temperature for 0.13 g of P in a quartz sample tube

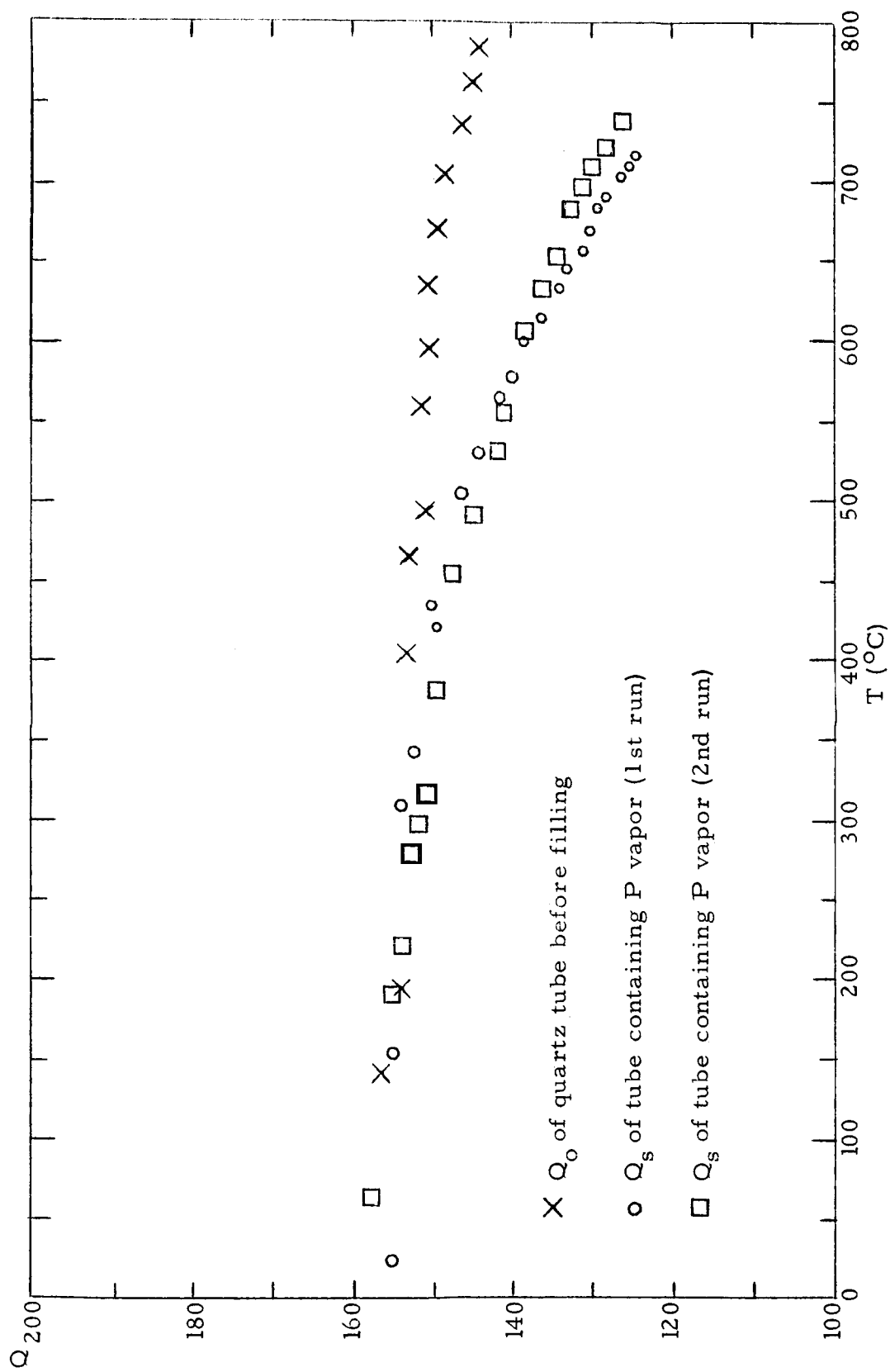


Fig. 24 -- Q as function of temperature for 0.3 g of P in a quartz sample tube

altered in the presence of the dense P to form a conducting layer of some pyrophosphate on the inner walls of the tube.

To examine the last possibility, the second tube (from Fig. 24) was reopened, the sample material was removed, and measurements were made with the tube opened in the air. As shown in Figure 25, the measured Q dropped off in exactly the same manner as shown in Figure 24. It is therefore evident that the measured conductivity was not due to the vapor. Conclusive evidence on the conductivity of P must await the solution of some rather difficult experimental problems.

If the phosphorous vapor were actually conducting, the conductivity must have been small enough that it did not show above the background given by Figure 25. One can estimate that the conductivity must have been less than about 7×10^{-2} ohm⁻¹/m.

3.3.3 Measurements on solid AgBr

As a final check of the reliability of our measuring technique before placing the high pressure autoclave into operation, we used the interim experimental apparatus to measure the Q of solid AgBr. This material was first melted (M.P. = 433°C) and poured into the Lucalox sample tube and allowed to cool to room temperature. Figure 26 shows the variation of the Q of the sample (Q_s) with temperature. Also shown is the apparent resistance of the sample (R_z) computed as described in Appendix III. Figure 27 illustrates the conductivity of the sample plotted as a function of temperature. Also shown in Figure 27 is the conductivity-versus-temperature curve of Teltow,⁽²⁸⁾ who employed bridge measuring techniques. Note the close agreement of the slopes of the two curves in Figure 27. The actual data points of the two curves seem to differ by a common factor, probably due to the uncompensated end effects associated with the spacing of the electrodes used in our measurements. Our data are therefore in good agreement with the data of Teltow. It should be noted that for our computations, we assumed a constant value of 169 for the Q of the empty tube (Q_0).

3.3.4 Measurements with Hg:Cs

In planning for making measurements on Hg doped with Cs in the high-pressure autoclave, it became evident that the sample filling system shown in Figure 18 would require modification due to the special characteristics of Cs. Accordingly, the modified filling system shown in Figure 28 was constructed and connected to the interim apparatus for testing. As shown in the figure, the system is connected to the stainless steel tubing by a length of rubber tubing. The required amount of liquid Cs (5 atomic percent of the amount of Hg) was placed in a Pyrex cell and the following filling procedure was followed:

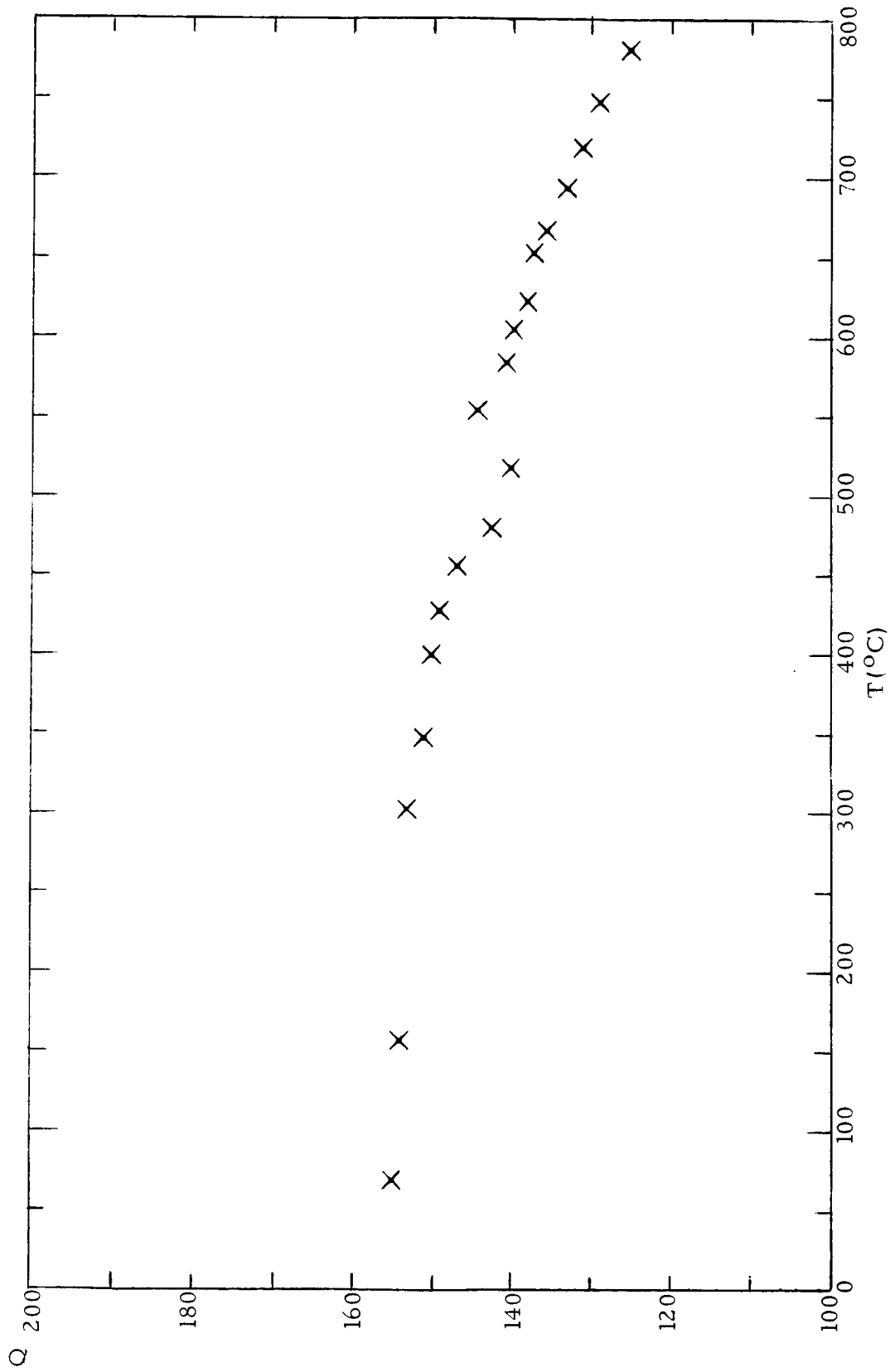


Fig. 25--Q of empty quartz tube from which P has been removed. Interior of tube was open to air.

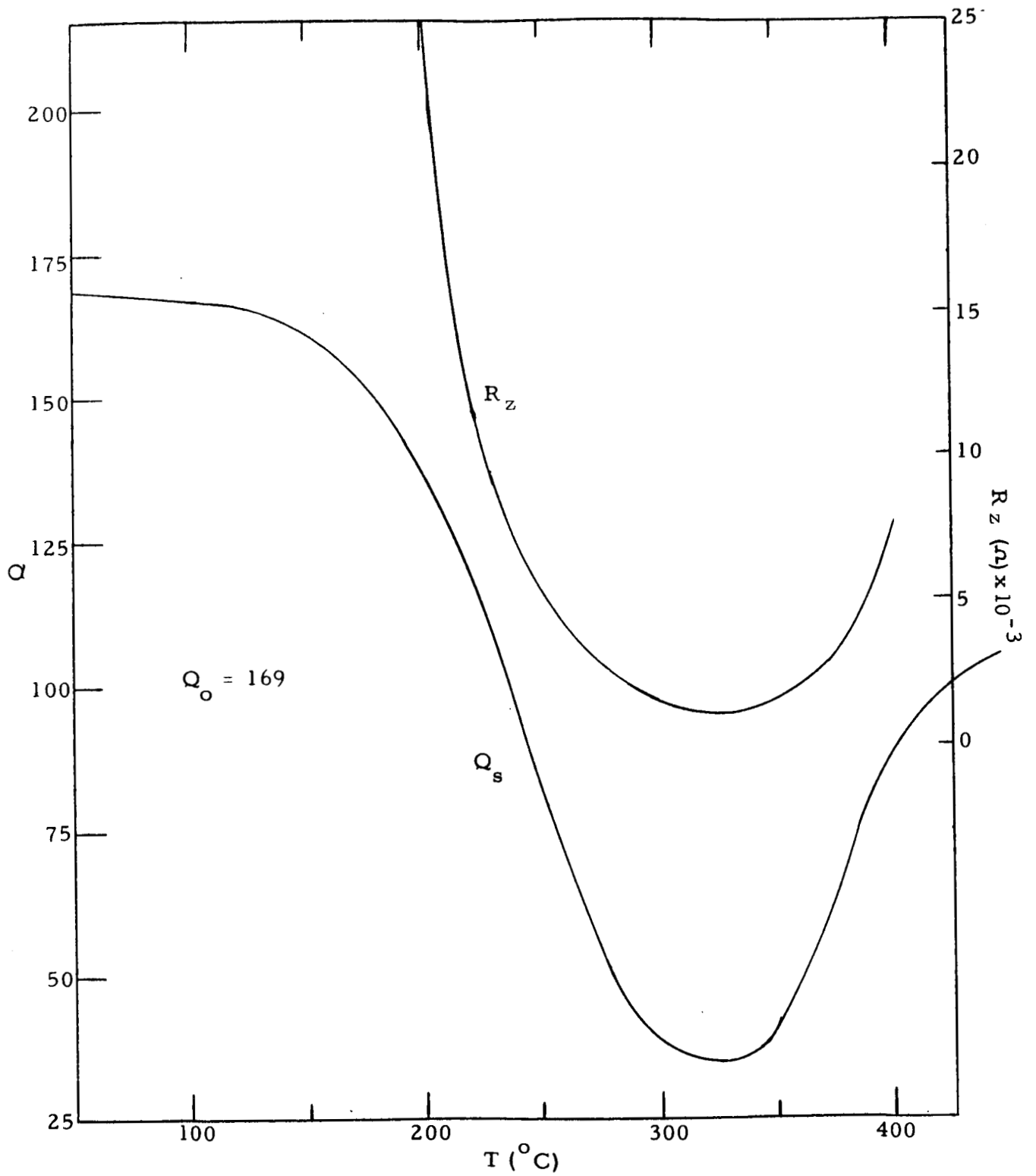


Fig. 26--Measured Q (Q_s) and computed apparent resistance (R_z) of AgBr as functions of temperature. $\omega = 20$ Mc, $C_0 \approx 237$ pF. The equivalent capacitance in series was 10.7 pF.

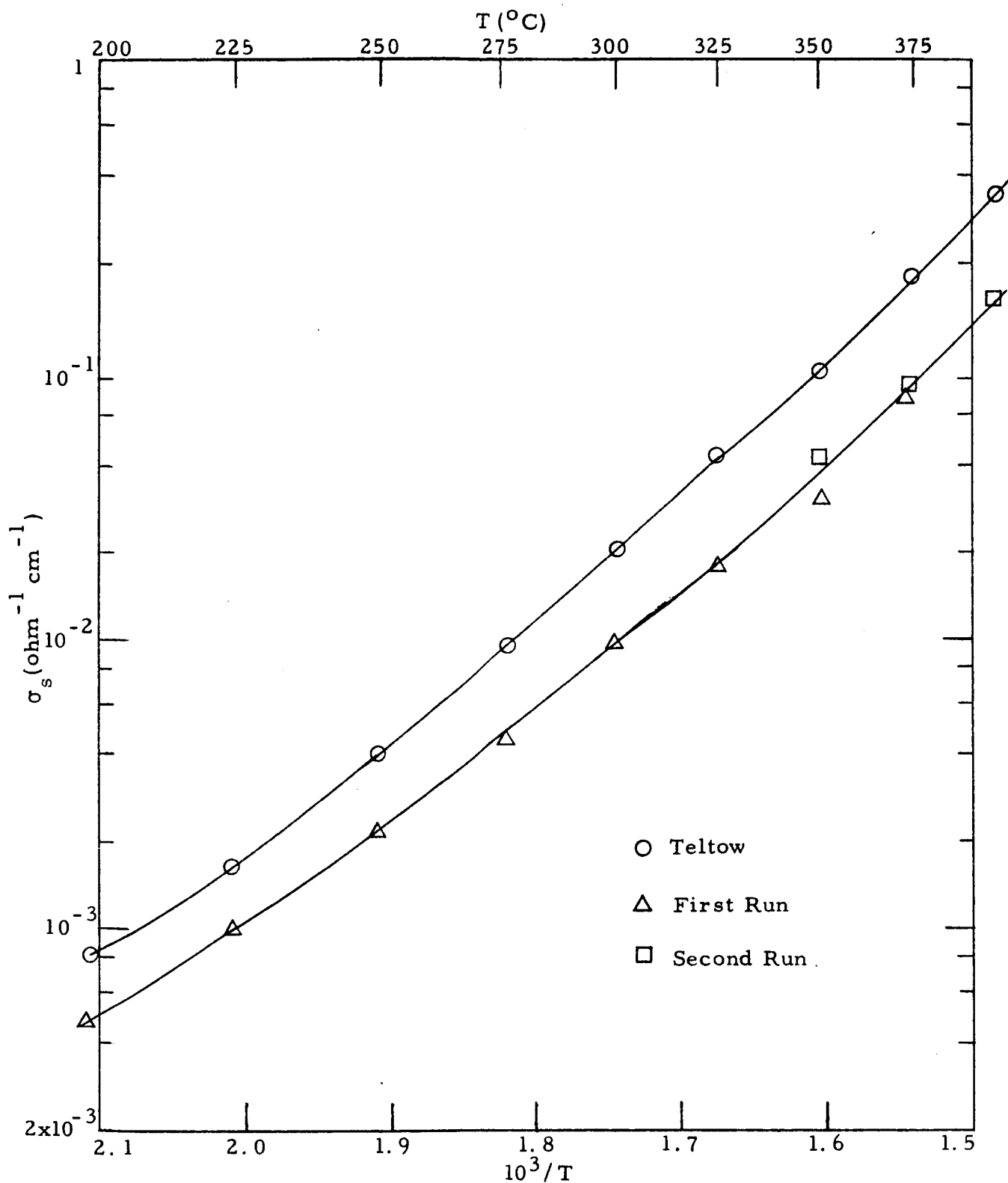


Fig. 27--Conductivity σ_s of AgBr as a function of temperature compared with that of Teltow. Based on R_z of Figure 26 with a C_3 of 10.7 pF. $\sigma_s = 14/R_s \text{ ohm}^{-1} \text{cm}^{-1}$

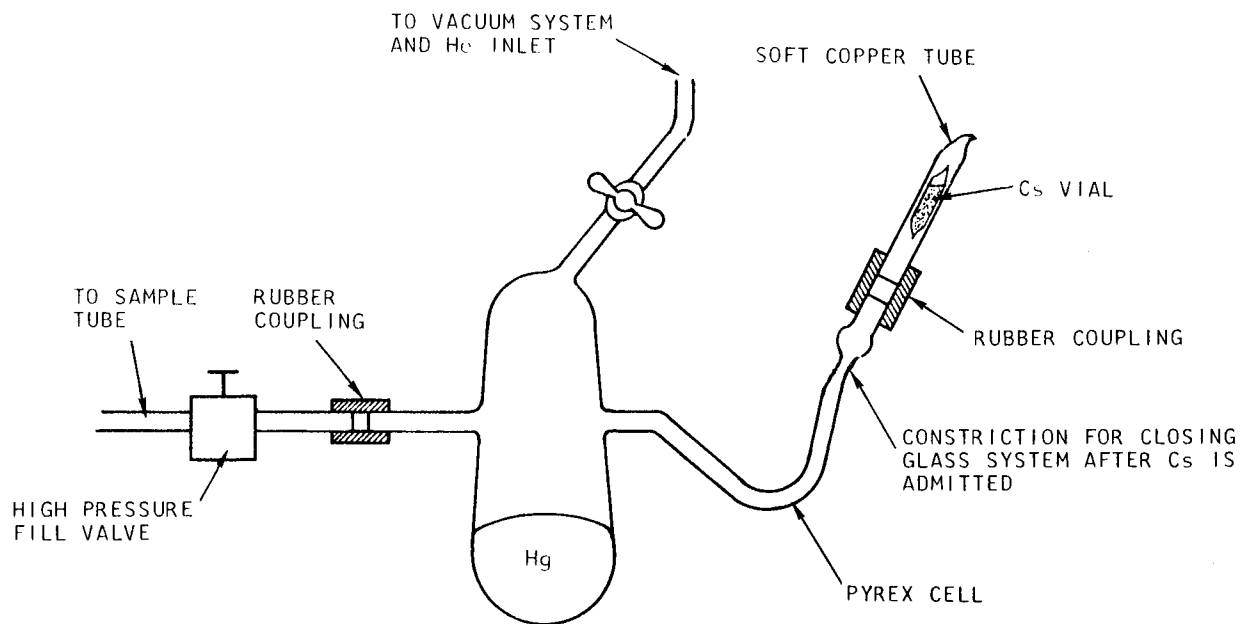


Figure 28---Modified sample filling system for use with Hg:Cs

- a. Prior to breaking the Cs vial, the system is evacuated and purged several times with He.
- b. The Cs vial is then broken by pinching the copper tube. After the Cs has run down into the V-shaped Pyrex tube, the copper tube is removed by burning off the Pyrex tube at the constriction.
- c. The tube is then tipped repeatedly, allowing only a small amount of Cs to mix with the Hg each time.
- d. After the mixing is complete, the cell is rotated 90 deg so that the long dimension of the cell is horizontal. The Hg:Cs sample is then forced up into the sample tube to the desired height by admitting He gas via the stopcock. When the desired level is achieved, the high-pressure fill valve is closed.

While the main purpose of this test was to check the modified sample filling apparatus for use with Hg:Cs, the Q of the system was recorded up to 1050°C and 3000 psi, the maximum pressure attained. At this point, the sample tube ruptured causing sufficient damage to the interim equipment to cause its retirement. No appreciable conductivity was encountered; however, none had been expected at that pressure.

In the preceding experiment the concentration of liquid Cs in liquid Hg at room temperature was about 5 atomic percent as determined by the phase diagram shown in Figure 9.⁽¹⁹⁾ It is evident from the shape of the liquidus curve that the amount of Cs which is soluble in Hg is limited if the melting point of the alloy is to be $< 50^{\circ}\text{C}$. Since we are restricted to the use of liquid in the transfer system, it is obvious that the system must be heated up to 150°C or more to permit a concentration of 10 atomic percent of Cs in Hg.

3.4 Experiments with the Autoclave

After arrival, installation, and checkout during September, 1964, the autoclave and associated systems were ready for initial tests in October. Because of the lack of time remaining in the program and because each experimental run takes from 24 to 30 hours to complete, experiments with the autoclave were limited to pure Hg and Hg doped with Cs.

The long time period required for each experimental run is a result of the characteristics of the furnace heater elements. These elements consist of an alloy of Mo and Re which is noted for its low resistance at low temperatures and relatively high resistance at elevated temperatures. For this reason it was necessary to increase the temperature slowly in order to reduce the temperature gradients. It takes about 12 hours to reach 600°C.

The experiments were performed with $\omega/2\pi = 14$ Mc and $C_0 \approx 450$ pF. The geometry of the bands gave a coupling capacity of 12 pF and the sample conductivity is expressed as $\sigma_s = 14/R_s$ in $\text{ohm}^{-1} \text{cm}^{-1}$.

3.4.1 Experiments with pure Hg

A total of 7 experimental runs were made with pure Hg vapor. In the earlier experiments, the maximum temperatures and pressures were limited by heat losses and pressure leaks. As these problems were reduced, the upper limits in succeeding experiments were gradually increased until 1650°C and 10,800 psi (~ 735 atm) were reached (but not simultaneously) in the last run. In this section, some of the experimental problems, together with their solution, are discussed. However, only the last run is discussed in detail.

Initial experiments with Hg and modifications to apparatus - The principal factor limiting sample pressure and temperature was that of poor heat transport between the furnace and the sample tube. Much of the thermal output of the furnace was lost to the water-cooled walls of the autoclave and was not available to heat the sample. This heat loss was reduced but not eliminated by:

- a. Using helium instead of argon as the pressurization gas surrounding the sample tube. Because of its large kinematic viscosity (~ 10 times that of argon), convective losses with helium are much lower than with argon. This change alone permitted the pressure of Hg vapor to be increased to ~ 5500 psi (compared to a maximum of 3000 psi with argon),
- b. Inserting boron nitride (BN) plugs in the well of the furnace above the sample tube, and by
- c. Placing additional packing around the sample tube, but not around the conductivity measuring bands.

An additional modification made before the last experimental run with Hg, was the installation of a piston (a modified gauge protector) in the sample tube supply line (see Fig. 18). The piston could be moved by a simple screw attachment, thereby changing the volume within the supply line, thus changing the height of the liquid/vapor interface in the sample tube. This also permitted us to raise the pressure of the vapor when required by raising the interface into a higher temperature zone. As previously described in Section 3.2.1, the height of the interface is measured by means of a height sensing strip whose capacitance is measured with a "Q" meter.

Final experiment with Hg - In the last experiment with Hg, temperature readings from thermocouples (T.C.) 2, 3, 4, 5 (see Fig. 20) were plotted as a function of time as shown in Figure 29. Time for this experiment is a rather arbitrary variable but it is a convenient parameter for labeling events. Simultaneous readings were made of sample pressure and Q as shown in Figure 30. The autoclave pressure (He) is maintained at a nominal 300-400 psi above sample tube pressure. The heat loss due to convection is evident in the behavior of the curve for T.C. 4 (see Fig. 29) which is seen to fall away from the curves for the other thermocouples after about three hours. It then levels off and starts to decrease. The curves for T.C. 3 and 5 start to decrease after eight hours.

At this point, it became interesting to see how high a temperature could be reached. The sample liquid/vapor interface was therefore lowered from the hot part of the furnace to reduce sample pressure. The autoclave pressure (He) was bled off simultaneously, care being taken to maintain the required differential over sample pressure. This was done from eight to eleven hours as shown in Figure 30. As the heat loss due to convection was reduced, T.C. 5 approached the maximum rated furnace temperature (see Fig. 29). The curve for T.C. 4 remained disappointingly low, however.

After eleven hours, it was decided to see how high a vapor pressure could be reached. The He pressuring gas was pumped in at the maximum rate obtainable and the level of the Hg liquid/vapor interface was elevated into the furnace hot zone as rapidly as possible without creating an overpressure in the sample tube. (This phase was referred to as the "bootstrap" operation.) The resulting fast rise in pressure is shown in Figure 30. Unfortunately, after a slight time lag, the higher He pressure (permitting more convection losses) caused a sharp drop in temperature (see Fig. 29).

At about 11.8 hours, the Hg interface had reached the hottest zone in the furnace; from then on, the temperature of the interface dropped, so the vapor pressure also dropped.

The Q of the sample tube actually rose by a large amount after eleven hours. Actually, it is shown in Appendix III that a slight increase in Q is possible when the sample fluid becomes conducting. However, in this case, the Q at identical temperatures correlates with the dry run, which was taken at a few atmospheres of He pressure. This is shown in Figure 31 where the measured Q is plotted against temperature (from T.C. 2), both with and without Hg in the sample tube. The final points extending the wet run and designated by (χ) were taken by extending the run with the booster piston. In this case, thermocouple readings were taken with T.C. 5 instead of T.C. 2. Except for a constant offset and scatter, the two curves are parallel and seem to provide no indication of any appreciable conductivity of the vapor.

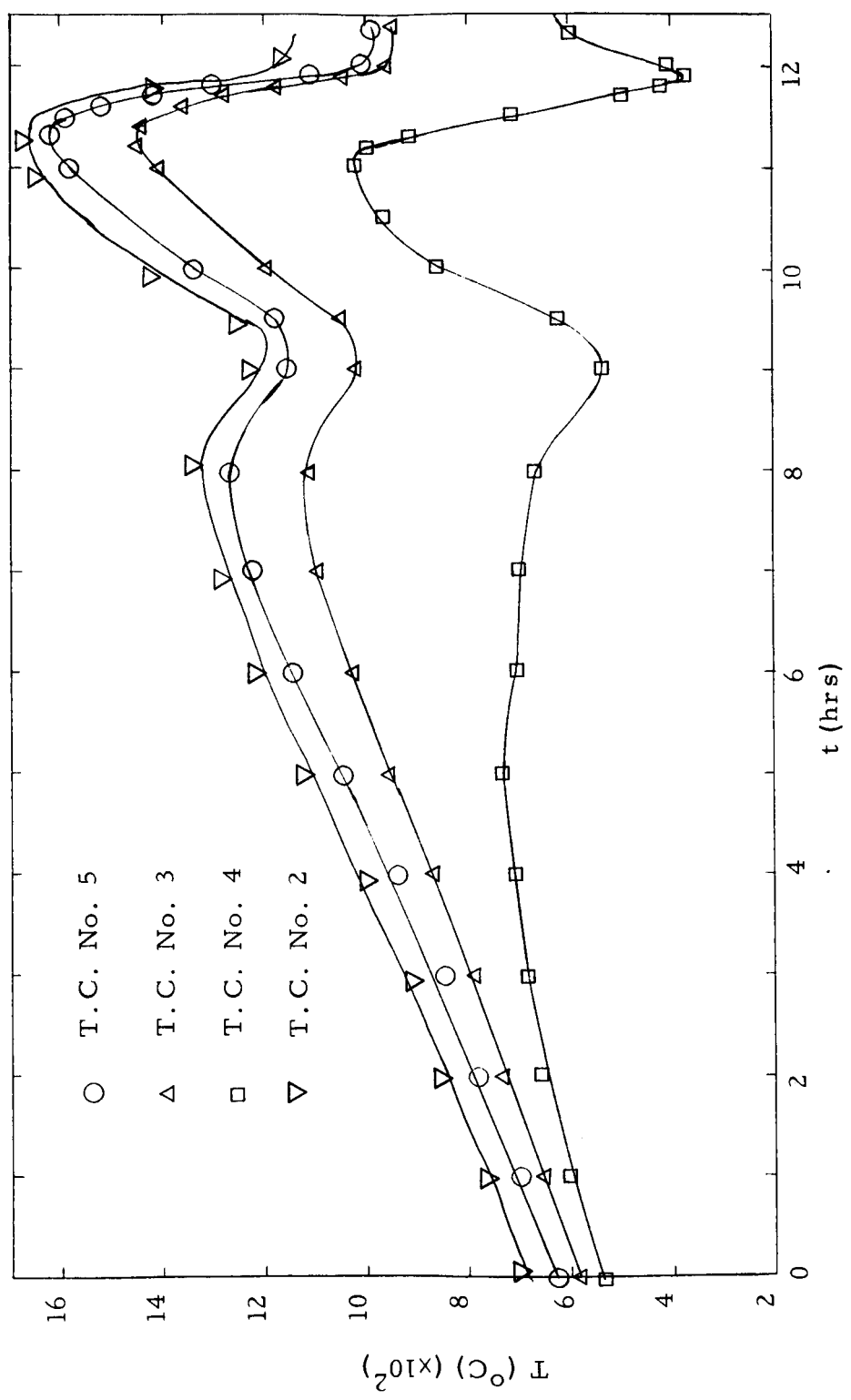


Fig. 29-- Temperature versus time for experiment with Hg vapor

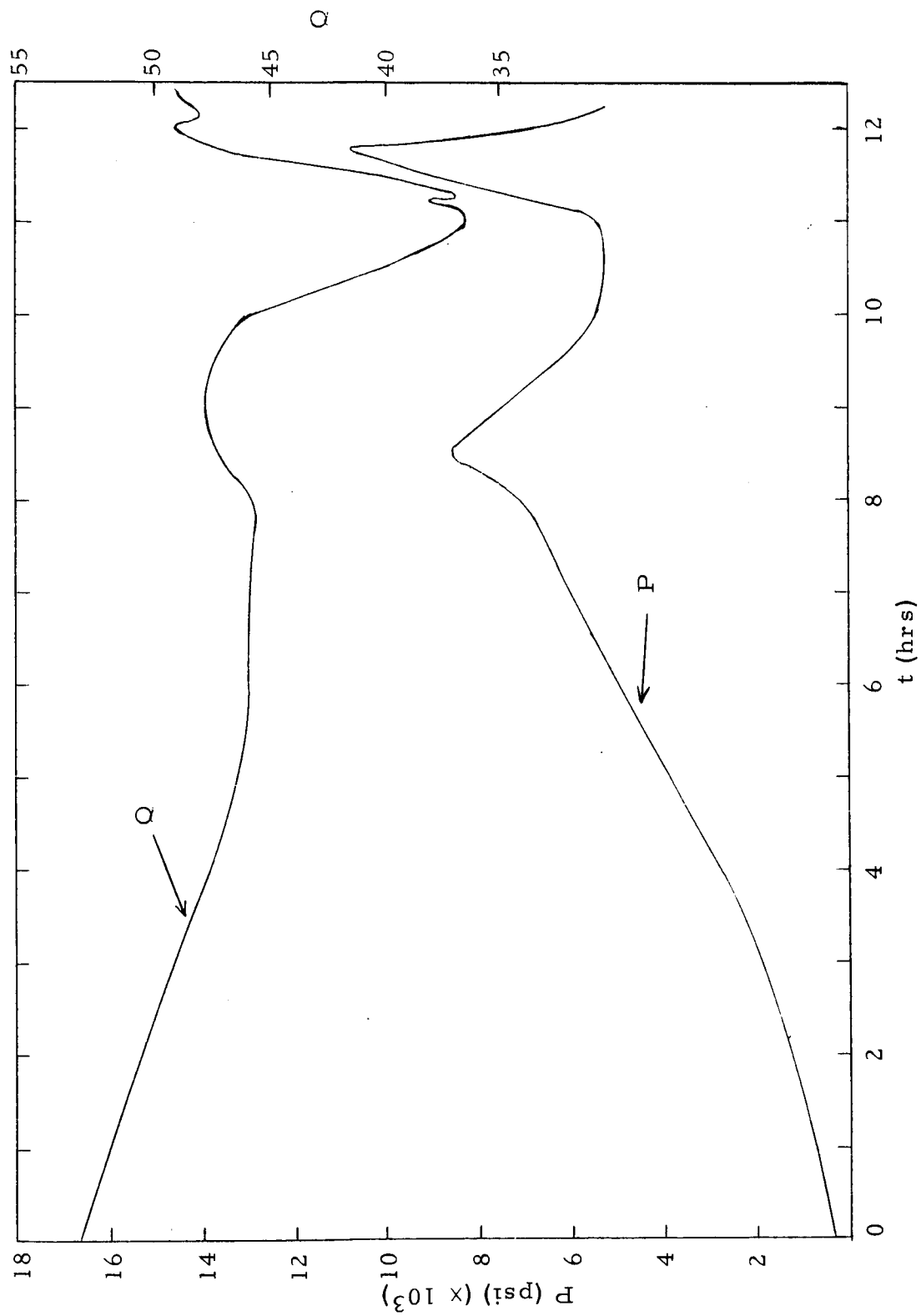


Fig. 30--Sample tube pressure and Q versus time for experiment with Hg

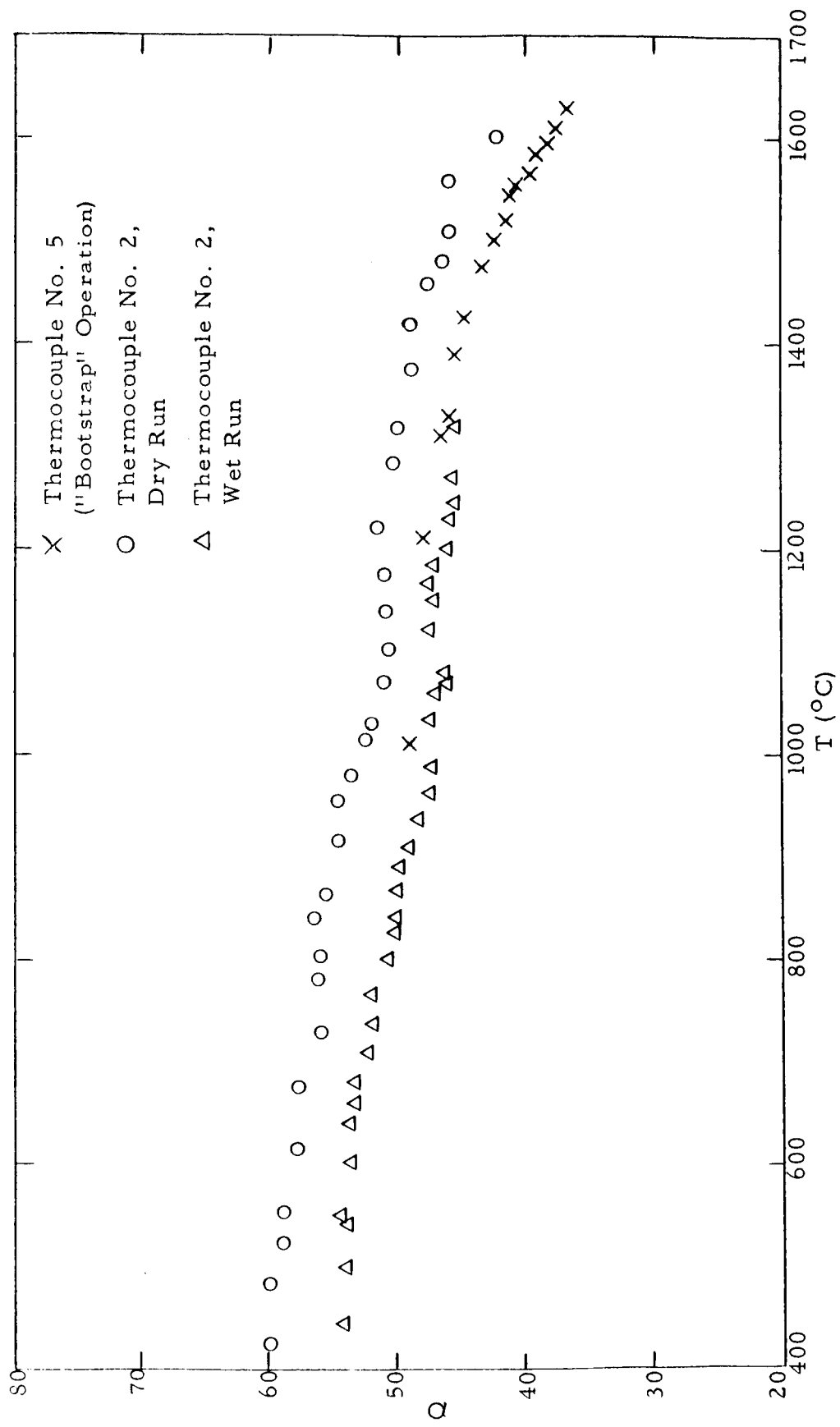


Fig. 31--Q as a function of temperature for pure Hg

Final modifications - To this point, experimental progress continued to be limited by convective heat losses from the autoclave furnace despite various attempts at providing better packing around the sample tube. These losses limited the pressure attainable in experiments with Hg vapor to a maximum of 10,800 psi (~ 735 atm). After the last run, described above, it was finally concluded that the furnace itself must have been packed improperly by the vendor (Marshall Furnace Products). The furnace was dismantled, and inspection revealed large voids in the bubble alumina used by the vendor. After repacking with reagent-grade alumina oxide, a dry run was made in which the pressure reached 13,000 psi (1400°C) with no sign of temperature stagnation in the lower regions of the furnace as observed in previous runs.

The above test run was limited to 13,000 psi by a leak in the pressure gland. This leak was eliminated by sending the head cover to the shops and reworking both the seat and the surface of the Conax head.

3.4.2 Experiments with Hg doped with Cs

After the experiments described above, it was decided to discontinue work with pure Hg and to devote the remaining effort to measurements on Hg doped with a small amount of Cs. The theoretical estimates indicate that this system should show a larger conductivity than pure Hg and it was deemed vital to see if this were indeed true.

Remaining problems of heat losses and pressure leaks were reduced so that the furnace-autoclave system could be operated up to its design limit. During this time, however, the background electrical losses were observed to increase above those shown, for example, in Figure 31. To ascertain the origin of this loss, the powdered alumina used as a packing material was placed in a crucible. The crucible was placed in a furnace and the losses were measured with metal tabs whose geometry factor was roughly the same as the bands on the sample tube. These losses were found to be identical with the recently observed background losses. The background losses persisted, however, even when care was taken to ensure that capacity coupling into the powdered alumina was small. The sample tube was then removed and inserted into an external furnace. Exactly the same losses were observed in this experiment as for the powdered alumina and the background in the autoclave. The losses, converted to resistance values, are shown in Figure 32. It seems possible that some contaminant had deposited itself on both the powdered alumina and the Lucalox tube, giving rise to a surface resistance that is the same for the two materials and that is also less than that of a clean surface. Whether or not this is the case, efforts to reduce the background losses by heating the sample tube and powdered alumina in an oxygen atmosphere were not successful. The run was made with the increased losses.

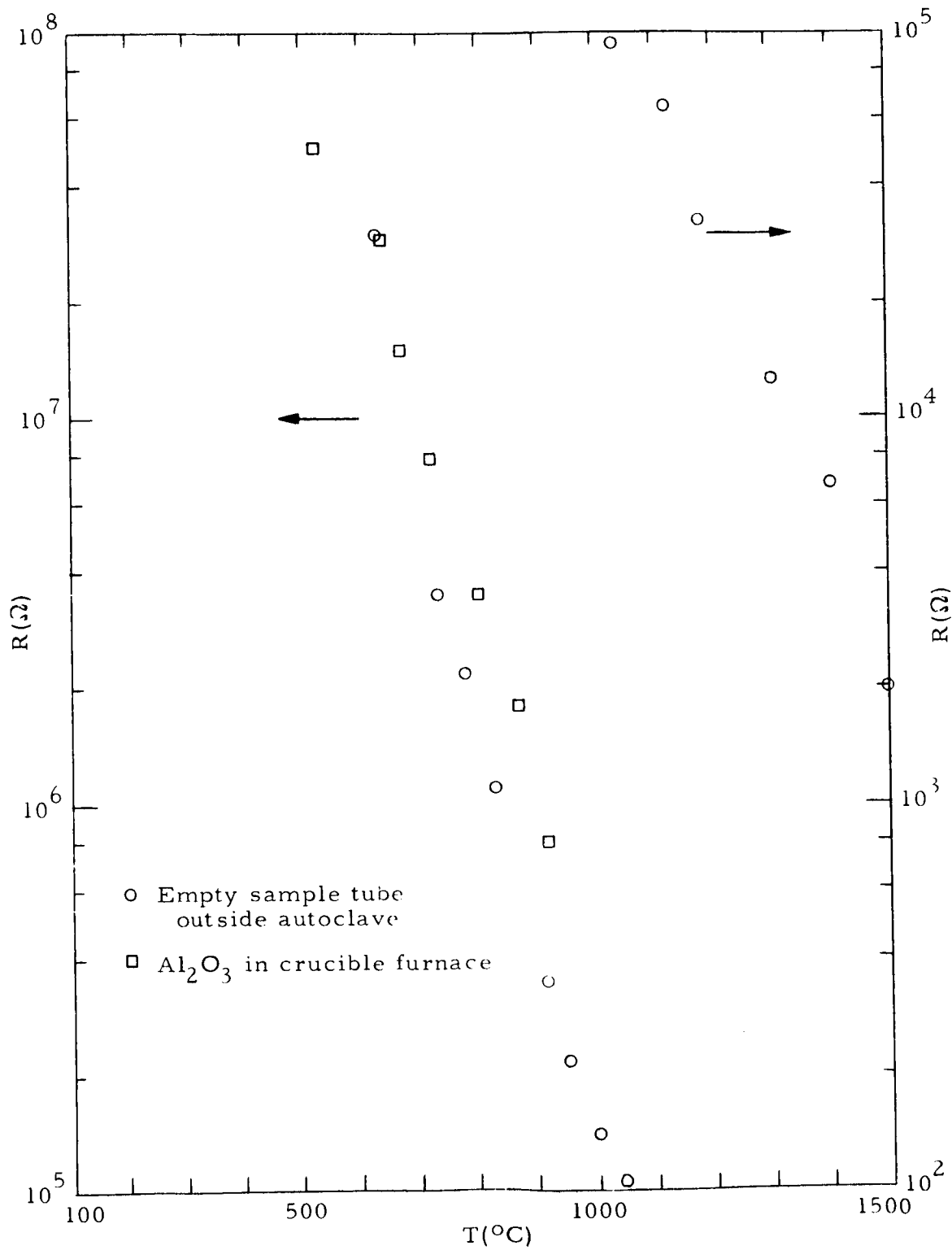


Fig. 32--Resistance of powdered alumina

During this final experiment, an increase in the measured Q was noted, starting at $\sim 1100^{\circ}\text{C}$ and continuing up to $\sim 1400^{\circ}\text{C}$. As shown in Figure 33, the differences in Q (between the wet run and a "dry" run) are barely large enough to be significant. At two points, marked by crosses in Figure 33, the temperature was held constant and the pressure was increased. This increased the Q at the lower temperature but not at the higher. Thus it is not really clear whether the difference is due to the sample vapor or to some other experimental variable that was inadvertently different between the wet and the dry runs. For example, since the dry runs were made at only a few atmospheres, then the change in Q may be due to a relaxation effect in the sample tube itself. However, such an effect has not been studied in Lucalox. Also the temperature profile may not have been exactly the same during the wet run as for the dry run.

There is also evidence that there was some helium leakage into the tube as the temperature was increased. This evidence shows up in the pressure versus temperature data to be presented in Section 3.4.3. The amount of helium is apparently not large but may be sufficient to provide extra scattering mechanisms that would decrease the conductivity. As the temperature was decreased, we know a malfunction occurred that admitted a significant amount of helium into the sample tube. The increase in Q was not present during this part of the run.

We now attempt to see whether the observed behavior is consistent with the type of conductivity outlined in Section 2.2.4 (in particular in Fig. 10). It should be stated that the above terminology was carefully chosen; in our opinion the calculation will not prove that the vapor was conducting but will only show that it is possible that it was. The reason is that the conductivity is not derived from the data, but rather, values of Q are calculated assuming that there exists a conductivity which is given function of pressure. Various other ad hoc assumptions have been made, as will be seen.

The analysis presented in Appendix III indicates that Q will be larger during a wet run only if there is some loss which is coupled into the Q meter by the same capacitance that is coupled to the sample. This model seems somewhat artificial; however, the Lucalox sample tube does have some losses and may be coupled into the bands capacitatively if the bands do not make good ohmic contact (see sketch on page 120 of Appendix III). In this case, the sample tube resistance is broken into two parts: R_4 , the loss from the inner to the outer wall which one would measure if R were zero; and R_3 , the loss which can be associated with the high temperature change in conductance of the sample tube.

As an ad hoc assumption to simplify the analysis, we have, however, assumed R_4 could be omitted from the circuit and thus used Eq. (88), with the left-hand side replaced by Eq. (93). The experimental values of ΔQ

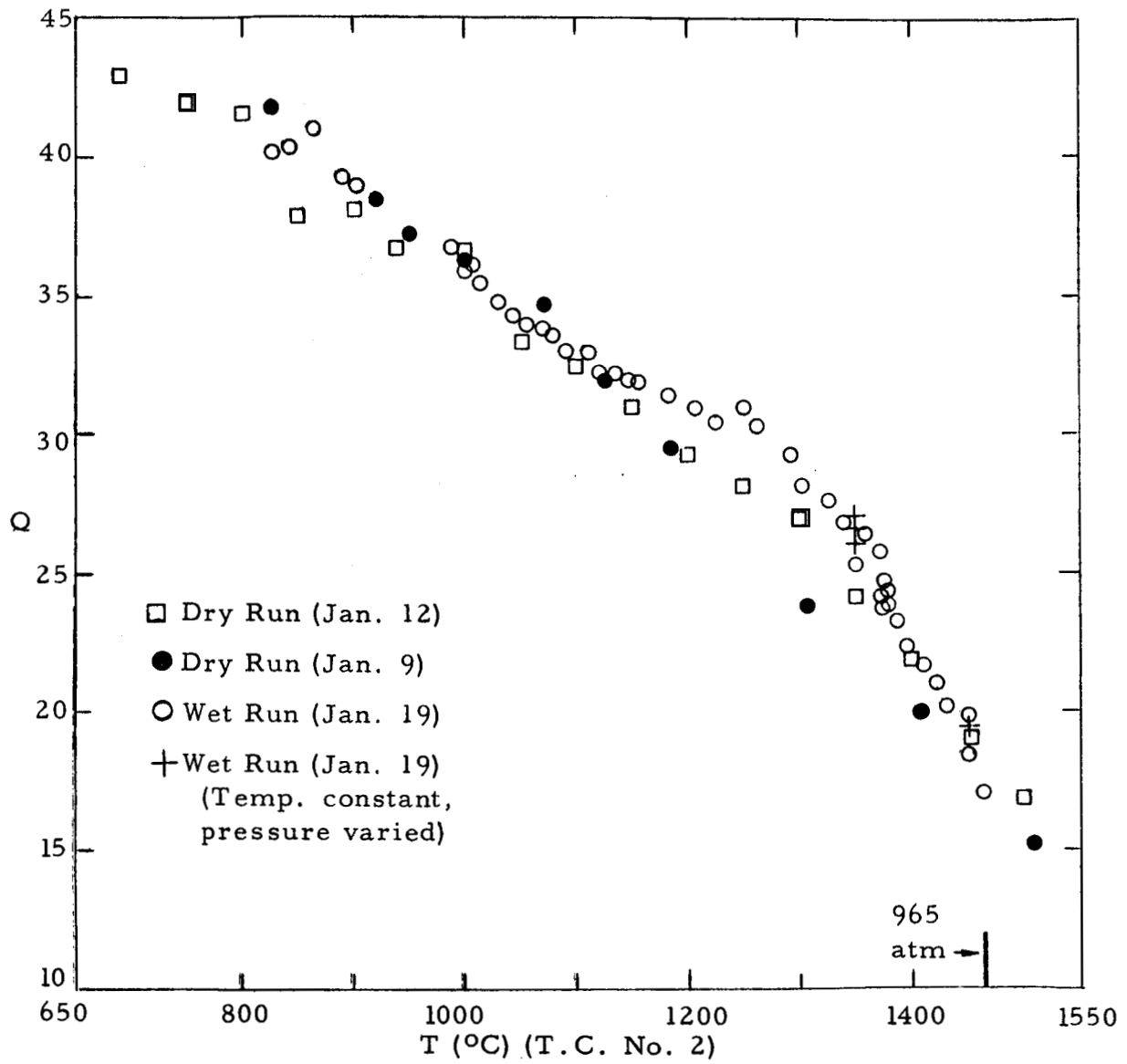


Fig. 33--Q as a function of temperature for 95% Hg:5% Cs

and \bar{Q} are shown in Figure 34 as a function of pressure. These may be combined into the form $\Delta Q/\bar{Q}^2$; it is then our aim to fit this expression as well as possible.

The fit is done in this fashion: At the pressure of 435 atm the measurements are still consistent with $\Delta Q = 0$. This value of ΔQ will be obtained, according to Eq. (88), if R satisfies

$$R_3/R = (\omega C_3 R_3)^2 - 1 \quad (46)$$

at the given temperature and pressure. The resistance R_3 was then assumed to be variable in magnitude but to have a temperature dependence as given by typical background losses shown in Figure 32. The magnitude of R_3 was varied until the calculated values of $\Delta Q/\bar{Q}^2$ agreed, in overall form, with the observed values. Throughout this procedure, R was completely fixed by assuming a magnitude at 435 atm given by Eq. (46), and a pressure dependence consistent with the conductivity shown in Figure 10.

The results of the fit, and the values of the parameters used, are shown in Table V. It can be seen that the main differences between the experimental values and the calculated values are that the calculated values predict a small positive peak at low pressure and that they approach zero relatively slowly. The value of R that is listed can be converted to σ by using the nominal value of 14 cm^{-1} for the geometrical constant: $\sigma = 1.1 \times 10^{-2} \text{ ohm}^{-1} \text{ cm}^{-1}$ (or $1.1 \text{ ohm}^{-1} \text{ m}^{-1}$) at 435 atm. This is about 20 times larger than predicted in Figure 10.

There is one observation that seems to indicate that the higher Q was associated with the vapor and was not just an artifact of the temperature profile. When the temperature was held constant at 1350°C , thereby holding the background losses constant, the Q did rise as the pressure was increased (see Table V). This observation is not pertinent if the background losses (the empty Lucalox tube) are pressure dependent. This rise was small and somewhat irregular, but does seem to be significant.

3.4.3 Vapor pressure measurements

While no large effort was devoted to measuring the vapor pressure of the samples under investigation, the temperature and pressure were taken during the electrical measurements. These values, along with the theoretical calculation from Section 2.1, are shown in Figure 35.

A temperature gradient did exist along the sample tube so in order to know the temperature of the liquid/vapor interface, its position must also be known. The interface position was monitored electrically, with a

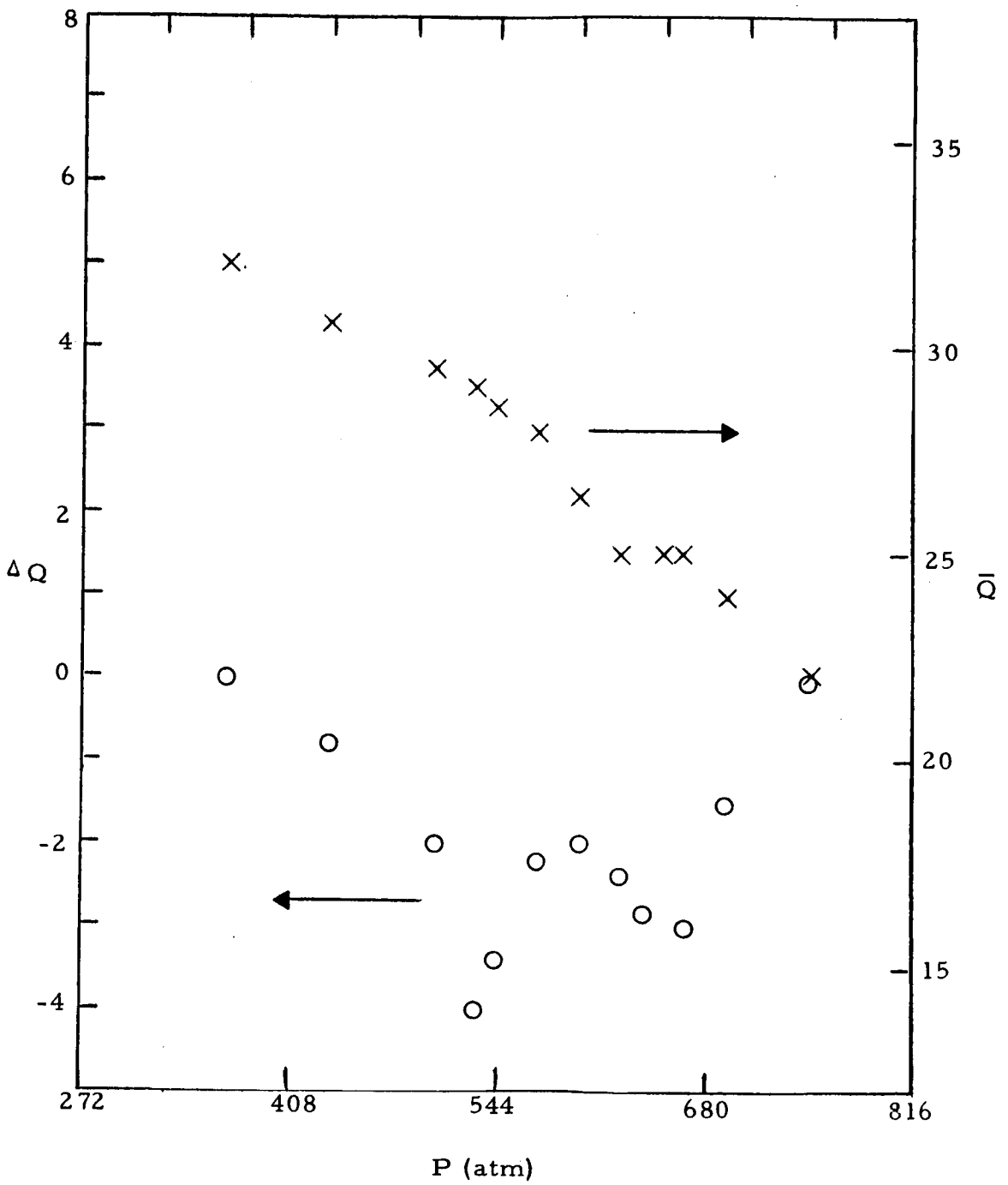


Fig. 34-- ΔQ and \bar{Q} as functions of pressure for 95% Hg:5% Cs

Table V
 VARIATION OF Q FOR 95% Hg:5% Cs*

T(°C) (T. C. 2)	P (atm)	$\Delta Q/\bar{Q}^2 (\times 10^{-3})$	
		Experimental	Calculated
1070	-	0.0	+0.6
1116	368	0.0	+1.2
1178	435	-0.9	0
1220	504	-2.3	-2.9
1248	530	-1.8	-4.1
1260	544	-1.2	-4.2
1300	572	-2.9	-4.0
1325	599	-2.9	-3.9
1350	626	-3.8	-3.7
1350	666	-4.8	-4.2
1375	694	-2.6	-3.4
1400	748	0.0	-3.1
1450	-	0.0	-1.1

* Parameters used in calculations: $C_s = 0.12$ pF, $\omega/2\pi = 14$ Mc,
 R_3 (at 1178°C) = 750 Ω , R (at 435 atm) = 1.25 k Ω , $C_3/C_0 = 2.4 \times 10^{-2}$

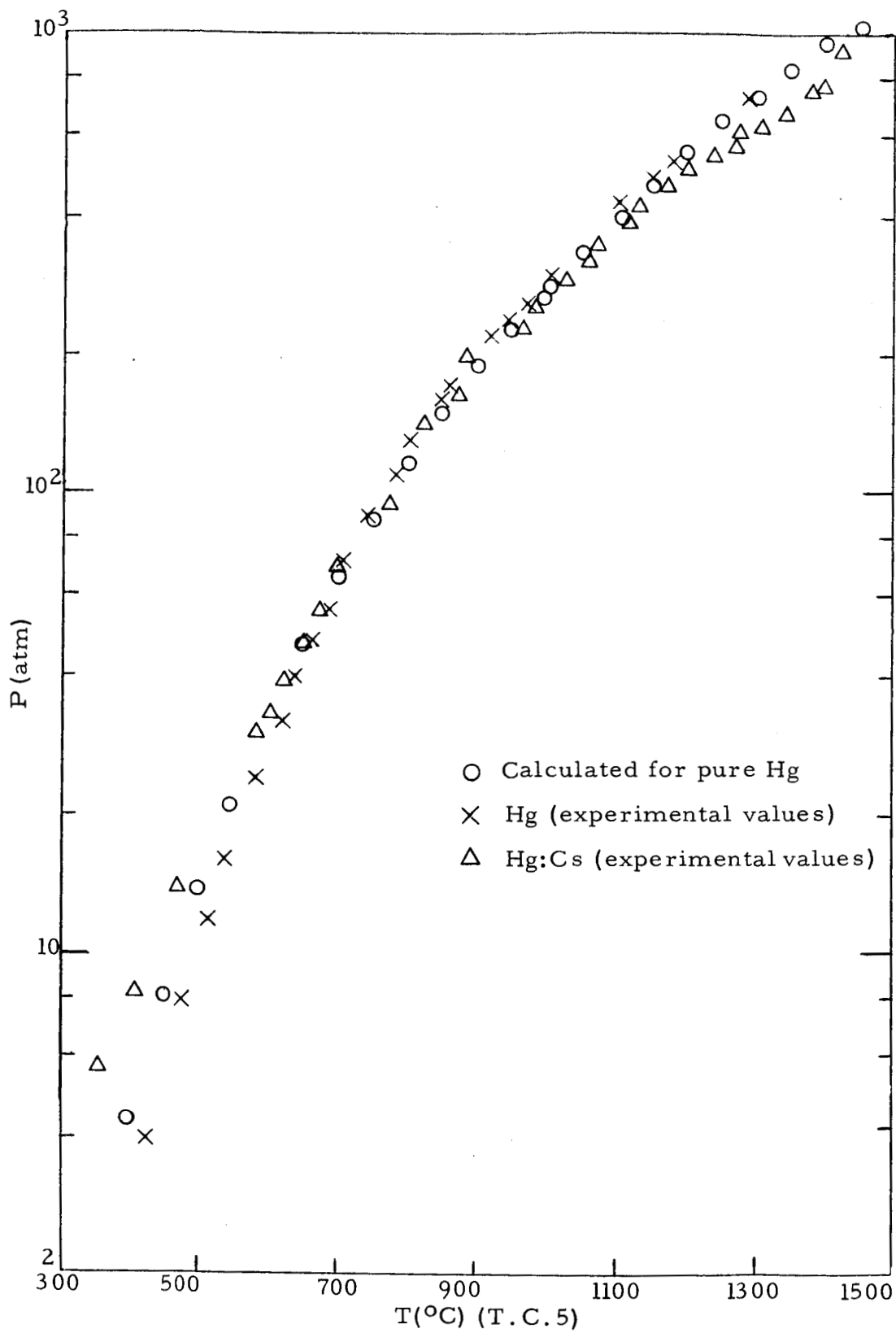


Fig. 35--Vapor pressures of pure Hg and 95% Hg:5% Cs as function of temperature

sensitivity that fell off as the temperature increased. For this reason, the head may be below the region of T. C. 5, which would explain the deviation during the Hg-Cs run. Raoult's law, Eq. (41) of Section II,¹³ would predict a 5 percent deviation, far less than the deviation observed. Some scatter at low pressures is understandable because the accuracy of the high pressure gauges is perhaps two atmospheres.

The fact that the observed pressure is too high at the lower pressures during the Cs-Hg run is also attributed to the fact that a small amount of He was observed to diffuse into the sample chamber at low temperatures (perhaps through the O-ring seal). The rate was apparently small enough to cause the partial pressure of He to be less than a few tens of atmospheres, however, since the Cs-Hg run recrosses the theoretical curve at around 200 atmospheres. How much these foreign atoms may lower the conductivity is not known.

In conclusion, the van der Waal's law seems to predict the vapor pressure of Hg to the accuracy at which measurements were made.

V.

RECOMMENDATIONS

On the basis of this work, one can not recommend any engineering evaluation of devices based on conductivity of dense vapors. On the other hand, in view of the utility of such devices, one can recommend further study of the dense vapors.

It is crucial to continue work on Cs-Hg alloys, with somewhat improved technique to be mentioned below, in order to see if a conductivity does exist. Phosphorus, in view of its modest critical temperature and pressure, would greatly simplify future device engineering and, for this reason alone, warrents further study.

Pure Hg holds great scientific interest, however, it may not be worth a great deal of attention from a strictly technological point of view.

If these systems are studied, it is recommended that the resistance of the sample tube be increased by decreasing the wall thickness, thereby increasing the electrical sensitivity. It will also be helpful to decrease the tube o. d. to reduce losses capacitively coupled from the heated furnace walls. The generous sample tube dimensions used in this work were thought to be necessary to provide mechanical strength, however, the technique of maintaining a small pressure differential between the sample tube and autoclave appears to be so successful that this strength is not needed.

For phosphorous, a sample tube other than quartz (chosen here partly because it can be relatively easily worked with a consequent saving in time) must be used. Lucalox again appears to be useful. Also either all of the sample must be kept above the melting point (590°C) or else a different technique for pressure transmission must be used.

IV.

CONCLUSIONS

Various experimental problems prevented a thorough investigation of the vapors of all of the materials which offer hope of being conductive at reasonable pressures or suggested as good possibilities. However, conclusions which can be drawn concerning those materials (P, Hg, and Hg doped with Cs) on which experiments were performed are summarized below.

Phosphorus - A chemical reaction apparently occurred between the phosphorus and the quartz sample tube, giving rise to a material with a conductivity large enough to mask any conductivity of the phosphorus vapor $< 7 \times 10^{-2} \text{ ohm}^{-1}/\text{m}$. Thus, although the experiments were by no means conclusive, the conductivity of the phosphorus vapor appeared to be very small below 85 atm.

Pure Hg - Theoretical estimates showed that pure Hg may be disappointing as a conductor because the two valence electrons in the atomic s level may form a filled, non-overlapping band and thus exhibit the small conductivity characteristic of an insulator. The highest pressure achieved during an experiment with Hg was ~ 735 atm, significantly below the design limit of the autoclave because various malfunctions were not yet corrected during this run. No evidence of conductivity was seen, indicating a conductivity $\leq 10^{-2} \text{ ohm}^{-1}/\text{m}$.

Hg doped with Cs - A 95% Hg: 5% Cs alloy was measured up to $\sim 1460^\circ\text{C}$ and 14,180 psi (~ 965 atm). The electrical sensitivity during this run was not good, but a small deviation from previous "dry" runs was noted. These deviations are barely significant and, furthermore, are anomalous in that they indicate a larger Q with the vapor present. One can assume a model for the background losses such that the observed behavior is consistent with a vapor conductivity of an amount about 10 times the theoretical estimate, which was $\sim 0.2 \text{ ohm}^{-1}$ at the pressure range where the anomaly was largest. This model appears to be an ad hoc assumption that is not based on independent evidence. Helium in an unknown amount, but presumably less than around 30 atmospheres, was present in the sample tube during this run. This would presumably lower the conductivity to some unknown extent. Thus, for this sample, there is no conclusive evidence for conductivity.

VI.

PERSONNEL

Engineering and scientific personnel who have contributed to this program are listed below:

- (a) S. W. Kurnick, Staff Member, Experimental Physics, has served as Principal Investigator.
- (b) J. F. Colwell, Staff Member, Theoretical Physics, has performed the theoretical analysis.
- (c) M. O. Stern, Staff Member, Experimental Physics, has computed the vapor pressure and densities for various systems and assisted in conducting experiments.
- (d) C. E. Mallon, Staff Associate, Experimental Physics, has assisted in apparatus design and in conducting experiments.
- (e) R. Durstenfeld, Staff Member, Mathematics and Computing, has contributed to computer programming and mathematical analysis.
- (f) B. W. Roos, Staff Member, Mathematics and Computing, has contributed to computer programming and mathematical analysis.
- (g) J. E. Gratteau, Staff Associate, Mathematics and Computing, has assisted in setting up programs for the digital computer.
- (h) E. Metzner, Staff Associate, Mathematics and Computing, has assisted in setting up programs for the digital computer.
- (i) M. J. Gerber, Research Assistant, Mathematics and Computing, has contributed to the programming for the digital computer.
- (j) W. J. Dougherty, Research Assistant, Engineering, has assisted in apparatus design.

REFERENCES AND FOOTNOTES

1. Greene, M. P., and W. Kohn, Phys. Rev. 137, A513 (1965).
2. Kubo, R., J. Phys. Soc. of Japan 12, No. 6, p. 570 (1957).
3. Bonch-Bruевич, V. A., and S. V. Tyablikov, The Green Function Method and Statistical Mechanics, (North Holland Publishing Co., Amsterdam, Holland, 1962).
4. Naiditch, S., "Electrical Conductivity of Sodium-Ammonia Solutions," presented at Colloque Wehl, Universite Catholique, Lille, France, June, 1963.
5. Birch, F., Phys. Rev. 41, 641 (1932).
6. Ecker, G., and W. Kröll, Phys. Fluids 6, 62 (1963).
7. Weatherford, Tyler and Ku, WADD - TR - 61 - 96 (1962).
8. Shapiro and Meisl, GE Report R 60 FPD 358 - A (1960).
9. See any standard text on thermodynamics, such as Zemansky, Heat and Thermodynamics.
10. Ziman, J. M., Electrons and Phonons, (Oxford-Clarendon Press, 1960) Sec. 1.5.
11. Mott, N. F., Phil. Mag. 6, 287 (1961).
12. Kohn, W., Phys. Rev. 133, A171 (1964).
13. Knight, B. W., and G. A. Peterson, Phys. Rev. 132, 1085 (1963).
14. See Ref. 10, Sec. 71. and 10.4.
15. Cusack, N., and J. E. Enderby, Proc. Phys. Soc. (London) 75, 395 (1960).
16. Robinson, L. B., Phys. Rev. 127, 2076 (1962).
17. Shockley, W., Electrons and Holes in Semiconductors (D. van Nostrand Co., 1950), p. 245.
18. See Wilson, A. H., Thermodynamics and Statistical Mechanics, (Cambridge University Press, 1957), p. 413; or any standard text on chemical thermodynamics.
19. Atomic Energy Commission and Bureau of Ships, Department of the Navy, Liquid-Metals Handbook, NAVEXOS P-733 (Rev.) R. N. Lyon, Ed-in-Chief, 2nd ed. (Rev.). (U.S. Government Printing Office, January 1954), p. 79.

REFERENCES AND FOOTNOTES (Cont' d.)

20. Latter, R., Phys. Rev. 99, 510 (1955).
21. Slater Functions are exponentials times r to some (positive) power and are somewhat more appropriate for describing atomic behavior. See, for example, Lowdin, P. O., and K. Appel, Phys. Rev. 103, 1746 (1956).
22. Phillips, J. C., and L. Kleinman, Phys. Rev. 116, 287 (1959). See also B. J. Austin, V. Heine, and L. J. Shaw, Phys. Rev. 127, 276 (1962).
23. Gupta, S. R., and G. J. Hills, J. Sci. Instr., 33 313 (1956); and R. Calvert et al., J. Phys. Chem. 62, 47 (1958).
24. Zimmerman, J. E., Rev. Sci. Instr., 32, 402 (1961).
25. Weingarten and Rothberg, J. Electrochemical Soc., 108, 167 (1962).
26. ASD-TR-61-628, Part II, "Studies of the Brittle Behavior of Ceramic Materials" (April 1963).
27. van Wazer, J. R., Phosphorus and Its Compounds (Interscience Pub., New York, 1958). Vol. I, Chemistry, p. 113.
28. Teltow, J., Ann. Physik (6) 5, 63 (1949).

APPENDIX I

THE ELECTRONIC AND THERMODYNAMIC
NATURE OF DENSE VAPORS

by

J. A. Krumhansl[†]
(Consultant)

[†]Professor of Physics and Director of the
Laboratory of Atomic and Solid State Physics,
Cornell University, Ithaca, New York

SUMMARY

To discuss the electronic properties of dense vapors at moderate temperatures, the systems should be envisaged as falling into two categories:

- a. Single species or "pure" systems which are either insulating or metallic, depending on density (pure crystals in solid state terminology),
- b. Mixed systems which may take two limiting forms, i. e., doped insulating vapors (semi-conductors) or alloys.

The nature of matter at densities between 1 and 10 percent of that of normal solid or liquid metals is a most important problem. On the basic side, it is of the essence of a "many-body" system where electron correlations play an essential role in determining both the equilibrium and transport properties. An increasing amount of theoretical attention is currently being devoted to this subject.

Technologically, the possibility of achieving essentially metallic conductivity at fractional densities of solids or liquids is of great potential importance both in MHD and thermoelectric systems, provided it is possible to attain the conditions at temperatures of 10^3 to 10^4 °K.

From current considerations, we conclude in the present discussion that the electrical properties of "pure" systems, such as alkali metal vapors, will likely be those of insulators until the density becomes so high that a discontinuous first order phase transition to a condensed metallic state of essentially normal solid density takes place. Experiments should provide for the detection of phase separation.

Several existing theoretical calculations of the electronic conductivity of single species systems are believed to be qualitatively and quantitatively unreliable in the range of potential interest (1 to 10 percent of solid density) because they do not incorporate electron correlations properly at low density.

By contrast, mixed (doped) vapor systems, consisting of a majority species whose density is well below that which would lead to an insulator-metal transition and a minority species which can donate electrons to the majority species, appear to be important both scientifically

and technologically. Suggested combinations include Hg as the majority species, with Cs as the minority "donor", and either Se, P, or As as a majority species with halogens or alkali metals as donors. It is desirable that the majority species become a negative ion upon accepting a donor electron, since a negative ion will have a large "electron radius" and thus lend itself well to electron transfer by tunneling.

The conducting behavior of mixed systems is likely to be more accessible to proper theoretical treatment by methods similar to those used for hopping and impurity band conduction in semi-conductors.

It is quite possible that mixed systems will be found to have considerable technological value, either in MHD or thermoelectric applications. Both practically and scientifically, it is believed that this is a most fruitful area for study, where the current state of only-qualitative understanding represents a serious inadequacy in the basic foundation which should exist for a technology such as energy conversion.

Finally, it should be remembered throughout the present discussion that the transition from the insulating solid to a metallic solid, which is due to overlapping bands, occurs at much higher densities than those under consideration here. There is no relation between these transitions and the ones discussed herein.

1. INTRODUCTION

This is not a report of completed work on a well developed subject. It cannot be, for the subject is only in a preliminary state. Thus, instead of providing definite answers, we will define the nature of the questions which should be asked, particularly of theory. The writer believes it to be a most interesting topic about which all too little is known; the experiments will be difficult, but the reward can be the deeper understanding of the physics of matter under most unusual circumstances.

Our purpose is to examine the probable behavior of dense vapors or low-density liquids (i. e., matter in a form with a density of perhaps 1 to 10 percent of normal solid or liquid density). We restrict consideration to temperatures less than about 2500°K , above which direct thermal ionization effects will occur. Well above that temperature one makes a transition to high temperature plasma ($10^4 - 10^5^{\circ}\text{K}$) where the electronic considerations of crucial importance in the present problem no longer play a role.

The immediate interest in this subject derive from the specific objective of examining the electrical conductivity of dense vapors at high pressures and intermediate temperatures to determine their possible application to MHD systems.¹ An early appreciation of the interesting possibilities was due to Miller.² However, the questions which must be answered to understand the experiments and delineate the range of applicability are of much broader intrinsic importance.

As a basic scientific problem, dense vapors have not received nearly as much attention as the limiting dense solid or dilute vapor form, particularly for elements which are metallic in their condensed phase. The reasons are apparent in regard to both experimental and theoretical aspects. Experimentally, high pressures and difficult materials problems arise. Theoretically, neither in constitution nor transport properties can we apply the time-honored and fortuitous self-deception embodied in the one-electron approximation and the Boltzmann transport equation.

Recently, a significant development of interest in the theoretical aspects of this problem was made possible by the introduction of proper many-electron descriptions of the state of such matter³⁻⁶ as well as generalized techniques for describing hopping and tunneling transport in such systems when the Boltzmann equation is not applicable.⁷⁻¹⁰ Thus,

discussion of this subject involves an essential departure from the traditional methods of either solid state or plasma physics, and is therefore of some considerable scientific interest.

We have already referred to the technological motivation in studying this subject. In examining this potential use of conducting vapors, it occurred to the writer that some care must be taken to re-examine the validity of the basic MHD constitutive equations, since the mode of conductivity envisaged in dense vapor systems is rather different from the standard kinetic model of a gas of electrons, mixed ions, and neutral atoms.

In fact, it appears that the point in question will not be troublesome practically. However, for the record, it may be worth discussing anyhow. The defining equations for MHD converters¹¹ comprise several conservation conditions and the constitutive relation between current and fields. These relate hydrodynamic quantities to electrical (electronic and ionic) properties. The essential point which concerned us can be illustrated using the energy-conservation condition

$$\rho u \left[d/dx \left(\frac{u^2}{2} + c_p T \right) \right] = j \cdot \underline{E} \quad (47)$$

The left side of Eq. (47) is hydrodynamic and refers to the gas kinetic translational and thermal energy of the fluid, and the right side is electrical. More particularly, the current is carried quite predominantly by electrons $j_e \gg j_i$; thus, it is apparent that for Eq. (47) to hold, the electrical energy supplied by the electrical field to the electrons must be transferred to ion and atom translational motion. In ordinary electron-gas conduction, the electron does lose its electrically-gained energy by collision with the ions and atoms¹² and, as long as the system is large in size compared to the mean free path, the conservative condition is valid. In the present case, electronic conduction was to take place by tunneling from one atom to another; so, in principle, it might be possible for such electron transfer to take place without transferring kinetic energy to the ions. And this is just what would happen in the limit of a perfectly-ordered solid. But we know that electron mean free paths are usually quite short in any real system, so it can be assumed that, again as a result of disorder scattering, the electrons will transfer their transport energy to the ions and electrons. Still another example of the possible failure of Eq. (47) would be the (unlikely) production of significant electroluminescence in electron tunneling transport; such radiation energy would not go into the fluid motion.

We turn now to some remarks on thermoelectric applications of conducting vapor systems. The parameter which limits the efficiency of all known solid-state systems is the lattice thermal conductivity, which is an irreversible parasitic production of entropy.¹³ Dense, mixed vapor systems may attain thermoelectrically-desirable conductivity and thermoelectric power without attendant high lattice thermal conduction (it will be replaced by gas kinetic heat flow). In the writer's opinion, this is at least as important and potentially-practical an aspect of study as is the potential MHD usage.

Finally, to lend further perspective to any potential technological applications, it must be remembered that many of the properties discussed here vary significantly with temperature. Hopefully, the advantages are to be sought in the lower temperature region (750 - 2000°C) by using high pressures.

2. ELECTRONIC BEHAVIOR OF PURE SINGLE-SPECIES MATTER AT LOW AND HIGH DENSITIES

It has already been mentioned that there is a fundamental qualitative difference between the properties of a low-density potentially-metallic species (e. g., atomic hydrogen, monovalent alkali metals, etc.) and its high density form. (Substances which form insulators, with filled bands, at normal solid densities are neither of concern nor interest in the present discussion.)³ This essential and conceptual difference is as follows: If the one electron (Hartree-Fock) approximation were valid, we could, in principle, describe the valence electrons in a dilute alkali-metal gas by Bloch-like extended orbitals, half filling a "band" or continuum of states. Though the width of this band would decrease with decreasing density, the lowest lying excited states above the ground state would still, in principle, lie infinitesimally close and the behavior would be metallic in nature in all densities.

This one-electron view is substantially wrong, in essence, as Mott,³ Hubbard,⁵ and Kohn⁴ have pointed out. Correlation effects, which become significant in the low density limit when electrons are placed in the same atom, fundamentally modify the description. The appropriate wave functions at large atomic separations really localize electrons in disconnected regions of configuration space, and the ground state will be detached by a finite energy from a continuum of excited states. It is not a matter of degree, but it is essential that the configuration should be that of an insulator.

As the density is increased, a sudden transition to a quite different configuration is expected--namely, the metallic state described by the extended orbitals referred to above.

The essential nature of the problem is covered by the above remarks but additional physical feeling for the situation can be obtained from Mott's article,³ whose essential points we restate. Consider an alkali metal gas which we will compress through a range of densities, which might take us continuously up to solid or liquid densities. At low densities we expect the atoms to be described by atomic orbitals which place exactly one valence electron on each atom. However, this complete localization cannot be precisely correct and we must examine the nature of electron transfer and exchange. There are two competing factors:

- a. When two atoms are brought together, and assuming an "atomic orbital" (AO) basis, there is possible an electron transition from the m-th to n-th atom which is quantum-mechanically specified by an overlap potential-energy matrix element, $m|v|n$, (v_{mn} for brevity). We do not wish to define this quantity too precisely here, nor do we need to do so for the purpose at hand. It is this interaction matrix element which leads to molecular binding, or relates to the band widths in a tight binding description of solid-state electron energy levels. In either of these cases, its magnitude is several electron volts at normal molecular and atomic densities. As the density decreases, this overlap integral falls off rapidly, usually exponentially.¹ To summarize, this overlap matrix element between atomic orbitals can produce delocalization of the electrons by interatomic transfer.

- b. When an electron is envisioned as transferring from the m-th to n-th atom, without allowing the other electrons on the n-th atom to "make way" by transferring in turn, a substantial amount of "correlation" energy must be provided. In essence, in the very low density limit, a positive and negative ion are produced requiring an amount of energy $I-A$, where I is the ionization energy and A is the electron affinity for formation of a negative ion. This quantity ($I-A$) is typically several eV in pure systems, and may depend also on the magnetic state which results. In any case, this effect opposes preceding factor (a) and tends to localize electrons in a quota of just one per atom (in the present case), and also leads to a ground state detached by finite energy from the excited state.

The formalization of this state of affairs may be embodied in a Hamiltonian^{4, 5} written in second quantized form with an AO or Wannier function basis. A reasonable approximation is to include only the correlation correction for electrons on the same atom. Since we will not use the equations specifically here, we refer to references 4 and 5 for further details.

Detailed calculations may differ, but there is no disagreement on the general behavior to be expected. At low densities, factor (b) dominates and the system is truly insulating. At higher densities, many-electron (transfer) effects become important and can relieve the electron excess on any one atom by compensating transfer. Mott's criterion is that this takes place when v_{mn} becomes comparable to $I-A$, whereas a dramatic change to metallic character takes place. This criterion can hardly be wrong by an order of magnitude, though much remains to be done theoretically to

develop a relevant and tractable model; however, Mott's criterion allows us to draw some conclusions about the likely conditions for achieving the metallic transition; namely, pure vapors would have to be very dense indeed (an estimate is 10 percent of solid densities) before transition to the metallic state occurs. This follows from requiring $v_{mn} \approx I-A \approx 1$ eV. However, it must also be noted that we have no way of estimating how density fluctuations, which could be significant in the present situation, will affect multiple transfer. This, of course, is the nastiest part of the problem. None the less, it is the writer's view that, in any case, the transition can take place only at such high densities that far more important questions of thermodynamic stability dominate the situation. These questions are discussed in Section 5.

Young⁶ has estimated the critical densities for the metallic transition in the alkali metals to be about 20 percent of solid densities. The pressures necessary to achieve such densities in the gaseous state may well be 10^5 atm.

From these considerations, it follows that computations of conductivity which do not specifically take electron correlation effects into account¹ will be quite inapplicable to vapors of single species at low densities, i. e., densities less than, say, 10 percent of solid and lower densities. We comment further on this matter in Section 4.

3. MIXED OR "SEMI-CONDUCTING" VAPOR SYSTEMS

We have developed the view that in a "pure" vapor, very high densities will be required for a transition from the insulating vapor state to a metallic vapor state. In Section 5, even the thermodynamic stability of such a state will be shown to be questionable. It is worth reconsidering an alternative possibility, therefore. A natural analog to a solid state system would be the doped insulator or "semi-conducting" vapor.

By semi-conducting vapor we mean that a majority species is the principal component of the vapor, which also includes a minority component whose function is either to donate or accept an electron from the majority component. We examine first the nature of the conducting process, next the criteria for desirable combinations, and third, a few particular combinations.

The problem of describing and analyzing electron transfer at low densities is much simpler now. Presuming a low concentration of donors or acceptors, electron transfer in donor systems takes place by interchange of an electron from one majority atom to another and merely amounts to changing the identity of the negative ion (or positive ion in the case of acceptor systems). Thus, there is no net change in correlation energy; the intra-atomic correlation has been accounted for in forming the ions in the first place and does not alter when the identity of the ion is simply interchanged. Thus, there is conceptual justification in using one-electron models for conductivity. For these there exist two limiting cases:

- a. The band model for a system with a small carrier concentration (of either electrons or holes), including impurity bands in compensated semi-conductors; or
- b. An atomic model with transport by hopping from one site to another.

An application of the former approach is contained in Reference 1, and we believe it to be appropriate, to a degree, in the case of doped insulators (but not for pure systems). The latter view is developed in various discussions of hopping and tunneling conductivity in dilute or narrow-band semi-conductors.¹⁴⁻¹⁶ In either case, the density dependence of overlap potential matrix elements, which determine electron transfer, can be estimated with some order of magnitude confidence in

the absolute and relative trends among possible mixtures. We will return to the transport problem in greater detail in the next section.

The criteria for useful combinations follow from the above discussion of mechanism, supplemented by some obvious physical chemical considerations:

- a. In a solid there is not too much a priori difference between donor and acceptor systems; this is not true for vapors. Electron transfer is to take place at low densities by interaction transition due to overlap potentials. Negative ions are much larger than positive ions, so that for a given density, electron transfer between a negative ion and the same-species neutral is far more likely than in the positive ion case. Thus, donor systems are overwhelmingly preferable.
- b. It is apparent that a minimum energy should be required to ionize the donor to transfer an electron to the majority species. Furthermore, the majority species should be capable of forming stable negative ions. Thus, we wish to minimize $(I_d - A_m)$, where I_d is the donor ionization energy, and A_m is the majority electron affinity. (Note that in the single species system, the "intrinsic activation energy", I-A, referred to ionization and electron attachment of the same species and is certainly substantially larger than that obtainable by judicious combinations envisaged here.)
- c. In addition to work in the vapor phase, we desire a majority species with as high a vapor pressure as possible, and which is chemically compatible with a minority donor which also has sufficient vapor pressure to be present in reasonable concentration.

These are the general conditions which must be met. Specific data relevant to these criteria must be obtained from a variety of sources. Electron affinities and ionization potentials are obtainable from the literature.^{17, 18} Vapor pressure data may similarly be calculated from thermochemical data; a particularly useful compilation for solid and liquid elements is given by Honig.¹⁹

It must be emphasized that to proceed significantly beyond our present qualitative and semi-quantitative knowledge, many difficult experiments are needed. Thus, though a number of possible mixed systems should be considered, we restrict our remarks to a few illustrations.

One combination which might be regarded as the prototype of the "donor" system is an "insulating" Hg vapor doped with Cs; that is, Hg is the majority species. The following data are relevant. At 643°K, Cs has a vapor pressure of 10 torr, while Hg has a vapor pressure of 10^3 torr; this represents a relative donor concentration of 1 percent, though at a relatively low pressure. At 980°K, Cs has a vapor pressure of 10^3 torr (1.32 atm), while Hg has a pressure¹ of approximately 60 atm. Thus, the donor concentration of Cs would probably be adequate. With regard to electronic properties, the ionization potential of Cs is 3.87 eV, and the electron affinity of Hg to form Hg^- is 1.79 eV; the difference $I_d - A_m = 2.08$ eV is significantly less than any single-species ionization potential. Chemically, it is likely that Cs and Hg will be compatible. This appears to be a promising system for study.

Metallic negative ions such as Hg^- are an exception: they are expected to be smaller in size than molecular negative ions or the negative ions formed from elements from the right hand side of the periodic table. Examination indicates that materials such as Se, S, P, As, Cl, CN, and I all have reasonably high vapor pressures and also form negative ions. The majority of these are known to have high electric polarizability, indicative of large size. However, the choice of a donor is not obvious, since alkali metals, for example, will likely form polar molecules.

Much of the chemical physics of this subject is unknown, and in concluding this section, we emphasize the need for appropriate application of chemical thermodynamics in choosing mixed systems.

4. ELECTRON TRANSPORT IN DENSE VAPOR SYSTEMS

An attempt to analyze electrical conductivity in systems such as those discussed herein is a most interesting experience. It seems to illustrate how specialized the basic premises on which the great bulk of conventional transport theory is based really are.

The conventional method of describing electron transport is by means of a statistical theory. It is based on a one-particle distribution function (reduced from an N-particle), referring to a basis description (free particles or Bloch functions in a crystal) whose states are eigenstates of the electron current operator, and considers scattering to be a non-essential part of the transport process, except insofar as it is limited thereby. In addition to these ingredients, the distribution function itself must be obtained from a defining integro-differential equation (Boltzmann) which has validity only for a continuum of spatial and momentum states. With the origin of transport theory in gas kinetic problems, and with the variety of plasma and electronic systems for which the idealization to these conditions is not a troublesome approximation, this is not surprising.

In contrast to the preceding, electron transfer in high-density vapor systems seems to exemplify the most opposite kind of situation. Except at the very highest densities, the appropriate basis states are atomic orbitals which carry no current. The basis states do not form any simple continuum. In "pure" single-species systems, electron correlation must play an essential role. Thus, no one-particle distribution function obtained from a Boltzmann equation is applicable. Furthermore, scattering from one atomic state to another is an essential part of the transport process itself. Finally, the spatial distribution and correlation of the atoms which carry the electrons also play an essential role.

Fortunately, during the past few years there have been many developments in transport theory, particularly in many-body solid state theory, which may be used with greater generality. Principally, these comprise the general description of transport based on correlation functions⁷ and the development of Green's-function methods for finding these correlation functions, and are general enough to handle either the limiting case of nearly free particles,^{8, 9, 20, 21} or the opposite case of tightly bound electrons¹⁴. Of course, these methods are only manageable in the regime of linear response theory (ohmic conductivity).

It should be stated immediately that we have not applied these methods yet in detail to the vapor systems under discussion. Rather, the remarks just made are intended to call attention to the fact that transport calculations based on free-particle or Bloch-function states can only be valid in the limit of essentially solid densities and, just as in discussing the electronic constitution, must also fail in an essential qualitative manner for vapors. This situation has been encountered in narrow band solids, and in some semi-conducting systems when conduction takes place by hopping from site to site.^{15, 16, 22, 23} (In the case of semi-conductors, the transfer matrix elements are usually not the simple potential overlap terms, but also contain phonon contributions.)

The essential steps necessary to develop a proper theory now follow. First, according to Kubo's method,⁷ we must compute an appropriate transform of the current-current correlation function; this may be understood qualitatively by recognizing that an applied electric field couples energy into the system by acting on moving charges, and we subsequently also observe the effect by measuring the current associated with this charge distribution. Thus, (for an isotropic medium) the static conductivity is

$$\sigma = \lim_{s \rightarrow 0^+} \int_0^{\infty} dt \int_0^{\beta} d\lambda \exp(-st) \left[J(-i\hbar\lambda), J(t) \right] \quad (48)$$

where the meaning of the symbols is standard, and the review article by Chester¹⁰ or the paper by Matsubara and Toyozawa¹⁴ should be consulted for details. To use this equation, we need the equations of motion for the current operators $J(t)$, which are in Heisenberg representation.

To determine these J , the method of Green's function may be employed.⁹ We cannot now make an extensive excursion into the details, but can simply point out what seem to be the current important or unresolved aspects. The appropriate basis representation for the vapor case would be atomic orbitals or Wannier functions. The significant features will then be contained in a Hamiltonian, written in second quantized form using creation or annihilation at the i^{th} or j^{th} site:

$$H = \sum_{i,j} (t_{ij} + v_{ij}) a_{i,\sigma}^{\dagger} a_{j,\sigma} + \sum_{i,\sigma,\sigma'} E_{\sigma\sigma'} n_{i,\sigma} n_{i,\sigma'} \quad (49)$$

where $n_{i,\sigma}$ is the number operation; $a_{i,\sigma}^{\dagger}$ is the creation operator; $a_{j,\sigma}$ is the annihilation operator; and the σ 's are spin indices. The first term contains both the intra-atomic and interatomic one-electron kinetic-energy and potential-energy matrix elements (and thus would determine the usual one-electron energy bands and related parameters in the

crystalline case). The second term is an approximation mentioned before; it is the correlation energy which results from multiple occupation of the same i^{th} site and omits correlations between different sites. This type of Hamiltonian is considered by Hubbard⁵ and by Kohn⁴.

The electron-current operator has zero expectation for a single atomic orbital. But the solutions to the interacting system defined by Eq. (49) may definitely have non-zero value. The complete current operator would contain all the information about the average "intra-cell" current as well as the "inter-site" current where the electron is transferred through the system. It is the latter which is of interest, and Matsubara and Toyozawa¹⁴ give an appropriate expression which simply localizes the electron of the n^{th} nucleus as long as it is on the n^{th} atom. The current is then

$$J = (ie/\hbar) \left[H, \sum_m R_m a_{m,\sigma}^+ a_{m,\sigma} \right] \quad (50)$$

where the brackets are the usual commutator giving the time rate of change of this approximate electron-position distribution.

In the "pure" vapor at low densities, the electrons referred to in Eq. (45) are about one per atom of the whole and the correlation term in the equation dominates so that the ground state is an essential insulator (discussed in Section 2). To compute the conductivity properly in this limit, it is quite essential that the Hamiltonian, Eq. (49), be treated completely. Hubbard⁵ has made some progress along these lines, but expressions for the conductivity are not yet available. This is a difficult problem--again, due to the correlation.

By contrast, in doped vapors, a Hamiltonian similar to Eq. (49) could be written; however, for the much smaller average number of electrons per majority atom, the correlation term can be neglected. The computation in this case is far more tractable. Specifically, Matsubara and Toyozawa¹⁴ have carried out a development of just this model in connection with compensated majority-band conduction in a randomly-doped semi-conductor (partially compensated). The atomic orbitals are assumed to be hydrogen-like. They compute expressions for both the level density and conductivity in the limiting case where the Hamiltonian Eq.(49) is approximated by only the interatomic matrix elements of potential v_{ij} . The Green's function and the equation of motion, Eq.(50), of the current operator J have been obtained by averaging over various random configurations of the impurity atoms. It would seem that this model could be extended more directly to the case of mixed vapor systems than that of Thirring,¹

which is also done in the spirit of linear response theory and Green's functions, but so far has been restricted to one-dimension and delta-function random potentials.

The purpose of this section was to summarize the nature of the electron-transport problem in the dense vapor state. When conductivity data are available for mixed systems, there is some hope of applying existing methods to analyze the data.

5. THERMODYNAMIC CONSIDERATIONS - PHASE TRANSITIONS IN THE DENSE VAPOR

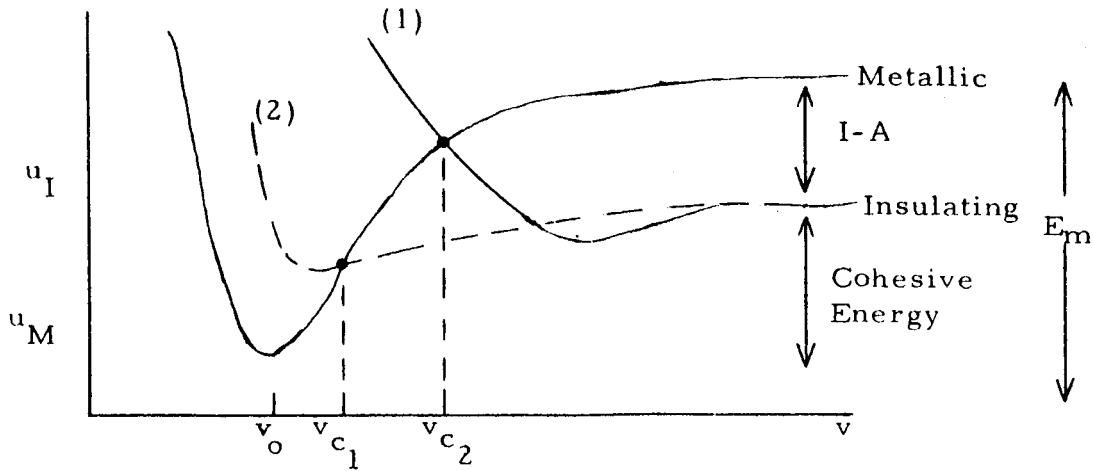
In the current literature on transitions from the insulating dilute gas to a metallic species of much higher density, attention seems to have been directed almost exclusively to the electronic constitution of two alternate configurations. For an alkali metal, the insulating state is described by atomic orbitals with one, and only one, valence electron per atom; in the metallic state, any one electron wave function extends over the whole system and, on the average, there is only one electron per atom. Moreover, attention has been directed particularly to the condition required for the energy of the two configurations to become equal, since this would mark the transition from one form to the other.

The question of the thermodynamic stability of such a transition configuration, which does not seem to have been examined, is the subject of this section. It develops that the transition configuration is very likely to be unstable, so that a "metallic vapor phase" is similarly unlikely. Rather, a first-order phase transition between a low-density insulating vapor and a high-density solid will occur.

The discussion is presented in several steps:

- a. We assume that there is only one insulating and one metallic configuration of importance.
- b. We consider the possibility of distinct ordered and disordered (liquid) metallic phases in addition to the insulating phases.
- c. We note general aspects of the phase transition problem; together with reference to other high pressure studies.

Consider the probable behavior of the (electronic) internal energy of a collection of alkali metal atoms. Assuming that we need consider only two possible configurations as a function of the specific volume $v = (V/N)$, the expected behavior is as shown in the following sketch.³



The principal features illustrated in this sketch are:

- The "insulating" phase is actually the dispersed gaseous atomic phase at large v , while the metallic phase is that which becomes the solid or liquid metal; the latter is known to have a definite cohesive energy relative to the gas phase, as indicated. The order of magnitude of this cohesive energy is a few electron volts.
- At relatively large distances, the metallic phase is higher in energy than the insulating phase by several electron volts (I-A in the sketch, where I is the ionization energy and A is the electron affinity of the metal atoms).
- As the specific volume of the metallic phase decreases, the valence electrons in the metallic configuration will behave approximately like an electron gas and the Hartree-Fock expression for the energy²⁴(corrected for correlation) will be

$$- [u_M^{(\infty)} - u_M(r_s)] = \left(\frac{2.21}{r_s^2} - \frac{0.916}{r_s} \right) + \left(-0.115 + 0.031 \log r_s \right) \quad (51)$$

where r_s is measured in Bohr radii units $\left[r_s = (3v/4\pi)^{1/3} \right]$, and the energy is given in Rydbergs. The zero temperature (solid phase) equilibrium values of r_s , corresponding to a minimum of u_M at v_0 , are typically $5-10^5$ atomic units and $E_m \approx 5$ eV. The shape of the metallic phase curve in the preceding sketch is seen to follow from this expression. For small r_s the ion-core repulsive effects would also have to be included, but do not pertain to the considerations at large r_s which are of interest here. Note: For $v > v_0$, $-(\partial u_M / \partial r_s) < 0$ in the "metallic" phase.

- d. The insulating phase is indicated to have a slight dip with decreasing v resulting from van der Waal's interactions between the neutral atoms. The dip is certainly only a few tenths of an electron volt. Van der Waal's energies are known to be quite inadequate to explain the observed cohesive energy of metals.²⁵ At small separations the repulsive exchange and coulomb energies will increase rapidly causing $u_1(v)$ to increase again with decreasing v . Two possible behaviors, (1) and (2), are shown in the sketch.

The zero temperature properties of this system have an important feature: once the metallic phase is reached as v decreases (i. e., the crossings at either $v_c(1)$ or $v_c(2)$) the system is unstable against contraction to v_0 , since the pressure is $p = (\partial u_M / \partial v)$. (p is negative for $v > v_0$.) Thus, although the condition for transition to the metallic (i. e., conducting) phase might occur for $v = v_{c1} > v_0$, the system would not be stable.

If we were to argue only in terms of the energy, we would conclude that all of the material should condense into the solid phase. To describe realistically what will actually happen, we must consider the behavior at finite temperature. We must apply standard thermodynamic arguments; for the following development, a standard text²⁶ on statistical mechanics may be used as a reference. At finite temperature, we deal with the free energy rather than the energy. For a single-component system,

$$F = F(T, V, N) = U - TS, \quad (52)$$

and since F is extensive, we may also use molar quantities denoted by lower case symbols:

$$F = N f(T, V/N) = N f(T, v). \quad (53)$$

The standard derivative relations apply,

$$p = - \left(\frac{\partial F}{\partial V} \right)_{N, T} = - \left(\frac{\partial f}{\partial v} \right)_T, \quad (54)$$

$$\mu = \left(\frac{\partial F}{\partial N} \right)_{V, T} = f(T, v) + N \left(\frac{V}{N^2} \right) \left(\frac{\partial f}{\partial v} \right)_T \quad (55)$$

$$= f(T, v) - v \left(\frac{\partial f}{\partial v} \right)_T = f + pv. \quad (55')$$

The condition for equilibrium between the two phases will be

$$\mu_M = \mu_I \quad (56)$$

where each is a function of T and v .

To find $f(T, v)$ for the two phases, we must add the finite temperature thermal energy and entropy terms to the zero-temperature energy contributions discussed above (see the preceding sketch). We cannot possibly give exact expressions because of the limited knowledge which we have of these systems, but the essential features are the following:

- a. At low densities, in either the metallic or insulating phases, we should have the standard contribution (kinetic theory) of the free energy of a gas:

$$f_T^{(A)} = -KT \log \left(\frac{v}{\lambda^3} \right), \quad (57)$$

where $\lambda = h(2\pi MKT)^{-1/2}$.

- b. At higher densities, when the density approaches that of solid or liquid metals, an Einstein or Debye approximation will take over and

$$f_T^{(B)} = -KT \log \left(\frac{KT}{h\omega_c} \right), \quad (58)$$

where ω_c is a characteristic frequency which increases with decreasing specific volume v .

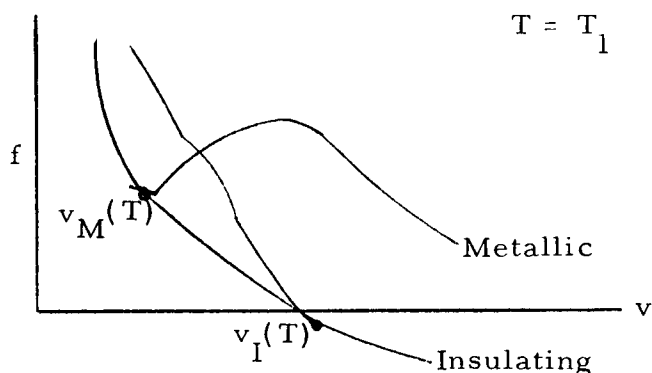
- c. An electron gas contribution in the metallic state, which seems to be small compared to either of the above in the range of interest here.
- d. At large v , we expect $f_T^{(A)}$ to be nearly the same for either phase. At smaller v , we can expect some difference between $f_T^{(B)}$ for the metal and insulating phase respectively, but both are an order of magnitude less than the cohesive energy, being measured in units of KT which is a few tenths of an electron volt at the moderate temperatures under consideration, and their differences will be smaller still.

A plot of the free energies

$$f_M = u_M - f_T^{(A)} \text{ large } v$$

$$f_M = u_M - f_T^{(B)} \text{ small } v \quad (59)$$

for the insulating phase is shown in the following sketch for a particular temperature T_1 . At large v , the term from $f_T^{(A)}$, namely $KT \log (v/\lambda^3)$, dominates. Also, at large v the difference in free energies will approach I-A (see preceding sketch).



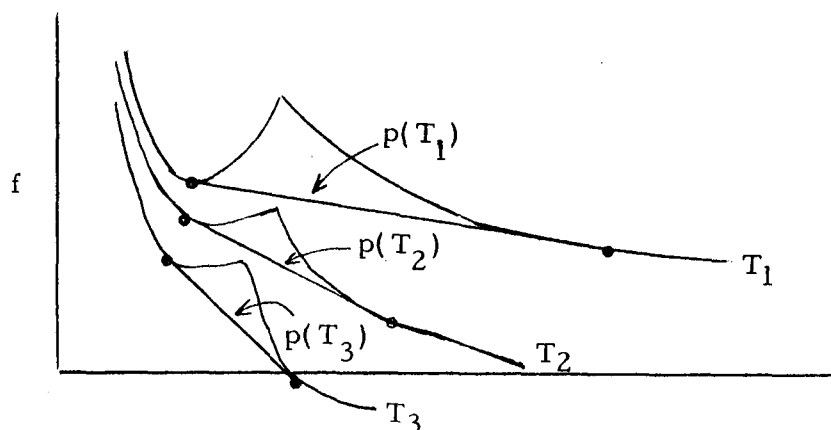
Now Eq. (55') can be substituted in (10) to give the condition for equilibrium:

$$f_M - v_M \left(\frac{\partial f_M}{\partial v_M} \right)_T = f_I - v_I \left(\frac{\partial f_I}{\partial v_I} \right)_T,$$

$$f_M + p_M v_M = f_I + p_I v_I; \quad (60)$$

however, since we are considering the possible equilibrium between one phase and another in the same container, the pressures must be equal, (i. e., $p_M = p_I = p$). Thus Eq.(60) is simply the condition under which curves f_M and f_I have a common tangent, as indicated in the last sketch. This well-known construction determines the equilibrium vapor pressure. The result is a first-order phase transition with a substantial change in volume, i. e., an abrupt transition from insulating vapor to dense metal.

The temperature dependence is determined by the varying thermal contributions to free energy, Eqs. (57) and (58). A temperature-series of plausible curves showing the metallic modification for $v < v_c$ and insulating for $v > v_c$ is shown in the following sketch.



It is to be noted that as the temperature increases ($T_1 < T_2 < T_3$), the transition pressure increases and the first-order volume change decreases. However, it seems completely unlikely that the upward indentation of the two free-energy curves above their common tangent can ever be eliminated, except for thermal energies KT which are comparable to the several electron volts by which the intersection of the insulating-metallic intersection in the first sketch lies above the minimum in the metallic phase.*

The common tangency equilibrium condition will lead to two well separated phases: one (insulating) of volume substantially greater than v_c , and one (metallic) with volume substantially less, i. e., approximately solid or liquid. A "highly conducting vapor" (of a single species) will simply not be attained because it is thermodynamically unstable; even at the highest pressures the equilibrium observed will quite probably be that between an insulating gas and a metal of essentially solid density.

As noted in the beginning of this section, these conclusions need some qualification and some placement in the context of changes of state generally.

* The pressure necessary to flatten out the metallic curve may be estimated from the volume derivative of Eq. (5.5); this would be a lower limit for the pressure needed to eliminate the first order transition. It is approximately 10^5 atm for representative values of specific volume.

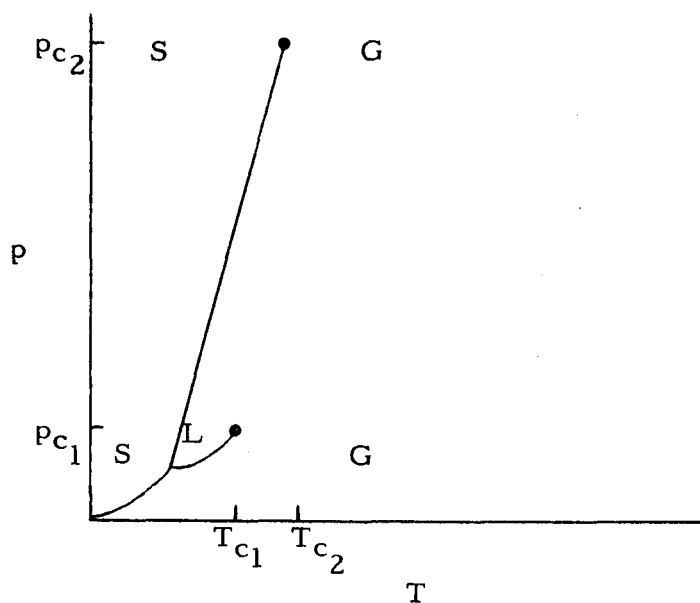
In the first instance, we know that the metallic state may well exist in either an ordered or disordered state. At ordinary temperatures and pressures the former is a crystalline state, while the latter is a liquid.

Actually, liquid metals do not differ so greatly from crystalline metals in most of their properties. The electronic constitutions are very similar²⁷; the thermodynamic properties and the solid-liquid transition can be discussed quite well in terms of a cell model in which the vibrational free energies of liquid and solid are quite similar²⁸, and finally we know there is not a large specific volume change on melting.

For all these reasons, we do not believe that disorder modifies our considerations for essentially solid densities. At lower densities corresponding to the insulating-metallic crossing, it is possible that some advantage might be taken of fluctuations in the spatial distribution of the atoms to lower the energy curves somewhat. However, it is unlikely that this would eliminate the several-electron volt indentation.

Should this surmise prove experimentally to be wrong, it would indicate some fascinating correlation effects indeed. An atomic or electronic configuration with either cluster or "fibrous" connectivity is highly speculative.

Finally, to place the question of a continuous transition from an insulating to metallic vapor phase in yet another perspective, we draw a conventional p, T phase diagram for a single species system (see following sketch). Ordinarily we direct attention to the lower pressure and temperature behavior where a critical temperature T_{c1} and pressure p_{c1} for the liquid gas transition is commonly observed and above which there are no separated liquid and gas phases. What we are now asking is whether there is another critical point (T_{c2}, p_{c2}) for the solid-gas transition, which marks the disappearance of a sharp separation into two phases. Though such an idea has been discussed²⁹ for molecular solids, there seems to be essentially no evidence for any such transition in metallic systems to date. It is presumed that such a critical point would involve pressures of megabars. Reference is made to the reviews by Bradley³⁰; Bundy, Hibbard, and Strong³¹; and several papers by Drickamer^{32,33}.



Thus, even with additional qualifications to the simple models for the insulating and metallic states, we still conclude that at any reasonable pressures ($< 10^5$ atm) and for temperatures of the order of $1-3 \times 10^3$ °K, we expect to find a discontinuous first-order phase transition from an insulating vapor to metallic solid in a single component system such as alkali metal. This is a challenge to the experimentalist since theory has been wrong before.

ACKNOWLEDGMENTS

The author wishes to acknowledge the stimulating hospitality of many members of the General Atomic Research Laboratory. Particular thanks are due Drs. J. F. Colwell and G. W. Hinman.

Appendix I

REFERENCES

1. Colwell, J. F., et al., The Effect of High Pressure on the Conductivity of Vapors, First Quarterly Report on Contract NAS 3-4119. General Atomic report GA-5253. May 15, 1964.
2. Miller, P. H., Jr., Unpublished studies.
3. Mott, N. F., Phil. Mag. 6, 287 (1961).
4. Kohn, W., Phys. Rev. 133, A171 (1964).
5. Hubbard, J., Proc. Roy. Soc. A276, 238 (1963); United Kingdom Atomic Energy Authority. Research group. Atomic Energy Research Establishment, Harwell. Report T/P-136 (1964).
6. Young, W. H., to be published.
7. Kubo, R., "Some Aspects of the Statistical-Mechanical Theory of Irreversible Processes," Lectures in Theoretical Physics, Lectures delivered at the Summer Institute for Theoretical Physics, University of Colorado, Boulder, 1958. W. E. Brittin and L. G. Dunham, eds. (Interscience, New York 1959) Vol. 1, pp. 120-203.
8. Kohn, W., and Luttinger, J. M., Phys. Rev. 108, 590 (1957).
9. Edwards, S. F., Phil. Mag. 3, 1020 (1958).
10. Chester, G. V., Reports Prog. Phys. 26, 411 (1963).
11. Rosa, R. J., Phys. Fluids 4, 182 (1961).
12. Lin, S. C., Resler, E. L., and Kantrowitz, A., J. Appl. Phys. 26, 95 (1955).
13. Krumhansl, J. A., "Thermoelectricity and Direction Conversion Systems," in Radiation Damage in Solids, proceedings of Course 18, Scuola Internazionale di Fisica "E. Fermi," Varenna, Italy. D. S. Bullington, ed. (Academic Press, New York, 1962) pp. 912-936.
14. Matsubara, T., and Toyozawa, Y., Progr. Theoret. Phys. (Japan) 26, 739 (1961).
15. Yamashita, J., and Kurosawa, T. J., J. Phys. Soc. Japan 15, 802 (1960).
16. Appel, J., "On the Small Polaron Motion in NiO," to be published.
17. Loeb, L. B., Fundamental Processes of Electrical Discharges in Gases, (John Wiley and Sons, New York, 1939), p. 297, Table 19.

Appendix I

REFERENCES (Cont.)

18. Branscomb, L. M., "Negative Ions," in Advances in Electronics and Electron Physics. L. Marton, ed. (Academic Press, New York 1957) Vol. 9, p. 46, Fig. 1. See also, standard handbooks on chemical and physical data.
19. Honig, R. E., RCA Review 23, 567 (1962).
20. Chester, G. V., and Thellung, A., Proc. Phys. Soc. (London) 77, 1005 (1961).
21. Langer, J. S., Phys. Rev. 127, 5 (1962); *ibid.* 128, 110 (1962).
22. Herring, C., "The Current State of Transport Theory," in Proc. Int. Conf. Semi-Conductor Phys., 4th Prague (1960), (Academic Press, New York 1961), p. 60.
23. Holstein, T., Ann. Phys. (N.Y.) 8, 325 (1959).
24. Kittel, C., Quantum Theory of Solids (John Wiley and Sons, New York 1963) p. 92, 114.
25. Mott, N. F., and Jones, H., Properties of Metals and Alloys, (Oxford Press, London 1936). Ch. 4.
26. Huang, K., Statistical Mechanics, (John Wiley and Sons, New York 1963).
27. Zinman, J. M., Phil. Mag. 6, 1013 (1961).
28. Vinyard, G. H., "The Theory and Structure of Liquid," in Liquid Metals and Solidification, Seminar during 39th National Metal Congress and Exposition, Chicago, Nov. 2-8, 1957. (American Society for Metals, Cleveland, 1958), pp. 1ff.
29. Temperly, H. N. V., Changes of State, (Cleaver-Hume Press, London 1956), p. 110.
30. Bradley, R. S., High Pressure Physics and Chemistry, (Academic Press, New York 1963).
31. Bundy, F. P., Hibbard, W. R., Jr., and Strong, H. M., Progress in Very High Pressure Research, proceedings from Conference on Very High Pressure Research, (John Wiley and Sons, New York 1961), p. 152.
32. Riggelman, B. M., and Drickamer, H. G., J. Chem. Phys. 38, 2721 (1963).
33. Stager, R. A., and Drickamer, H. G., Phys. Rev. 132, 124 (1963).

APPENDIX II

MATHEMATICAL DETAILS FROM SECTION II

Two integrations which occur during the theoretical discussion will be performed here. The first is that of Eq. (19) when the pseudo-potential $v(r)$ has the form given by Eq. (21). Ignoring factors of 2 and π (which can be absorbed into the normalization constant A), the integration is thus

$$\tilde{v}(q) = \int d^3 q e^{-i q \cdot r} v(r). \quad (61)$$

Now

$$q \cdot r = qr \cos \theta, \quad (62)$$

and

$$\int_0^\pi \sin \theta d\theta e^{i qr \cos \theta} = \frac{2 \sin qr}{qr}, \quad (63)$$

when the pseudo-potential from Eq. (44) is placed in Eq. (61) and Eq. (63) is used. One thus obtains

$$\tilde{v}(q) = (A/q) \sum_n B_n \int_0^\infty r dr \exp(-\lambda_n r) \sin qr = A \sum_n \frac{B_n}{q^2 + \lambda_n^2}. \quad (64)$$

The quantity desired, as given by Eq. (4), is

$$f(\ell) = A^2 \sum_{nm} B_n B_m \int \frac{d^3 q e^{iq \cdot \ell}}{(q^2 + \lambda_n^2) (q^2 + \lambda_m^2) (q^2 + E_k)}. \quad (65)$$

Now employ Eq. (63) to obtain

$$f(\ell) = A^2 \sum_{nm} \frac{2B_n B_m}{\ell} \int_0^\infty \frac{q dq \sin q \ell}{(q^2 + \lambda_n^2) (q^2 + \lambda_m^2) (q^2 + E_k)}. \quad (66)$$

Now we write the sine as the sum of a positive and negative exponential and change the sign of q in the latter to obtain an integral along the entire real axis;

$$f(\ell) = A^2 \sum_{nm} \frac{B_n B_m}{i\ell} \int_{-\infty}^{\infty} \frac{q dq e^{iq\ell}}{(q^2 + \lambda_n^2)(q^2 + \lambda_m^2)(q^2 + E_k)} \quad (67)$$

Equation (67) may be evaluated by contour integration, completing the contour around the upper half plane to obtain convergence. Thus only the three poles above the real axis are enclosed and one obtains

$$f(\ell) = A^2 \sum_{nm} \frac{B_n B_m}{\ell} \left\{ \frac{1}{(\lambda_n^2 - \lambda_m^2)} \left[\frac{\exp(-\lambda_m \ell)}{E_k - \lambda_m^2} - \frac{\exp(-\lambda_n \ell)}{E_k - \lambda_n^2} \right] + \frac{\exp(-\ell \sqrt{E_k})}{(\lambda_n^2 - E_k)(\lambda_m^2 - E_k)} \right\} \quad (68)$$

Equation (68) is indeterminate for the diagonal terms ($\lambda_n = \lambda_m$) and for $\ell = 0$, but L'Hospital's rule may be applied to find that the diagonal members of the sum are

$$\frac{B_m^2 \left[\exp(-\ell \sqrt{E_k}) - \exp(-\lambda_m \ell) \left(1 + \frac{\lambda_m^2 - E_k}{2} \right) \right]}{\ell (\lambda_m^2 - E_k)^2} \quad (69)$$

For $\ell = 0$ a similar application shows

$$f(0) = A^2 \sum_{nm} \frac{B_n B_m}{(\lambda_n + \lambda_m)(\lambda_n + \sqrt{E_k})(\lambda_m + \sqrt{E_k})} \quad (70)$$

The normalization, A , is found by requiring that $f(0)$ be unity if $E_k = E_0$, the atomic energy level.

The second integration is that of Eq. (4) in which $\bar{v}(q)$ is the Fourier transform of $v(r)$,

$$f(\ell) = \frac{A^2}{E_k} \int d^3 r \frac{e^{-\lambda r}}{r} \frac{e^{-\lambda r'}}{r'}, \quad (71)$$

where

$$\vec{r}' = \vec{r} - \vec{\ell}. \quad (72)$$

We use spheroidal coordinates ξ and η defined by

$$\xi = \frac{r + r'}{\ell}, \quad \eta = \frac{r - r'}{\ell}, \quad (73)$$

and

$$d^3 r = \frac{2\pi\ell^3}{8} (\xi^2 - \eta^2) d\xi d\eta = \pi\ell r r' d\xi d\eta. \quad (74)$$

Thus Eq. (71) becomes

$$f(\ell) = \frac{\pi A^2 \ell}{E_k} \int_1^\infty d\xi e^{-\lambda \xi \ell} \int_{-1}^1 d\eta = \frac{2\pi A^2 e^{-\lambda \ell}}{\lambda E_k}. \quad (75)$$

We now make use of the fact that E_0 is determined by $f(0)$ to arrive at Eq. (22)

$$E_0 = \frac{2\pi A^2}{\lambda}. \quad (22)$$

We can now use Eq. (22) to write Eq. (75) in the form used in Eq. (23):

$$f(\ell) = (E_0/E_k) e^{-\lambda \ell}. \quad (23)$$

* Refer to J. Stratton, "Electromagnetic Theory", Sec. 1.18(6), p. 56 (McGraw Hill Book Company, New York, 1941).

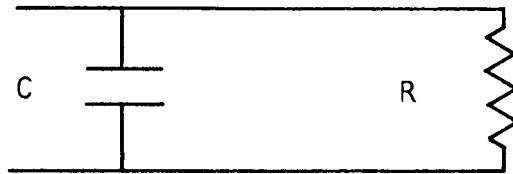
APPENDIX III

CONVERSION OF Q MEASUREMENTS TO RESISTANCE

As used in these experiments, the "Q" meter measures the Q of an equivalent parallel circuit. That is, the circuit must be cast into the form shown in the sketch below and the Q is then of the form

$$Q = \omega CR, \tag{76}$$

where ω is 2π times the frequency.

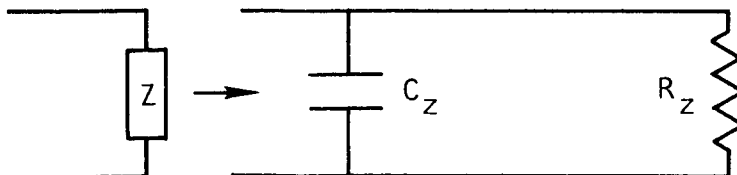


Before any circuit is added, there are some losses associated with the coil and internal circuitry used in the "Q" meter. These losses, together with the tuning coil, will be represented as in the sketch above, except with a sub zero. The Q of this circuit is simply

$$Q_o = \omega C_o R_o. \tag{77}$$

When the element to be measured is connected to the "Q" meter and the mathematical expression for its impedance is cast into a real and an imaginary part (as indicated symbolically in the next sketch), then the Q becomes

$$Q = \omega(C_t + C_z) \frac{R_o R_z}{R_o + R_z}. \tag{78}$$



In Eq. (78), C_t is the value of the tuning capacitor needed for the resonant frequency to remain ω . If Q is larger than about 10, the value of Q does not affect the resonant condition, so the total capacity must remain constant:

$$C_o = C_t + C_z \quad (79)$$

Since the Q meter deals with parallel resistances, it is apparent that it is much easier to use the reciprocal of Q than Q itself. When this is done, and Eq. (79) is used, Eq. (78) becomes

$$1/Q = (1/\omega C_o) \left(\frac{1}{R_o} + \frac{1}{R_z} \right). \quad (80)$$

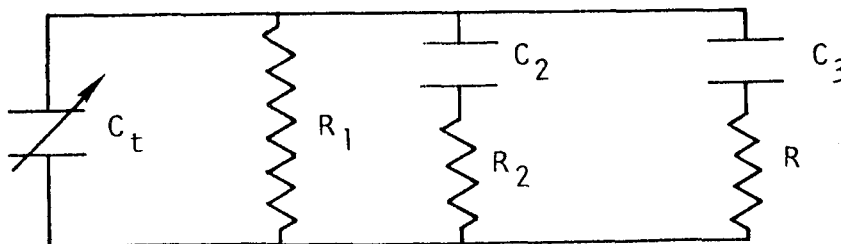
The value of the apparent resistance R_z can now be found by subtracting Eq. (77) from Eq. (79),

$$1/Q - 1/Q_o = 1/(\omega C_o R_z), \quad (81)$$

or

$$R_z = \frac{Q_o Q}{\omega C_o (Q_o - Q)}. \quad (82)$$

We now discuss how the wet and dry runs must be combined to find the sample resistance. The procedure depends on the model one takes for the losses during the dry run. We shall discuss two such losses. In the first case (see following sketch) the background losses are R_1 (appearing directly) and R_2 (appearing capacitatively coupled). The vapor resistance is R . Note that R_1 is actually the parallel combination of R_o and any new losses that appear by connecting the sample tube to the Q meter.



The resolution into real and imaginary parts is

$$1/Z = i\omega C_t + 1/R_1 + \frac{i\omega C_2}{1 + i\omega C_2 R_2} + \frac{i\omega C_3}{1 + i\omega C_3 R} \quad (83)$$

which reduces to the imaginary and real parts

$$1/Z = i\omega \left[C_t + \frac{C_2}{1 + (\omega C_2 R_2)^2} + \frac{C_3}{1 + (\omega C_3 R)^2} \right] + 1/R_1 + \frac{R_c (\omega C_2)^2}{1 + (\omega C_2 R_2)^2} + \frac{R (\omega C_3)^2}{1 + (\omega C_3 R)^2} \quad (84)$$

Now, during the dry run, all of the above losses are assumed to be present except the sample resistance, R , which is infinity. Call the Q measured during the dry run Q_d and that measured during the wet run simply Q ; then Eq.(80) and (84) may be used to find

$$1/Q - 1/Q_d = (1/\omega C_o) \frac{R (\omega C_3)^2}{1 + (\omega C_3 R)^2} \quad (85)$$

Since R is positive, by definition, Q must always be smaller than Q_d . Also, Q approaches Q_d as $\omega C_3 R$ becomes either much smaller or much larger than one.

Equation (85) can be solved for R , the actual resistance, in terms of R_z , the measured apparent resistance. R_z , in turn, is found from Eq. (82), using Q_d instead of Q_o . The result for R is

$$R = (R_z/2) \left\{ 1 \pm \left[1 - (2/\omega C_3 R_z)^2 \right]^{1/2} \right\} \quad (86)$$

It is worth mentioning that both the labor and the arithmetical errors involved in finding R may be reduced by the substitution

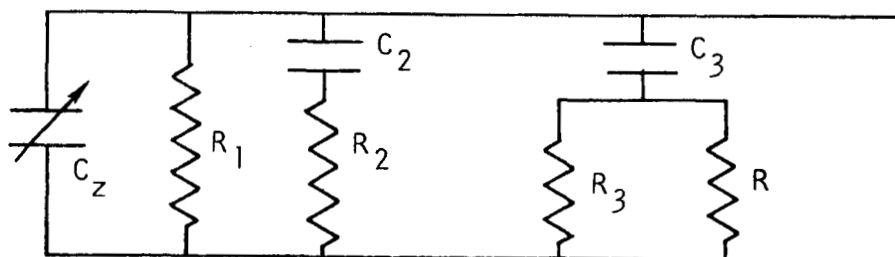
$$\sin y = 2/\omega C_3 R_z \quad (86')$$

Equation (78) now becomes

$$R = R_z \frac{\cos^2(y/2)}{\sin^2(y/2)} \quad (86'')$$

The resistance is a double-valued function of R_z . Which value is to be used can be decided by a simultaneous measurement of C_z or, in practice, by assuming that R is a continuous function of the temperature or pressure. One then uses whichever value assures such continuity.

The second model for the background losses is very similar to the last sketch except that another loss is coupled in by the same capacitor that couples to R . This may be the insulating tube containing the sample, for example. This circuit is shown below.



The resolution into real and imaginary parts is exactly the same as Eq.(84) except that where R appears, we must now use the parallel combination of R and R_3 . The dry run Q is again found by letting R go to infinity. A little self-evident algebra can now be used to find

$$\frac{1}{Q} - \frac{1}{Q_d} = R_3 \omega C_3 \frac{C_3}{C_o} \left\{ \frac{R/(R+R_3)}{1 + \left[\frac{R R_3 \omega C_3}{R+R_3} \right]^2} - \frac{1}{1 + (R_3 \omega C_3)^2} \right\} \quad (87)$$

This in turn may be reduced to

$$Q^{-1} - Q_d^{-1} = \frac{\frac{C_3}{C_o} (R_3^2 \omega C_3) \left[-1 + \frac{R (R_3 \omega C_3)^2}{R + R_3} \right]}{(R + R_3) \left\{ 1 + \left[\frac{R R_3 \omega C_3}{R + R_3} \right]^2 \right\} \left[1 + (R_3 \omega C_3)^2 \right]} \quad (88)$$

Note that in this case, Q_d can be smaller than the Q during the run if $1 + R_3/R \leq (\omega C_3 R_3)^2$.

The general form of Eq. (88) is shown in Figure 36 which gives the difference in the reciprocal Q 's as a function of R/R_3 with $\omega C_3 R_3$ as a parameter. The value of 2.4×10^{-2} , which is appropriate to the experiments, has been used for the ratio C_3/C_0 .

It should be noted that the left-hand side of Eqs. (85) and (88) can be written

$$Q^{-1} - Q_d^{-1} = \frac{\Delta Q}{Q Q_d} \quad (89)$$

where

$$\Delta Q = Q_d - Q \quad (90)$$

It is also frequently convenient to introduce an "average Q ", \bar{Q} :

$$\bar{Q} = \frac{Q_d + Q}{2} \quad (91)$$

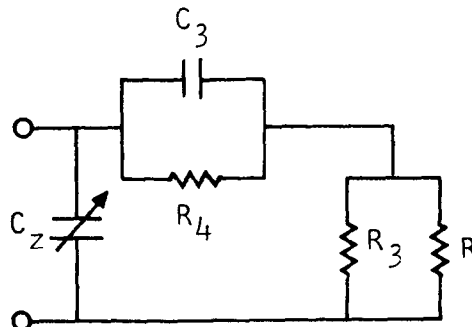
The product occurring in Eq. (89) may be written in terms of ΔQ and \bar{Q} as

$$Q Q_d = \bar{Q}^2 - \left(\frac{\Delta Q}{2}\right)^2 \quad (92)$$

Finally, if ΔQ is small, Eq. (89) reduces to

$$Q^{-1} - Q_d^{-1} = \frac{\Delta Q}{\bar{Q}^2} \quad (93)$$

The losses may be more complex than indicated by the preceding model (see last sketch); for example, the sample tube may be represented by a capacitor in parallel with a resistance as shown below. No analysis was performed on this rather complex circuit.



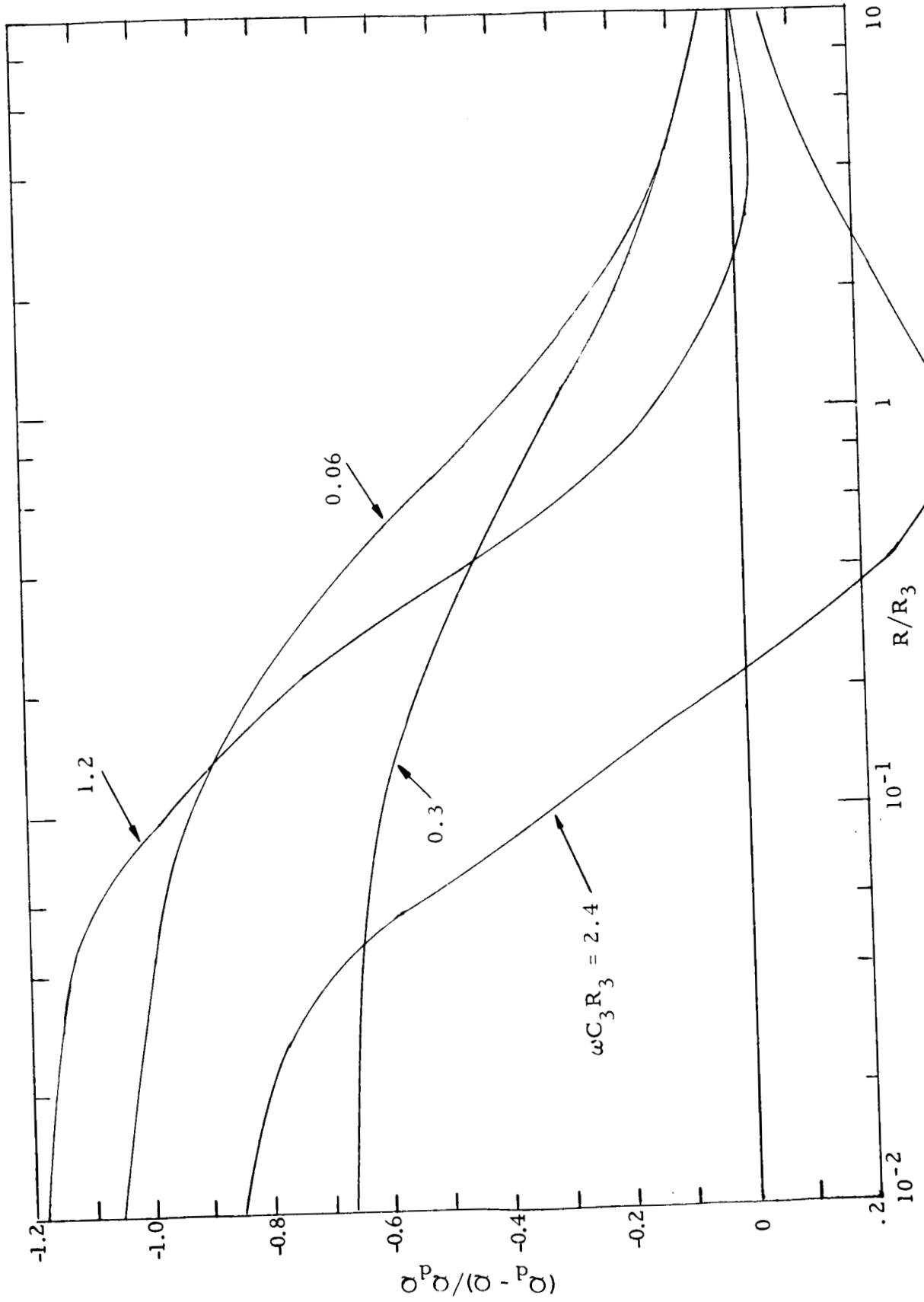


Fig. 36-- $(Q_d - Q)/Q_d Q$ versus R/R_3 for various values of $\omega C_3 R_3$

REPORT DISTRIBUTION LIST FOR
CONTRACT NO. NAS3-4119

National Aeronautics & Space Adm. (1)
Washington, D.C. 20546
Attn: Dr. H. Harrison (RRE)

National Aeronautics & Space Adm. (1)
Washington, D.C. 20546
Attn: Dr. F. Schulman (RNP)

National Aeronautics & Space Adm. (2)
Washington, D.C. 20546
Attn: J. Lazar (RNT)

National Aeronautics & Space Adm. (1)
Washington, D.C. 20546
Attn: Dr. K. H. Thom (RRP)

National Aeronautics & Space Adm. (2)
Washington, D.C. 20546
Attn: J. Lynch (RNP)

NASA Lewis Research Center (1)
21000 Brookpark Road
Cleveland, Ohio 44135
Attn: John H. DeFord

NASA Lewis Research Center (1)
21000 Brookpark Road
Cleveland, Ohio 44135
Attn: J. H. Childs

NASA Lewis Research Center (2)
21000 Brookpark Road
Cleveland, Ohio 44135
Attn: N. J. Stevens

NASA Lewis Research Center (1)
21000 Brookpark Road
Cleveland, Ohio 44135
Attn: L. D. Nichols

NASA Lewis Research Center (1)
21000 Brookpark Road
Cleveland, Ohio 44135
Attn: Henry O. Slone

NASA Lewis Research Center (1)
21000 Brookpark Road
Cleveland, Ohio 44135
Attn: Bernard Lubarsky

NASA Lewis Research Center (1)
21000 Brookpark Road
Cleveland, Ohio 44135
Attn: James Couch

NASA Lewis Research Center (1)
21000 Brookpark Road
Cleveland, Ohio 44135
Attn: Norman T. Musial
Patent Counsel

NASA Lewis Research Center (1)
21000 Brookpark Road
Cleveland, Ohio 44135
Attn: Library

NASA Lewis Research Center (1)
21000 Brookpark Road
Cleveland, Ohio 44135
Attn: Reports Control Office

NASA Lewis Research Center (1)
21000 Brookpark Road
Cleveland, Ohio 44135
Attn: Technology Utilization Officer

Air Force Systems Command (1)
Aeronautical Systems Division
Wright-Patterson Air Force Base, Ohio
APIE-2/Robert Barthelemy

Office of Naval Research (1)
Power Branch (Code 429)
Washington, D. C.
Attn: Dr. Ralph Roberts

U. S. Air Force (1)
Office of Scientific Research
Washington, D. C.
Attn: M. M. Slawsky

AVCO-Everett Research Laboratory (1)
2385 Revere Beach Parkway
Everett, Massachusetts
Attn: T. Brogan

Electrical Engineering Department (1)
Massachusetts Institute of Technology
Cambridge 39, Massachusetts
Attn: Prof. H. H. Woodson

Electrical Engineering Department (1)
Massachusetts Institute of Technology
Cambridge 39, Massachusetts
Attn: Dr. J. Kerrebrock

MHD Research, Inc. (1)
1535 Monrovia Street
Newport Beach, California
Attn: Dr. V. H. Blackman

TRW-TAPCO Group (1)
7209 Platt Avenue
Cleveland, Ohio 44135
Attn: W. C. Davis

RCA (1)
Astro Electronics Division
Princeton, New Jersey

Curtis-Wright (1)
Wright Aeronautical Division
Woodridge, New Jersey

Republic Aviation Corporation (1)
Farmington, Long Island
New York

NASA Sci. & Tech. Info. Facility (6)
P. O. Box 5700
Bethesda, Maryland 20014
Attn: RQT-2448/NASA Representative

Melpar, Inc. (1)
3000 Arlington Boulevard
Falls Church, Virginia
Attn: Dr. Roger C. Jones

Westinghouse Res. & Dev. Ctr. (1)
Beulah Road, Churchill Boro
Pittsburgh, Pennsylvania
Attn: Dr. E. V. Somers

General Electric Company (1)
Valley Forge Space Technology Ctr.
P. O. Box 8555
Philadelphia 1, Pennsylvania
Attn: Dr. A. Sherman

General Electric Company (1)
Valley Forge Space Technology Ctr.
P. O. Box 8555
Philadelphia 1, Pennsylvania
Attn: Dr. F. Shair

Plasmadyne Corporation (1)
Santa Ana, California
Attn: Phillip J. Wyatt

Martin-Marietta Corporation (1)
Baltimore 3, Maryland
Attn: Dr. W. Bienert

Unified Science Associates, Inc. (1)
826 South Arroyo Parkway
Pasadena, California
Attn: S. Naiditch

Stanford University (1)
Department of Mechanical Engineering
Stanford, California
Attn: Dr. R. H. Eustis

Jet Propulsion Laboratory (1)
California Institute of Technology
Research & Advanced Concepts Section
4800 Oak Grove Drive
Pasadena, California 91103
Attn: D. G. Elliot